ABSTRACT

KHALILZAD, MAHDI. Development of Deformation-Based Limit States for Reliability Assessment of Flood Protection Earth Dams and Levees. (Under the direction of Professor Mohammed Gabr.)

Traditional design approaches based on the concept of factor of safety do not provide a complete indicator of level of safety pertinent to earth structures given uncertainties in loading, soil properties, and changes in geometry that can take place with time. Thus, there has been a tendency to utilize probabilistic analysis in addition to conventional design methods. Work is presented herein to introduce performance limit states and incorporate them into probabilistic analysis, for water holding embankments and flood protection structures. Coupled flow/deformation analysis is employed in the numerical analyses to capture the interdependency of under-seepage and through-seepage with deformation associated with the development of plastic zones and shear bands. Limit states were defined in terms of deformations that correspond to levels of performance or extent of damage in the embankment.

The effect of various parameters on the flow and deformation response of embankment dams and the corresponding performance limit states are also investigated in this study. The parameters are pertinent to the geometry of dams, and applied loads in terms of intensity, duration, and cycles of loading and unloading which are equivalent to the rising and falling of water level in the reservoir. In addition, the effects of woody vegetation on soil hydraulic conductivity and the related probability of exceeding deformation-based performance limit states are investigated in this study.

Finally, the results of a series of numerical analyses simulating remedial measures conducted on embankment dams in order to mitigate the hazard. Three remedial measures

including constructing a berm at the toe, constructing drainage system within the toe area, and adding an impermeable curtain from the crest extending to three different depths are investigated.

The analysis showed as the water level increased in the reservoir, the probability of exceeding each limit state increased and the target deformation was changed to the next limit state. It is shown that in a larger embankment model, the shear zone propagates deeper for failure to occur. The time to exceed LS I, II and III increases as the size of an embankment model become larger. For example, failure occurs after 4.6 days in the model with a size factor of 0.1 compared to 12 days for a model with a size factor of 0.2. This is mainly because the saturation front reaches the critical level in less time in a small dam, considering that the hydraulic conductivities are the same. After two weeks of water rising in the reservoir and sustained at the maximum pool level, the magnitudes of horizontal deformations at toe are 0.16m, 0.08m, and 0.048m for embankment models with side slopes of 1:2.5, 1:3, and 1:4, respectively. The analyses demonstrated the importance of accounting for the storm loading history when assessing the stability of the flood protection earth structures under future flood events.

Even though the levee case used in this study (Elkhorn) was in a marginal condition of stability based on limit equilibrium analysis, the probability of exceeding LS III after 10 days of a sustained high water level was 2%. This probability, however, increased over time to 37% and 72% after 20 and 30 days of sustained water loading, respectively, which signifies the importance of considering the transient nature of hydraulic loading in making condition assessments after a storm event.

Development of Deformation-Based Limit States for Reliability Assessment of Flood Protection Earth Dams and Levees

by
Mahdi Khalilzad

A dissertation submitted to the Graduate Faculty of
North Carolina State University
in partial fulfillment of the
requirements for the degree of
Doctor of Philosophy

Civil Engineering

Raleigh, North Carolina

2013

APPROVED BY:

Mohammed Gabr Committee Chair	Roy Borden
Shamim Rahman	Ranji Ranjithan

BIOGRAPHY

Mahdi Khalilzad was born and raised in Ardebil, Iran. In 2001, he was admitted to Iran University of Science and Technology to study in Civil Engineering program. After completing his Bachelor's degree in 2005, he found his passion in soil and foundation field and started his Master's degree in Geotechnical Engineering at University of Tehran in the same year. While doing his Master's thesis, he was working in the Reinforced Earth Company in Tehran. As he was moving on in his career and after he completed his Master's degree in 2008, he realized he needed to deepen his knowledge and make a contribution to the Geotechnical field. Hence, in the next big step he moved to the United States to pursue his Ph.D. in Civil Engineering with a Geotechnical focus. To cultivate his interests, Mahdi accepted a job at Geocomp Corporation in 2012.

ACKNOWLEDGMENTS

Sincere appreciation is extended to my faculty mentor, scientific colleague and friend, Professor Mo Gabr. Through his guidance, this thesis was initiated to challenge the breadth of my research potential. Finally, his friendship has made my four-year tenure at NC State an enjoyable one. I would also like to thank Professors Roy Borden, Shamim Rahman and Ranji Ranjithan for accepting to be in my doctoral committee, for evaluating my research, and for their valuable advice and support. Finally, it is important to recognize my family, without whose support, such achievements would never be possible.

TABLE OF CONTENTS

LIST OF TABLES

LIST OF FIGURES

CHAPTER 1

1. OVERVIEW

1.1 Introduction

Traditional design approaches based on the concept of factor of safety do not provide a complete indicator of level of safety pertinent to earth structures given uncertainties in loading, soil properties, and changes in geometry that can take place with time. Thus, there has been a tendency to utilize probabilistic analysis in addition to conventional design methods. Work is presented herein to introduce performance limit states and incorporate them into probabilistic analysis, for water holding embankments and flood protection structures. Coupled flow/deformation analysis is employed in the numerical analyses to capture the interdependency of under-seepage and through-seepage with deformation associated with the development of plastic zones and shear bands. Limit states were defined in terms of deformations that correspond to levels of performance or extent of damage in the embankment.

The effect of various parameters on the flow and deformation response of embankment dams and the corresponding performance limit states are also investigated in this study. The parameters are pertinent to the geometry of dams, and applied loads in terms of intensity, duration, and cycles of loading and unloading which are equivalent to the rising and falling of water level in the reservoir. The analysis of a model dam is conducted using the finite element approach and the results of the numerical analyses are incorporated into

deformation-based probabilistic analyses and the probabilities of exceeding three pre-defined limit states are presented.

In addition, the effects of woody vegetation on soil hydraulic conductivity and the related probability of exceeding deformation-based performance limit states are investigated in this study. A summary of results obtained from laboratory and field hydraulic conductivity tests, as reported by Brizendine (1997), for four levee sites are presented. Limit states, as defined based on the framework of critical state soil mechanics, are developed and simple probability analyses are used to quantify the probability of exceedance under hydraulic loading. A case study of Elkhorn Levee near Sacramento, California, is presented to demonstrate the applicability of the limit states concept.

Finally, the results of a series of numerical analyses simulating remedial measures conducted on embankment dams in order to mitigate the hazard. The work is performed through a deformation-based probabilistic analysis which employs coupled flow and deformation finite element analysis along with the Taylor's series approach to calculate the probabilities of exceeding pre-defined performance limit states. The results are studies in view of deformations and gradients at the key points. The limit states (LS) values were established in a previous publication by the authors (Khalilzad and Gabr, 2013) and the current paper is employing those LS values in the probabilistic analysis performed herein. Three remedial measures including constructing a berm at the toe, constructing drainage system within the toe area, and adding an impermeable curtain from the crest extending to three different depths are investigated.

1.2 Thesis Content

Chapter 2 introduces the basics of proposed deformation limit states and illustrates its use with simplified reliability analysis of deformation in an embankment dam. In Chapter 3, a parametric study has been performed on deformation-based limit analysis and the effects of factors such as geometry and side slopes, loading condition in terms of rate of rise, and cycles of rise and fall are investigated on the magnitudes of deformation and strains corresponding to pre-defined limit states criteria. Chapter 4 presents a case study to investigate the effects of woody vegetation on seepage-induced deformation using limit state analysis of levees. In Chapter 5, remedial measures to mitigate the hazard of failure in embankment dams are studied through the deformation-based limit analysis. Conclusions are presented in Chapters 6.

CHAPTER 2

2. DEFORMATION-BASED LIMIT STATES FOR EARTH EMBANKMENTS

2.1 Introduction

Past experience with levee failures, especially those caused by hurricanes Katrina and Rita, has highlighted the weaknesses in the current state of the nation's infrastructure. Consequences of such disasters involve loss of life and financial damage that present a burden to our nation. The Katrina incident, in particular, drew attention toward the condition assessment and rehabilitation of levees.

Several factors compromise levees stability over the design life. As identified by many in the literature (e.g. Tremaine et al., 2010; Chowdhury, 2010), uncertainties in design soil parameters, unforeseen failure modes, changes in geometry, scour, accumulated plastic strains, and local deficiencies due to burrowing animals and vegetation roots are among the many factors increasing the risk of levee failure in the absence of rehabilitative programs. As shown by "sunny day" failures, the use of a traditional value of factor of safety does not guarantee the stability of slopes in a dam or a levee subjected to fluctuating water levels. This traditional factor of safety value is usually specified as a *minimum* for all cases but a probability of failure, even if small, associated with each chosen factor of safety always exists.

Levees and dams are continually subjected to changes in water elevation in a reservoir. Apart from earthquakes, hydraulic and gravity loadings are the most dominant loading conditions in these water holding structures. Therefore, different approaches have been proposed to study seepage flow through embankment dams and levees and to investigate the stability of slopes under seepage conditions. For example, Fu and Jin (2009) developed a numerical model to simulate unsteady seepage flow through dams assuming saturation and hydraulic head as variables. Lu and Godt (2008) proposed a framework for infinite slopes under steady unsaturated seepage conditions, and showed instability may occur under high infiltration rates in the slope due to a decrease in the absolute value of suction stresses. Callari and Abati (2009) illustrated the hyperelastic response of three-phase porous media using a finite element formulation and studied reservoir bank response subjected to rapid drawdown. Based on their finite element model, deformations of reservoir slopes increased during drawdown and continued over time with a descending rate.

After hurricane Katrina, extensive investigations were performed on the geology of the area, performance of the levees and floodwalls and causes and consequences of their failures. The results of these studies were published in a special issue of ASCE JGGE (May, 2008). Sills et al. (2008) reported that: “In other cases levee failures occurred at water levels well below their design due to the combination of misinterpretation of geologic conditions and an unforeseen failure mechanism.” Bea and Cobos-Roa (2009) discussed the case of the 17th Street Canal floodwall levee, citing resistance to lateral forces from water was potentially reduced because of the significant uplift pressure. Such cases illustrated the

importance of considering multimodal failures (i.e. interdependency of seepage and slope instability modes) as well as uncertainties in the estimation of soil profile and soil parameters.

The use of probabilistic analysis in geotechnical engineering are covered in US Army Corps of Engineering (USACE) technical letters ETL 1110-2-547 (1997), ETL 1110-2-556 (1999), and ETL 1110-2-561(2006). In these documents probabilistic analysis is used to study seepage failure modes or slope instability modes in relation to the factor of safety. In the first reference from the abovementioned technical letters, the probabilities of exceeding unsatisfactory performance has been tied to the expected performance levels as expressed in Table 2.1.

Table 2.1 Performance levels associated with probabilities of unsatisfactory performance (from ETL 1110-2-547)

Expected Performance Level	Probability of Unsatisfactory Performance
High	0.0000003
Good	0.00003
Above average	0.001
Below average	0.006
Poor	0.023
Unsatisfactory	0.07
Hazardous	0.16

Work conducted for this paper utilizes a simplified reliability analysis of deformation in an embankment dam, and illustrates its use with proposed deformation limit states to

define various structure performance levels. The analyses are based on coupled flow/deformation behavior of an embankment dam section with a geologic profile representative of the lower Mississippi valley where an alluvium foundation is overlain by a blanket of relatively low permeability soil. In this analysis, no predefined limit equilibrium mode is being considered as the probable failure mode. Thus, either deformations or gradients are manifesting the *emerging failure mode* while the dam is subjected to a loading condition corresponding to a given storm event. Once emerging performance envelopes are defined on the basis of deformation /gradient levels, the deterministic analyses are extended to assess the probability of exceeding the proposed performance envelopes.

2.2 Deformation-Based Probabilistic Analysis

In general, the factor of safety concept is being used as the margin for stability of a structure. The general notion is such that the higher the value of factor of safety, the less the probability of failure occurrence although there is no statistical basis for this statement. For addressing such a limitation, probabilistic analysis has been used extensively in the literature (e.g. Wolff, 1985; Tang et al., 1999; Griffiths and Fenton, 2004). In this analysis, the probability is attributed to the occurrence of an event (e.g. failure). Even though the factor of safety is higher than one, it is still possible to have failure due to uncertainties not taken into account in deterministic analysis. There have been several cases where designed with an appropriate factor of safety but failed under critical loading conditions (USACE, 2006; Stark and Duncan, 1991). Furthermore, failure is a relative, rather than absolute term. A levee may

experience large deformations but retain its water-holding capacity. In this case, failure may have occurred based on the initial design criterion, but not from a functionality perspective.

In deformation-based probabilistic analyses, probabilities of unsatisfactory performances are calculated for performance aspects such as deformation, hydraulic gradient, stresses, etc. which are derived from response of the earth structure at any time step. The advantage of this method is the ability to consider the effect of previous extreme events and to assess the probability of unsatisfactory performance at the operational conditions, as well as under future extreme events.

2.2.1 Methodology

Deformation-based probabilistic analyses, as used in this study, employ a combination of finite element simulation, reliability index, and three-sigma rule to develop a probability of unsatisfactory performance in an earth structure. The main concept relies on the definition of performance criteria corresponding to various limit states. The criteria are currently selected with regard to functionality aspects. For example, horizontal deformation of crown can be a performance criterion related to the amount of damage of an embankment dam, or seepage gradient can be selected as another criterion for assessing limit states.

To assess the failure risk of a dam or levee, USACE proposes four steps including: annual loading probability, probability of unsatisfactory performance, performance levels, and consequences (USACE, 2006). In deformation-based probabilistic analysis presented herein, the second and third steps are combined into one step with probabilities of exceeding performance envelopes (limit states) being calculated.

To find the probability of occurrence for each limit state, a method similar to Duncan (2000) is employed. For this purpose, a finite element model of the embankment dam is constructed and a mean value of each analysis parameter is introduced into the model. The three-sigma rule is used to estimate the standard deviation of a parameter since generally limited data are available for finding standard deviation of earth parameters. The finite element model is processed for each random parameter, once with one standard deviation more than mean value and again for one standard deviation less than mean value. Deformation values of key points along the embankment are then normalized with respect to the proposed (pre-defined) limit state values. Next, the Taylor Series Technique (Wolff, 1994; USACE, 1997; 1999) is used to find the standard deviation and coefficient of variation of these normalized values. Finally, a reliability index is calculated based on the mean and standard deviation of normalized values and a probability of exceeding a pre-defined limit state is estimated.

2.2.2 Limit States Definition

It is proposed herein that limit states be defined based on the performance levels expected from the earth structure in terms of deformation and hydraulic gradients. In an embankment dam, the limit states can be defined as: i) minor deformations, no discernable shear zones, low gradients (i.e. $i<1$) throughout the dam and foundation (Limit State I); ii) medium (repairable) deformations, limited piping problems (i.e. $i>1$ within a depth less than 10 ft at the location of toe), dispersed plastic zones with moderate strain values, tolerable gradients less than critical (Limit State II); iii) major deformations, breaches and critical

gradients at key locations (i.e. boiling and fine material washing within a depth more than 20 ft at the location of toe), high strain plastic zones and emerging shear bands (Limit State III). At this point such definitions are subjective. Clearly, the definition of limit states for earth embankments is a challenging task since it requires large databases with quantifiable information on condition and corresponding functionality.

2.3 Model Description

The development of rehabilitation and retrofit measures as well as maintenance programs for critical earth structures requires the assessment of performance before, during, and after severe loading conditions representative of natural events. From a long term perspective, there is a need to assess the condition of the structure in terms of threshold performance limit states to effectively manage repairs, and distribute resources. In this study, a model is developed to represent an earth dam section with geologic profile representative of the lower Mississippi valley, where alluvial foundation soil is overlain by a blanket of a relative low permeability soil. The profile and dam geometry were analyzed in the USACE Technical Letter No. 1110-2-561 (2006). The analysis in this study utilized the finite element program ABAQUS 6.8 in a coupled flow/deformation mode to first investigate the mechanistic response with rising water level. Once deformation levels and their impact on the dam functionality were estimated, the deterministic analysis was extended to include probabilistic assessment of the exceeding a given limit state in order to address uncertainties associated with the structure response under a storm event.

2.3.1 Model Discretization and Properties

The dam was modeled as a two dimensional continuum system with three uniform isotropic layers. The geometry and meshing of the model including quadratic quadrilateral elements of type CPE8RP is shown in Figure 2.1. The finite element mesh consists of approximately 75,000 nodes and 24,000 elements. The top of the shale layer is located at an elevation of 550 ft and the top of the alluvium layer is located at 700 ft. The elevation of the crown is 1000 ft and horizontal distance from crown to the toe on each side is 500 ft (USACE, 2006). The width of the crown is 15 ft. The soil properties for embankment and foundation layers are presented in Table 2.2. The Mohr-Coulomb model is used in the finite element model to define the plastic behavior of the soil. Modeling steps included first generating the geostatic stress state in the foundation and then adding the embankment layer. "Sunny day" water loading was applied in a steady state condition, and then rising water level was simulated in transient steps where the water level and associated boundary conditions were applied consistent with the rising rate of the water level.

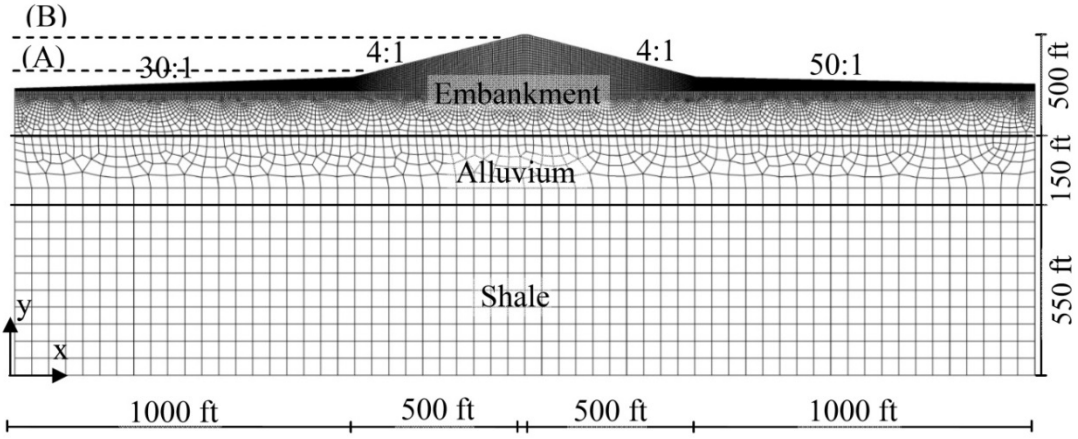

Figure 2.1 Model geometry and mesh (1 ft=0.3 m)

Table 2.2 Soil Properties (from ETL 1110-2-561) [1 pcf=16 kg/m3, 1 psf= 47.9 Pa]

Soil Type	Unit Weight (pcf)	Cohesion (psf)	Friction Angle
Embankment	125	0	27.1°
Alluvium	105	0	18°
Shale	128	0	20.8°

2.3.1 Boundary Condition

Deformation boundary conditions included restriction of horizontal deformation on the left and right edges of the soil profile as well as restriction of horizontal and vertical deformations at the bottom. Pore pressure boundary conditions on the upstream slopes corresponded to the water elevation in reservoir. In addition, a pressure load was also applied to the upstream elements representing the weight of water. Downstream boundary elements were assigned to be drainage elements. Zero flow boundaries included the bottom and sides

of the soil profile. Water level increased from normal pool elevation (900 ft, level A) to high water level (980 ft, level B) at a rate of 2 ft per hour.

2.4 Results and Discussion

As water rises in the reservoir, horizontal deformations begin to increase due to the stress applied by water pressure on upstream slopes as well as seepage forces associated with flow gradients throughout the dam. The horizontal deformations at crown, mid-slope and toe of the dam are shown in Figure 2.2.

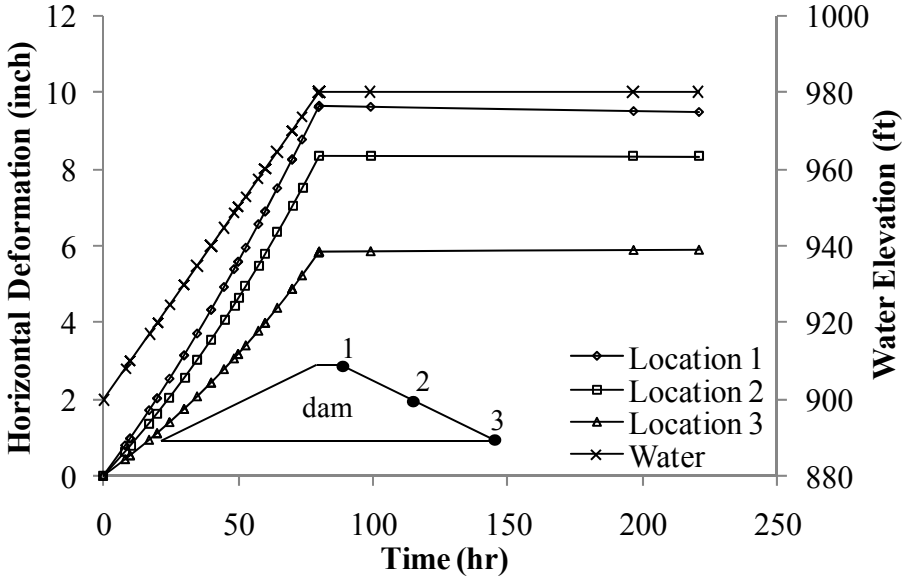

Figure 2.2 Horizontal deformation [1 inch=2.5 cm, 1 ft=0.3 m]

Based on the deformation levels, the probabilities of exceeding a given limit state are estimated as water rises in the reservoir. Table 2.3 shows a sample of a worksheet developed to estimate those probabilities when water is at its maximum level. As mentioned earlier, three limit states were defined for the horizontal deformation of the crown based on the development of shear zones and high gradient zones within the embankment dam. *Limit State I* (2.5 in) represents the condition where shear zones have not yet been developed but a small area of high gradient zones are being observed. *Limit State II* (5 in) is the start point of developing plastic shear zone as well as expanding high gradient zones. In *Limit State III* (10 in) shear bands have been developed and high gradient can be observed in a wide zone which can lead to compromising the stability of slopes.

When the water level is at elevation 940 ft, the probability of exceeding *Limit State I* is 100%, while probabilities of exceeding *Limit States II* and *III* are 0.51% and 0.00%, respectively. As water rises to elevation 960 ft, the dam has already experienced deformations exceeding *Limit State II* as indicated by 100 percent probability of exceedance, but it has not exceeded *Limit States III*. When water is at elevation 970 ft, there is a 2 percent probability of exceeding *Limit State III* while this probability is 73 percent when water reaches elevation 980 ft. The last finding is in agreement with USACE (2006) results since failure occurred (in the form of FS less than one) in the dam when it reached the high water level.

Table 2.3 Calculating Probability of Exceeding Limit States [1 pcf=16 kg/m^3]

Friction Angle					L.S.I (S_1=2.5 in)		L.S.II (S_2=5 in)		L.S.III (S_3=10 in)	
Soil Type	**μ**	**σ**	**μ+/-σ**	**S (in)**	**N=S_1/S**	**ΔN**	**N=S_2/S**	**ΔN**	**N=S_3/S**	**ΔN**
Embankment	27.1	2.56	29.66	10.0	0.2500	0.0119	0.5000	0.0238	1.0000	0.0476
			24.54	10.5	0.2381		0.4762		0.9524	
Alluvium	18.0	3.93	21.92	10.5	0.2381	-0.0046	0.4762	-0.0092	0.9524	-0.0185
			14.08	10.3	0.2427		0.4854		0.9709	
Shale	20.8	5.57	26.37	10.3	0.2427	0.0023	0.4854	0.0047	0.9709	0.0093
			15.23	10.4	0.2404		0.4808		0.9615	
Unit weight (pcf)										
Embankment	125	5.67	130.67	10.2	0.2451	0.0070	0.4902	0.0140	0.9804	0.0280
			119.33	10.5	0.2381		0.4762		0.9524	
Alluvium	105	2.33	107.33	10.3	0.2427	0.0046	0.4854	0.0092	0.9709	0.0185
			102.67	10.5	0.2381		0.4762		0.9524	
Shale	128	4.33	132.33	10.5	0.2381	-0.0094	0.4762	-0.0189	0.9524	-0.0377
			123.67	10.1	0.2475		0.4950		0.9901	

	L.S. I	L.S. II	L.S. III
Standard Deviation	0.0091	0.0181	0.0362
Mean	0.2418	0.4836	0.9672
C.O.V.	0.0374	0.0374	0.0374
β	-25.008	-12.803	-0.5993
R=Φ(β)	0.000	0.000	0.274
P(E.L.)=1- R	**1.000**	**1.000**	**0.726**

Notations:

μ=Expected value of friction angle/unit weight
σ=Standard deviation of friction angle//unit weight
L.S. i=Limit State i
S=Horizontal deformation
N=Normalized deformation
R=Reliability
C.O.V=Coefficient of Variation
β=Reliability index

P(E.L.)=Probability of exceeding the limit state

The progression of high gradient zones at the toe of the dam for different limit states is shown in Figure 2.3. At a deformation level associated with *L.S. I* only one data point is beyond the critical gradient line. This indicates the development of high gradient zones at a depth of 5 ft. At *L.S. II*, the high gradient zone expands to a depth of 10 ft, and at *L.S. III* gradients exceeding the critical values are observed throughout the foundation, as shown in Figure 2.4 (dark gray areas indicate the zones where gradient is equal or greater than critical gradient.) The flow rate through the dam for *Limit States I* is 200 gal/day per ft, but increases by over 60% with the progression of lateral deformations. This is while the flow rates through the dam increase to 320 gal/day per ft for *Limit States II* and 360 gal/day per ft for *Limit States III*.

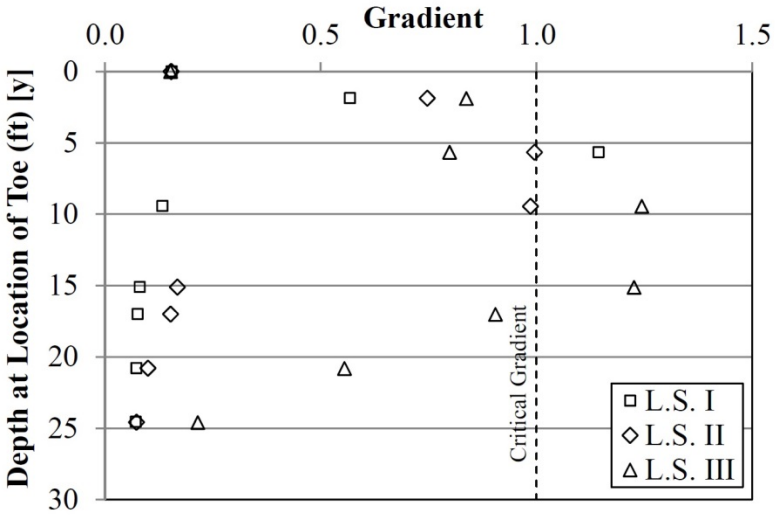

Figure 2.3 Gradient at toe (Datum is shown in Figure 2.4)

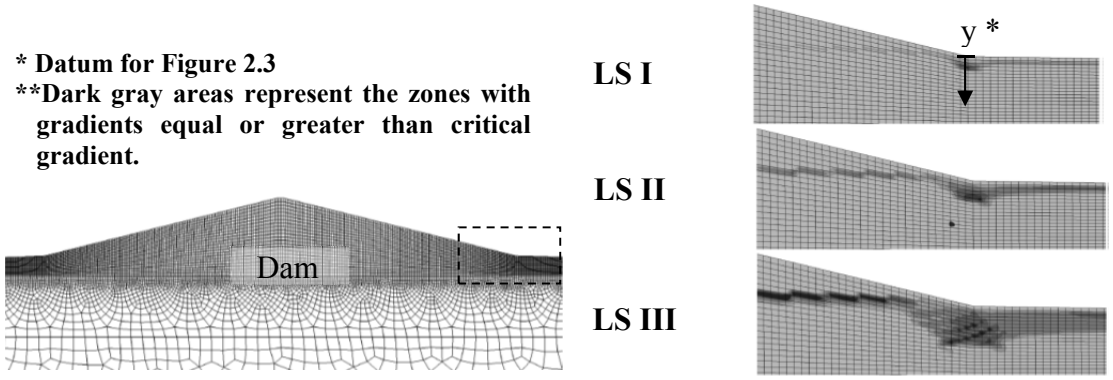

Figure 2.4 Expanding high gradient zones at toe

2.5 Summary and Conclusions

This paper presents the results of coupled seepage/deformation analysis with the aim of estimating the probabilities of exceeding a pre-defined deformation limit state, with a focus on water storage and flood protection earth structures. Finite element analyses of an embankment dam where failure was estimated to occur with high water level in the reservoir were performed. Limit states were defined on the basis of deformation level and area of high seepage gradients. The approach presented in this paper utilized limit states that were defined based on potential emerging failure zones instead of using probability of exceeding a predefined value of factor of safety. Based on the assumptions made in this study and the analyses results, the following conclusions are presented:

i. By considering uncertainties in design soil properties, analyses indicated the earth embankment has a 100% probability of exceeding *Limit State I* and *II* and a 73% probability of exceeding *Limit State III* when the water level is at the maximum elevation (980 ft).

ii. This is in agreement with the deterministic analyses in which a factor of safety of less than unity is estimated for the embankment slope at water elevation of 980 ft (USACE, 2006).

iii. Analyses results suggested that at *Limit State I*, corresponding to 2.5 inches of lateral deformation at the crown, zones of high hydraulic gradients began to emerge. At *Limit State II*, corresponding to 5 inches of lateral deformation at the crown, the high gradient zones (above critical gradient) expands to a depth of 10 ft below the toe. In case of *Limit State III*, corresponding to 10 inches of lateral deformation at the crown, a substantial area on the high gradient zones below the toe extends to a depth of 20 ft.

iv. In these analyses, *Limit State I* can be considered the serviceability limit state while *Limit States II* and *III* can be considered intermediate and ultimate limit states, respectively. The flow rates through the dam for *Limit States I* was 200 gal/day per ft, but increased to 320 gal/day per ft for *Limit States II* and to 360 gal/day per ft for *Limit States III*.

Finally, selecting the definition of limit states for earth embankments is a challenging task because it requires a large database with quantifiable information on condition and

corresponding performance levels. Coupled with modeling effort, mining databases such as the National Levee Database provided by the USACE may provide sufficient information for a better establishment of limit states in various modes. The advantage of this approach is not only in terms of avoiding confusion with factors of safety and their various definitions, but also in terms of a better communication of risk for county, city, state and federal officials.

CHAPTER 3

3. PARAMETRIC STUDY ON DEFORMATION-BASED LIMIT STATE ANALYSIS

3.1 Introduction

Modeling of embankment dams and levees has been widely employed in geotechnical engineering to assess the structures' stability through limit equilibrium and mobilized deformation levels (e.g. Seed et. al, 1990; Charles and Bromhead, 2008; Özera and Bromwell, 2012). In the cases where embankments slope stability is of concern, the main focus of analyses has traditionally been the limit equilibrium for which the soil is assumed to follow the Mohr-Coulomb failure criterion under fully plastic conditions. A factor of safety is computed as the balance between the capacity and the demand based on what is deemed as the most critical failure surface. Although, this type of analysis is easier to implement and many computer programs have been developed to facilitate limit equilibrium calculations, the approach has several drawbacks that were summarized by Yu et al (1998). A main drawback in this case is the lack of displacement compatibility in the analysis and the possibility of having slip surfaces that may not be permissible due to the assumptions of the failure wedge kinematically behaving like a rigid body and the assumption made regarding interstice forces. On the other hand, numerical approaches are usually employed in the analyses to estimate emerging failure modes within the lower and upper bounds, and can incorporate

steady state and transient flow, stress-deformation, and coupled flow and deformation analyses. Within the framework of risk assessment, however, these deterministic evaluations need to be supplemented with assessment of the probability of occurrence in order to be suitable as an input for assessing risk.

An approach for combining the deterministic evaluation with simple probability techniques was presented by Khalilzad and Gabr (2011) in the form of assessing the stability of levees and dam embankments using the concept of deformation-based limit states. In recent decades, instrumentation, monitoring and data management systems have vastly advanced and technology has allowed real time monitoring of many structures (for example in World Trade Center, Willow Island Hydroelectric Project, New Orleans levees, etc. and in Ahmed-Zeki et al., 2000; and Dickenson, 2007) . This has opened an area for a proactive management of risk; provided that the measured quantities in the field can be compared with pre-established limit states. In large and mega construction projects (e.g the Boston Artery), owners are mandating the contractors to employ instrumentations to monitor the response of new and existing structures during and after construction activities. A fundamental component of the interpretation of data from such a monitoring program is establishing limit states for measured quantities, as well as benchmarking for a due course of action to minimize either damage and/or impact of failure of earth structures.

In this paper, work is focused on the definition of deformation-based limit states for earth embankments through the performance of numerical analysis varying key parameters of earth embankments. A finite element model is established for a model earth dam using Plaxis

software, and parameters varied included geometry and side slopes, loading condition in terms of rate of rising and duration of high water level in the reservoir, and cycles of rising and falling water levels. The influence of these factors on magnitudes of deformation and strains corresponding to predefine limit states criteria is studied. The deterministic results are extended through simplified probabilistic analysis to define the probability of exceeding a given limit state as a function of the analyses parameters. Results are discussed including the effect of time history of hydraulic loading and unloading on the probability of exceedance of a given limit state.

3.2 Background

Modeling the earth embankments of dams and levees, including the effect of seepage, has been reported in the literature. Using kinematic approach of limit analysis, Viratjandr and Michalowski (2006) presented factor of safety charts for slopes under drawdown condition. While these charts are useful for estimation of the factor of safety for the slopes subjected to drawdown condition, there was no provision for time component (no rate of variation of water level) or hydraulic conductivity variation. Lu and Godt (2008) utilized the limit equilibrium approach and proposed an analytical framework for infinite slope analysis under steady unsaturated seepage conditions. They showed instability may occur under high infiltration rates due to a decrease in the absolute value of suction stresses, but the issue of time was not clearly indicated.

On the other hand, a large amount of work on seepage-deformation response of earth dams and levee embankments has been performed through numerical simulations, especially with the renewed interest in the subject after Hurricane Katerina in 2003. Kohgo et al. (2006) conducted a centrifuge test modeling on an embankment dam and compared the experimental results with those obtained from numerical simulations. They reported a good agreement between the vertical deformation results in both models. They also recorded similar responses from the experimental model during the wetting stage, as compared to results from the numerical model (e.g. location of the cracks). Berilgen (2007) studied the drawdown effect on the stability of slopes using numerical models and concluded that the hydraulic conductivity has a significant effect on deformations occurring within the slope. Huang and Jia (2009) implemented the shear strength reduction technique (SSRFEM) to calculate a factor of safety in an embankment dam under rapid drawdown. Comparing the SSRFEM method with the traditional factors of safety obtained from limit equilibrium analysis, they illustrated that the method can be utilized to calculate the factor of safety for the slopes under transient unsaturated seepage. Fu and Jin (2009) developed a numerical model to simulate unsteady seepage flow through dams. They showed that by assuming saturation and hydraulic head as variables, their numerical formulation can capture the distribution of pore water pressure and the advancement of saturation front throughout the embankment with an acceptable accuracy assuming a seepage zone composed of both saturated and unsaturated sections. Callari and Abati (2009) illustrated the hyperelastic response of three-phase porous media using a finite element formulation and studied

reservoir bank response subjected to rapid drawdown. Based on their finite element model results, the deformation of the reservoir slopes increased during drawdown and continued over time with descending water level rate.

3.3 Performance based design

The concept of performance limit states refers to damage levels in a structure that are corresponding to specific definitions in the design code (Wellington and Vlachaki, 2004). This subject is well established in the earthquake engineering and it has been incorporated into seismic design codes mainly for bridge foundation (AASHTO 2004). Generally, in the realm of geotechnical engineering, the serviceability limit states are still emerging for the different geostrctures and are yet to be fully incorporated into the state-of practice and design codes. With advancement of the instrumentation and monitoring field, the application of performance based design approach is however gaining acceptance but successful implementation requires the establishment of performance matrics (limit states).

Meyerhof (1982) described the ultimate limit states (ULS) as “mainly instability against sliding, bearing capacity, overturning, uplift, seepage and erosion” and the serviceability limit state (SLS) as “mainly total and differential movements, cracking and vibration”. Meyerhof defined tentative rotation limits in terms of “safe” and “danger” limits for structures such as retaining walls and bridge abutments. There are several published papers in the realm of serviceability and ultimate limit states in geotechnical engineering. Examples include the chapter in the “Reliability-based Design in Geotechnical Engineering”

book devoted to the serviceability limit state reliability-based design by Phoon and Kulhawy (2008). The authors presented a probabilistic hyperbolic model for reliability-based design with an application in foundation engineering. In the method, they fitted a hyperbolic function to the load-displacement curve, thus, the new random vector representing the uncertainty in the entire load-displacement curve included only the two parameters required to define the hyperbolic function. Other examples include work by Zhang and Ng (2005) and Bauer and Pula (2000) who also studied the serviceability limit state of foundations using probabilistic methods.

3.4 Limit States and Probabilistic Analysis

Khalilzad and Gabr (2013, 2011b) presented deformation-based limit states for embankment dams and incorporated these into simple probabilistic analysis using the approach by Duncan (2000). The performance limit states are defined in terms of horizontal deformation at the toe as a key location indicating basal stability of the embankment. At this location, the stress path follows the form of an axial extension loading. The horizontal deformations are then correlated to levels of shear strain on the potential failure surface. A qualitative definition of the performance limit states (LS) was expressed by the authors as: LSI: minor deformations, no discernible shear zones, low gradients (i.e. i<1) throughout the embankment dam and foundation ; ii) LSII: medium (repairable) deformations, limited piping problems (i.e. i>1 within a shallow depth at the location of toe), dispersed plastic zones with moderate strain values, tolerable gradients less than critical; iii) LSIII: major

deformations, breaches and critical gradients at key locations (i.e. boiling and fine material washing at the location of toe), high strain plastic zones and emerging shear bands (LS III). Although, it is challenging to quantify a set of limit states, representative of both flow and deformation response of an earth embankment, the authors in this paper endeavor to use coupled flow and deformation finite element model for the understanding these limit states, and their variation of various embankment parameters.

3.5 Numerical Model

An embankment dam is modeled using the finite element program Plaxis (Plaxis, 2010) and limit equilibrium program Slope/W (Slope/W, Ver. 5). The modeled dam geometry is obtained from the US Army Corps of Engineers technical manuals (USACE, 2006) and it represents an earth dam section with geological profile representative of the lower Mississippi valley where a three layers soil system includes a shale layer at the bottom that is overlain by a layer of alluvial soil with a relatively high hydraulic conductivity. Above the alluvial layer, a low permeability soil forms the top foundation layer and the body of the embankment dam. The side slopes are 4H:1V on both upstream and downstream sides of the embankment dam. The landside ground surface slopes at 50:1 and the river side slopes at 30:1.

In work presented herein, a model with a size factor of 0.5 (i.e. scaling down the original geometry by 50%) has been used as the base case with the soil properties adjusted such that the dam is in a marginal stability condition. To obtain the soil properties

corresponding to this condition, the dam is modeled in Slope/W (a limit equilibrium program) and the material strength is reduced until a factor of safety of 1.05 is reached. This factor of safety value is selected to represent the near-failure condition while avoiding numerical convergence issues. The geometry and meshing of the model are shown in Figure 3.1. The finite element mesh consists of approximately 47,000 nodes and 5800 elements. The 15-node triangular plane strain elements (Plaxis, 2010) are utilized to capture a better resolution of stress distribution and deformation magnitudes.

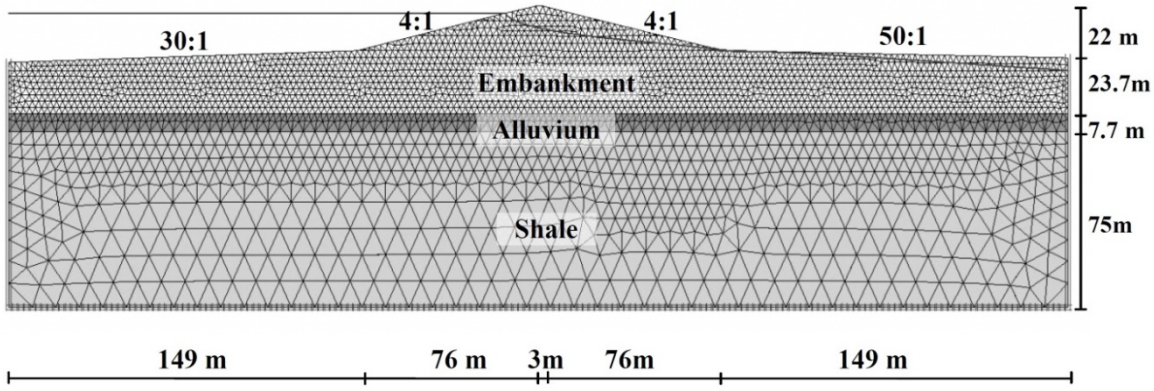

Figure 3.1 Model geometry and discretization

The soil properties of the embankment and foundation layers are presented in Table 3.1. As mentioned earlier, the soil strength parameters originally reported in USACE (2006) have been reduced by a factor of 1.55 in order to reach a safety factor of 1.05 in the model. This is consistent with the soil strength reduction method (SSRFEM) which is an approach to

find the factor of safety using the finite element analysis (Huang and Jia, 2009). The hydraulic conductivities were selected from the reported k values for the soil types (Morrice et al., 1997; Hart et al., 2006) and the stiffness parameters were selected using typical values presented by USACE (1990). It is assumed that the soils are homogeneous within each layer, thus, no spatial variability is taken into account except for the friction angle; this is assumed to be the only random parameter in the probability analyses.

Table 3.1 Soil properties

Soil Parameters	Embankment	Alluvium	Shale
γ (kN/m^3)	19.7	16.5	20.1
C (kPa)	0	0	0
Φ, Mean (°)	17.5	11.6	13.4
Φ, SD (°)	1.65	2.54	3.59
E_{50} (kPa)	6670	5000	33.3E3
E_{ode} (kPa)	5330	4000	26.7E3
E_{ur} (kPa)	20.0E3	15.0E3	100.0E3
k (m/day)	0.43	0.43	0.86E-9
θ_{res}*	0.074	N/A	N/A
α (1/m)*	1.6	N/A	N/A
n*	1.37	N/A	N/A

*** Van-Gunechten parameters**

The constitutive model of the analysis domain is defined by the Hardening Soil (HS) model, as incorporated in Plaxis (Schanz et. al, 1999). The HS model simulates both soft and stiff soils (Schanz and Vermeer, 1998). In comparison to the Mohr-Coulomb model, the yield

surface of the HS model is not fixed in the principal stress space and can expand due to plastic strain. The stiffness of the soil decreases under deviatoric stress, resulting in irrecoverable plastic strain. In a drained triaxial test, hardening soil model can be approximated with a hyperbola similar to the hyperbolic model by Kondner (1963) and Duncan and Chang (1970), but different in that it utilizes the theory of plasticity instead of the theory of elasticity, includes soil dilation effects, and provides for a yield cap (Plaxis, 2010). The two yield curves in triaxial condition are expressed by (Schanz et al., 1999):

$$f_{12} = \frac{q_a}{E_{50}} \frac{(\sigma_1 - \sigma_2)}{q_a - (\sigma_1 - \sigma_2)} - \frac{2(\sigma_1 - \sigma_2)}{E_{ur}} - \gamma^p \text{, and}$$

$$f_{13} = \frac{q_a}{E_{50}} \frac{(\sigma_1 - \sigma_3)}{q_a - (\sigma_1 - \sigma_3)} - \frac{2(\sigma_1 - \sigma_3)}{E_{ur}} - \gamma^p$$

where q_a is related to the ultimate deviatoric stress (q_f) with a parameter R_f described as:

$$q_f = \frac{6\,\mathrm{Sin}\,\varphi_p}{3 - \mathrm{Sin}\,\varphi_p}(p + c\,\mathrm{Cot}\,\varphi_p) \qquad \text{and} \quad q_a = \frac{q_f}{R_f}$$

The plastic shear strain (γ^p), which is the hardening parameter, is defined with the following equation assuming that the plastic volumetric strain (ε_v^p) is small:

$$\gamma^p = \varepsilon_1^p - \varepsilon_2^p - \varepsilon_3^p = 2\varepsilon_1^p - \varepsilon_\upsilon^p \approx 2\varepsilon_1^p$$

E_{50} is the stiffness modulus for primary loading given by:

$$E_{50} = E_{50}^{ref}\left(\frac{\sigma_3' + c\,Cot\,\varphi_p}{\sigma^{ref} + c\,Cot\,\varphi_p}\right)^m$$

where E_{50}^{ref} is the reference stiffness modulus at a reference stress (σ^{ref}).

For unloading-reloading, another stress-dependent stiffness modulus is used:

$$E_{ur} = E_{ur}^{ref}\left(\frac{\sigma_3' + c\,Cot\,\varphi_p}{\sigma^{ref} + c\,Cot\,\varphi_p}\right)^m$$

where E_{ur}^{ref} is the reference stiffness modulus at a reference stress (σ^{ref}).

Flow rule in the HS model is defined as:

$$\dot{\varepsilon}_\upsilon^p = \sin\psi_m\ \dot{\gamma}^p$$

where ψ_m is the mobilized dilatancy angle.

Unsaturated hydraulic properties are used for the embankment layer as all or some parts of the layer are above the phreatic surface at the different stages of modeling simulating rising reservoir level. The other two layers are saturated during the simulation time. The appropriate soil water characteristic curve (SWCC) is assigned to the top layer based on the saturated k value. The Van-Gunechten parameters pertinent to the SWCC are also presented in Table 3.1. No hysteresis effect has been considered for the SWCC in the analyses.

3.5.1 Loading and Boundary Conditions

Horizontal deformations are restricted on both sides of the foundation soil profile and both horizontal and vertical deformations are restricted at the lower boundary of the model. The flow boundary conditions include no-flow boundary at the bottom of the model and free-seepage boundary at the downstream face of the embankment. On the right side of the foundation layers, a constant head boundary equal to the total hydraulic head is applied.

A steady state seepage condition, representing a “sunny day” water elevation is first established through a model run, followed by a rise in water elevation with time to represent a flooding scenario. For the steady state step, the upstream side of the embankment and the left side boundary are modeled as constant head boundaries, while for the transient steps they are modeled as time-dependent head boundaries.

3.5.2 Modeling Steps

The dam is modeled using a staged construction. Geostatic stress state is generated in the foundation layers and the embankment is placed in three layers with water level assumed to be at elevation 101m (EL. 101m, see Figure 3.1) which is 8 m below the toe of dam. Next,

the water level is raised in several steps, allowing the steady state condition to occur, until it reaches around the mid-height of the dam (EL. 119.2 m). To model a storm situation, the water level is raised with an assumed rate of 0.08 m per hour until reaching to a maximum elevation of 125.3 m. This relatively high rate of rise was observed, for example, recently at Bourbeuse river levee (NOAA, 2011). The water level remains at this level for several days, and its effect on the flow and deformation responses of the embankment is investigated in view of the pre-defined limit states.

3.6 Parametric Study

3.6.1 Dam Size

While geometry does not impact the limit states predefined in the deviatoric strain versus mean effective stress ($\gamma_s - p'$) space, the objective of the analyses herein is to define the deformation and strain levels corresponding to the LS criteria. The embankment dam is modeled in 4 sizes with the size factors of 1, 0.5, 0.2 and 0.1, and the model with the size factor of 0.5 is taken as the base case. The results are examined in relation to the magnitude of deformation and strain, corresponding to target limit states, as well as time to failure as a function of the size/geometry of the dam embankment. .

3.6.2 Effect of side slopes

Similarly, the effect of the downstream and upstream slopes magnitudes on the strain and deformation levels is investigated using the geometry of the base case. Three side slopes (1:4, 1:3and 1:2.5) are modeled and the effects on the target parameters are studied. To be

able to study the side slope influence, and to cover a reasonable range of slopes, the strength parameters of the embankment layer is increased to 25° in these analyses.

3.6.3 Rate of rising pool level

Three different rates of rising water level in the reservoir are employed to simulate storms with different intensities. The sunny-day water level is assumed to be primarily at the mid-height of the reservoir and it starts rising with three different rates (0.04, 0.08 and 0.16 meter per hour) until reaching the maximum pool elevation (El. 125.3 m). The water is sustained at the maximum pool level for a period of time and the impact on probabilities of exceeding limit states is investigated at various time periods.

3.6.4 Cycles of rising and falling pool level

One of the merits of the deformation-based limit state analysis is the ability to capture a loading history applied to an embankment dam. It seems that one of the reasons for failure in an embankment dams is the accumulation of plastic shear strains with time and decreasing the soil strength in the plastic zone. The effect of cycles of rising and falling water level is studied in this section. A scenario is introduced to the model in which the water rises to the maximum pool level and remains at that level for 7 days. Then, a drawdown occurs and water remains for a long period of time at the mid-height level and this cycle is repeated until the failure condition is reached. A “plastic drained” phase is added between the first and second cycles meaning that in the first cycle, the water rises, drawdown occurs and then a “plastic drained” phase is used to simulate the time lag between two storms. Afterwards, the second cycle starts.

3.7 Results and Discussion

Figure 3.2a shows the failure surface obtained from limit equilibrium analysis using Slope/w program. This model is employed as a validation of the failure zone developed in the finite element model which corresponds to high magnitudes of shear strains (Figure 3.2b). Figure 3.3 shows the state of shear strain in a section under the toe at three different stages. Stage 1 corresponds to the modeling phase when the water rises in the pool and reaches the elevation 122.3 ft. Stage 2 is when water reaches the maximum pool level, and stage 3 is at the end modeling step where the water is sustained at the maximum pool elevation. It is evident that the high shear strains zone propagates from the toe into the foundation soil. In addition, data in Figure 3.4 show the strain levels at the different stages in relation to LS I, II and III at different depths. The shear strain corresponding to LS III decreases with a nonlinear trend as the mean effective stress decreases. This indicates that at a relatively small deviatoric stress, a point at a shallow depth is at LS III mainly since the basal toe area is subjected to an axial extension stress-path. This could be one of the reasons why failure zone starts at the toe and propagates to the deeper sections of the downstream slope. Moreover, seepage forces due to high gradients at the toe exacerbate the developing high shear strains at the toe area.

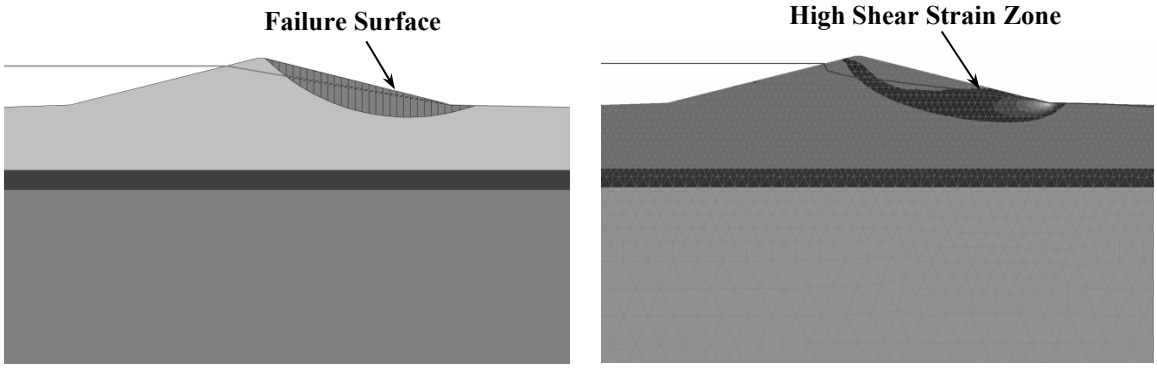

Figure 3.2 a) Failure surface in Slope/W (left) and b) shear zone in Plaxis (right)

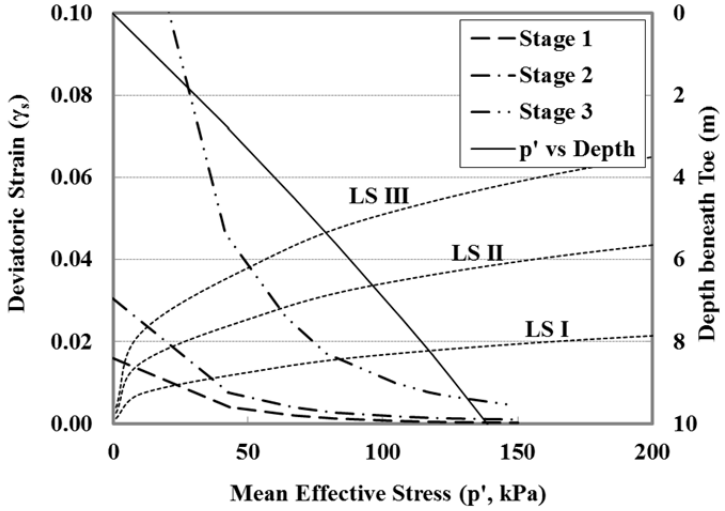

Figure 3.3 State of shear strain in a vertical section under toe of dam at three stages

Figure 3.4a shows the shear strain for Element A located on the failure surface under the toe. As the water rises in the reservoir, the data show the emergence of shear strains at the toe area in relation to LS I, II and III versus time. The magnitude of horizontal deformation corresponding to the emergent shear strains is shown Figure 3.4b. The levels of horizontal deformation of the toe at the three limit states are captured from these graphs and incorporated into probabilistic analysis as presented in Table 3.2. In the probabilistic analysis, it is assumed that the soil friction angle is the only random variable to simplify the analysis.

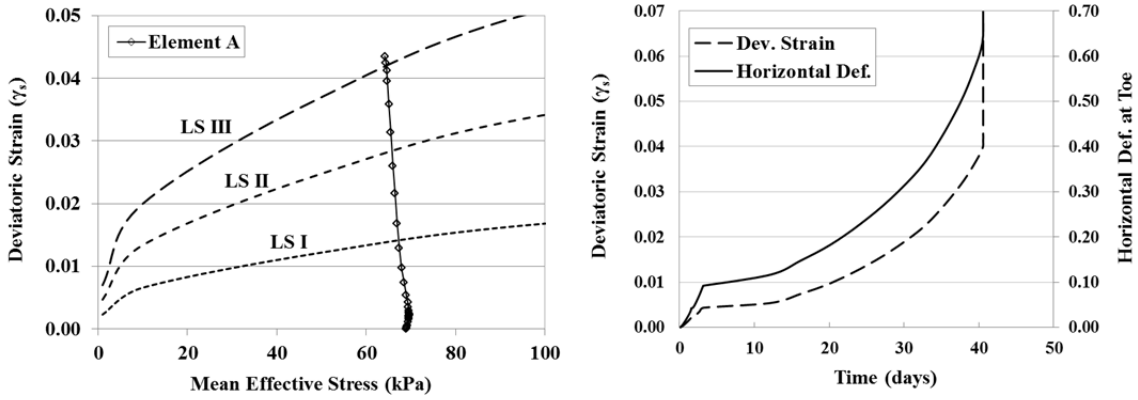

Figure 3.4 a) State of shear strain during simulation time for element A (left), and b) Strain and horizontal deformation at toe versus time (right)

Table 3.2. Calculating the probability of exceeding limit states (after 10 days)

Soil Type	Friction Angle μ (°)	σ (°)	μ+/-σ (°)	S (m)	LS I (S_1 = 0.23 m) N=S_1/S	ΔN	LS II (S_2 = 0.46 m) N=S_2/S	ΔN	LS III (S_3 = 0.76 m) N=S_3/S	ΔN
Embankment	17.5	1.65	19.15	0.07	3.286	-2.434	6.571	-4.868	10.857	-8.042
			15.85	0.27	0.852		1.704		2.815	
Alluvium	11.6	2.54	14.14	0.135	1.704	-0.426	3.407	-0.852	5.630	-1.407
			9.06	0.18	1.278		2.556		4.222	
Shale	13.4	3.59	16.99	0.14	1.643	-0.249	3.286	-0.498	5.429	-0.823
			9.81	0.165	1.394		2.788		4.606	

	LS I	LS II	LS III
SD	1.242	2.483	4.103
Mean	2.091	4.182	6.909
COV	0.594	0.594	0.594
β	1.067	2.328	3.242
R=Ψ(β)	0.857	0.990	0.999
P(E.L.)	0.143	0.010	0.001

Notations:

μ=Expected value of friction angle
σ=Standard deviation of friction angle S=Horizontal deformation of toe
N=Normalized deformation
COV=Coefficient of variation
β=Reliability index
R=Reliability

P(E.L.)=Probability of exceeding a limit state

3.7.1 Effect of dam size

The size of a dam is a geometric parameter that impacts the magnitude of deformation and strain levels corresponding to the various limit states. Table 3.3 shows the variation of these values at the corresponding limit states versus the dam size. It should be noted that although, limit states criteria are pre-defined in the shear strain-mean effective stress space, the corresponding magnitude in terms of shear strains, depend on the stress state of the target point selected to be under the toe. It is interesting to note that the larger the dam is the deeper the plastic zone propagates. Therefore, the magnitudes of deviatoric strain at which a given LS occurs is higher as the size increases (Figure 3.5). Accordingly, the horizontal

deformations at the toe are also higher for a larger dam. In this case, the strain nearly doubles and the deformation increases by a factor of 25 when the dam size is increased by a factor of 10 (from 0.1 to 1). On the other hand, it takes a longer time for the phreatic surface in the larger dam to rise and lead to a critical level of strain. Therefore, the time to exceed a given limit state increases as the size of a dam increases. Figure 3.6a shows the horizontal deformation of toe versus time for the four analyzed models. The time to exceed LS III versus the dam size is shown in Figure 3.6b. It appears these two parameters are related in a linear fashion.

Table 3.3 Effect of dam size on LS

Size Factor	Horizontal Deformation (m)			Deviatoric Strain		
	LS I	**LS II**	**LS III**	**LS I**	**LS II**	**LS III**
0.1	0.029	0.047	0.068	0.008	0.015	0.022
0.2	0.06	0.12	0.18	0.009	0.018	0.028
0.5	0.23	0.46	0.76	0.014	0.028	0.042
1.0	0.74	1.17	1.7	0.018	0.035	0.052

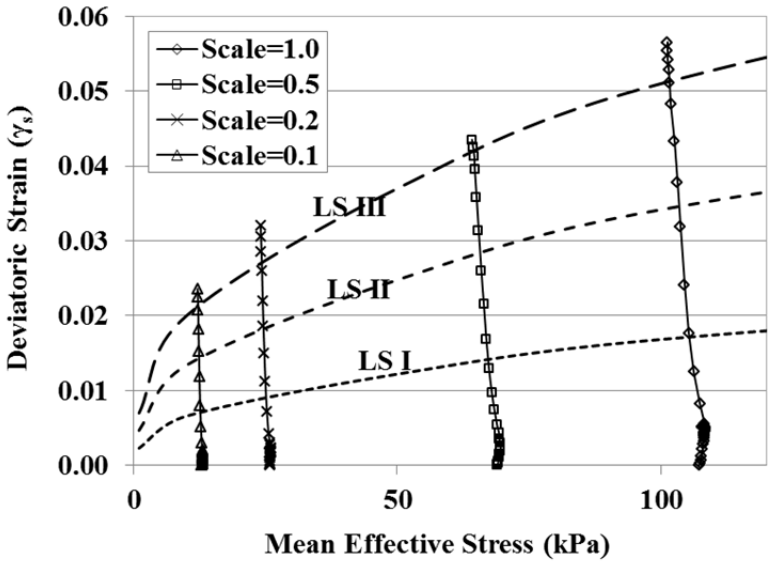

Figure 3.5 Shear stress state on failure surface for various dam size

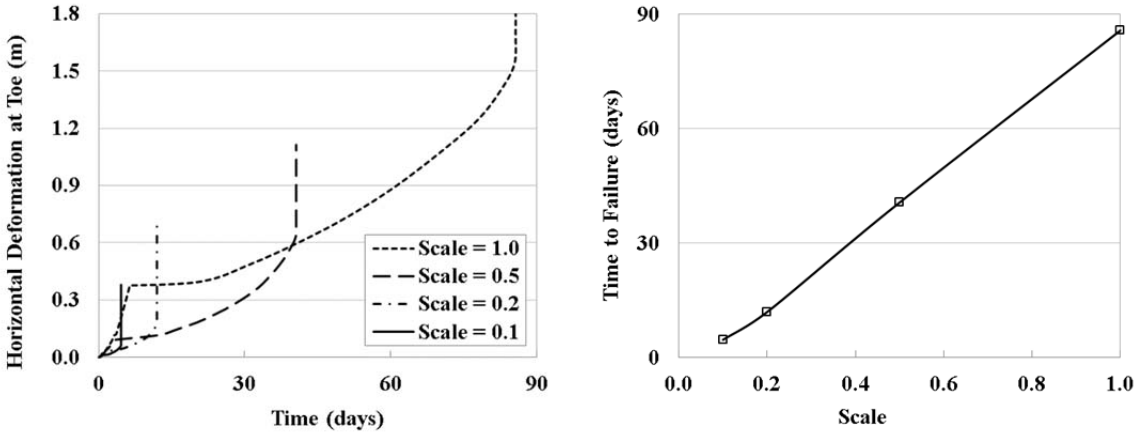

Figure 3.6 a) Horizontal deformation versus time, b) time to failure versus dam size

Figure 3.7 shows the phreatic lines in two dams with the size factor of 0.1 (on the left) and 1 (on the right) after two days of water remaining at the maximum elevation. It is evident that the saturated front is higher in the smaller dam, which leads to higher shear strain values at the toe area, and therefore the smaller size dam exceeding the predefined LS as will be shown later.

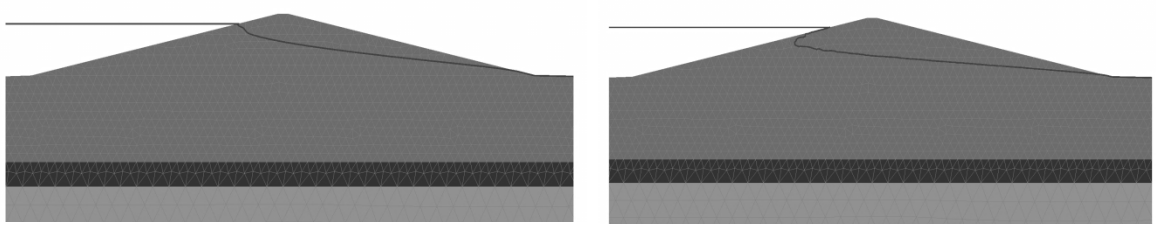

Figure 3.7 Phreatic surface after two days of water remaining at maximum elevation for a) size factor = 0.1, and b) size factor = 1

3.7.2 Effect of side slopes

Figure 3.8 shows the state of strains at the toe area relative to the LS I, II and III. The reason why the start points are different on the x-axis is because the mean effective stress at a specific depth increases due to a higher overburden stress in the vicinity, as the slope become steeper. At the beginning of each loading phase, a jump occurs in the strain due to an increase in the lateral loading. At the end of simulation time, the embankment model with side slopes of 1:2.5 is exceeding LS III, the embankment model with side slopes of 1:3 is

exceeding LS I but still below LS II, and the embankment model with side slopes 1:4 is below LS I. Figures 3.9 presents the deviatoric strains and horizontal deformation of the toe versus time. As the side slopes become steeper, deviatoric strains and horizontal deformations at the toe increase as well. This can be attributed to two factors. First, the distance between upstream and downstream side of slopes is lower for an embankment dam with steeper slopes. Thus, the saturation front rises more quickly and the impact of flow and pore pressure are higher. Second, the direction of major principal stress is steeper in a steep slope which leads to higher driving forces within the downstream slope and foundation. A comparison of mobilized shear stress for two side slopes (1:2.5 and 1:4) is presented in Figure 3.10. The figure shows 30 to 40 percent higher shear stress with depth for an embankment dam with side slopes of 1:2.5 compared to a dam with side slopes of 1:4.

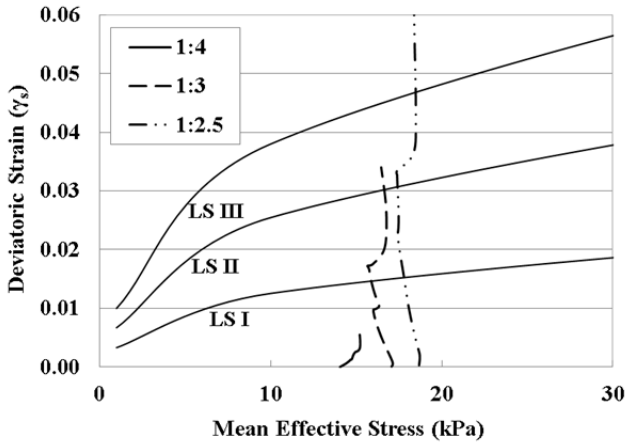

Figure 3.8 State of strains at toe relative to limit states

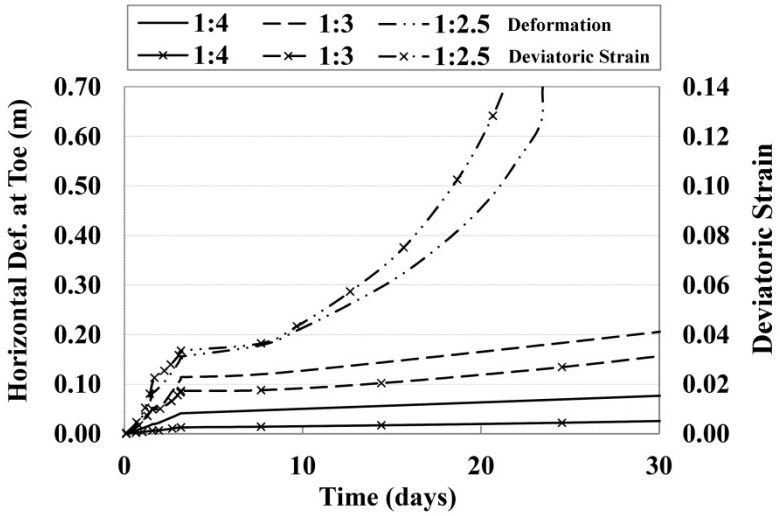

Figure 3.9 Effect of side slopes on shear strain and horizontal deformation of Toe

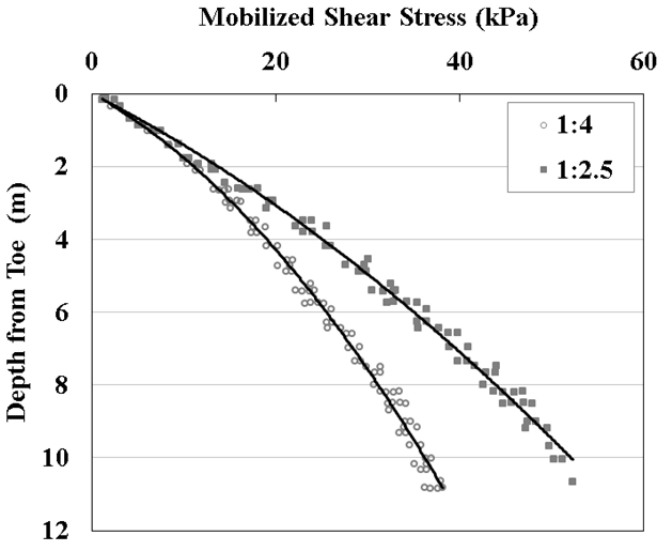

Figure 3.10 Mobilized shear stress under the toe for two side slopes

3.7.3 Effect of rate of rising water in the reservoir

Figure 3.11 shows the probabilities of exceeding LS I, II and III for three rising rates with three rising rates of water levels (assumed to represent storm intensities.) In all cases, the exceedance probabilities increase over time as water rises and remains at the maximum pool level. For example, for a rising rate of 0.16 m/hr, the probabilities of exceeding LS I, II and III increase by approximately 23%, 25% and 18%, respectively, in 20 days. This is mainly due to the advancement of saturation front over time within the dam that leads to a reduction of soil strength as a result of losing metric suction and increasing pore pressures. Correspondingly, the shear strains and deformations increase as well.

At a lower rate of rise (comparing 0.04 m/hr and 0.08 m/hr cases), there is a small difference in the probabilities of exceeding LS I, II and III (at most about 3%). In comparison, at higher rates of rise (compare 0.08 m/hr and 0.16 m/hr), the impact of rising rate is more pronounced on the probability of exceeding LS I; a rising rate of 0.16 m/hr results in about 22% higher exceedance probability after 10 days compared to a rising rate of 0.08 m/hr. The reason can be attributed to the magnitudes of shear strains and deformation developed during the rise of water at different rates due to loading and saturation front conditions at various time. As shown in Figure 3.12, the horizontal deformation of toe is higher for a rising rate of 0.16 m/hr but is approximately the same for the other two rates.

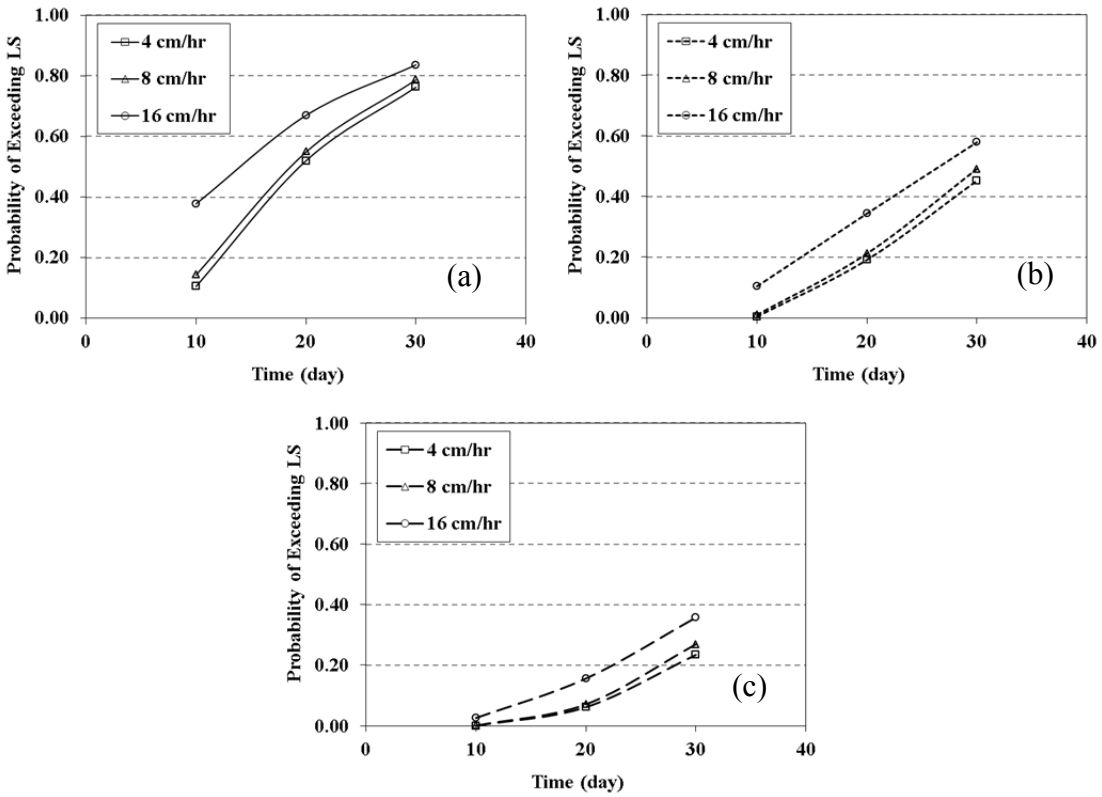

Figure 3.11 Probabilities of exceeding a) LS I, b) LS II, and c) LS III versus time for various rising rate

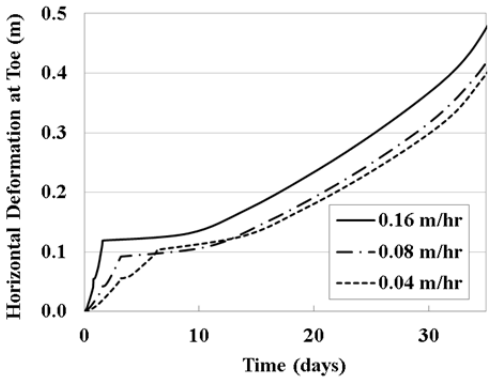

Figure 3.12 horizontal deformation levels at toe for three rising rates

3.7.4 Effect of cycles of rising and falling pool level

Cycles of rising and falling water level in the reservoirs lead to accumulation of plastic shear strain within the shear zone. Figure 3.13 demonstrates the progressive nature of zones with high shear strain magnitude. As observed in Figure 3.13a, when the water rises to the maximum elevation for the first time, a shear zone develops at the toe. At this time, the horizontal deformation at the toe is 0.11 m. In the next cycle (Figure 3.13b), the shear zone grows in size and the magnitude of shear strains also increase. At the end of this cycle, the horizontal deformation at the toe is 0.2 m. Ultimately, the shear zone becomes large enough during the third cycle and failure occurs. When the shear strain exceeds LS III over a potential failure surface, the entire zone start moving along the boundaries of the plastic zone and failure occurs. Figure 3.14 shows the state of strains at the toe relative to the limit states in each cycle. This analysis serves to illustrate the importance of accounting for the history of storms and loading cycles with time. Similar observation was originally made by Stark and Duncan (1991) in relation to the forensic analyses of the failure occurred at the St. Luis dam in California.

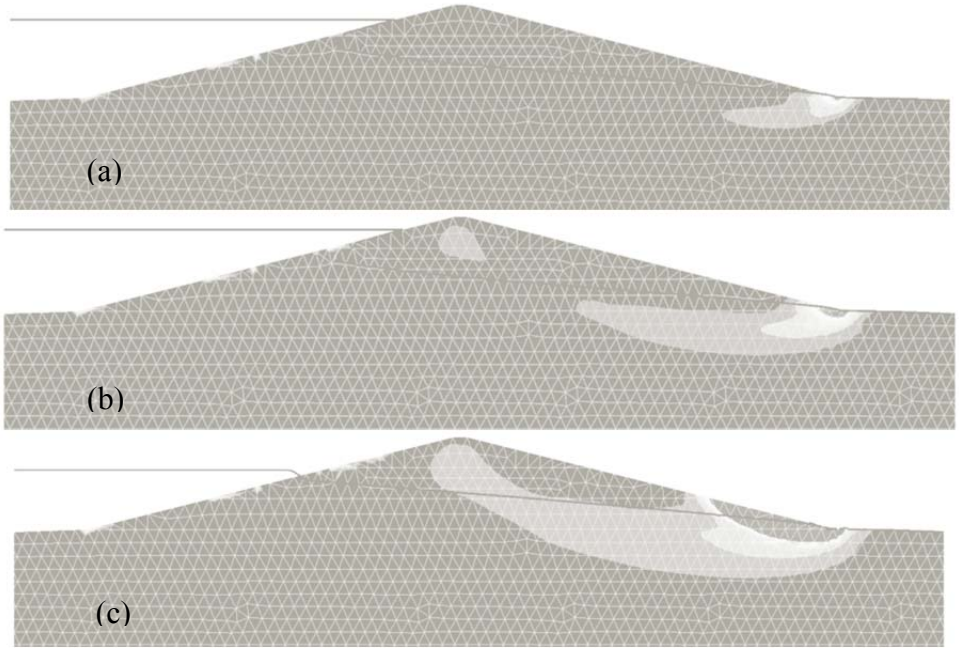

Figure 3.13 Developing high shear strain zones with cycles of rising and falling water

Figure 3.15 presents the above scenario in terms of probabilities of exceeding limit states. During the cycles of water rising and falling in the reservoir, the probabilities of exceeding all three limit states increase. For example, in case of LS III, the exceedance probability increases from 40% in the first cycle to 63% in the second cycle and 100% in the third cycle.

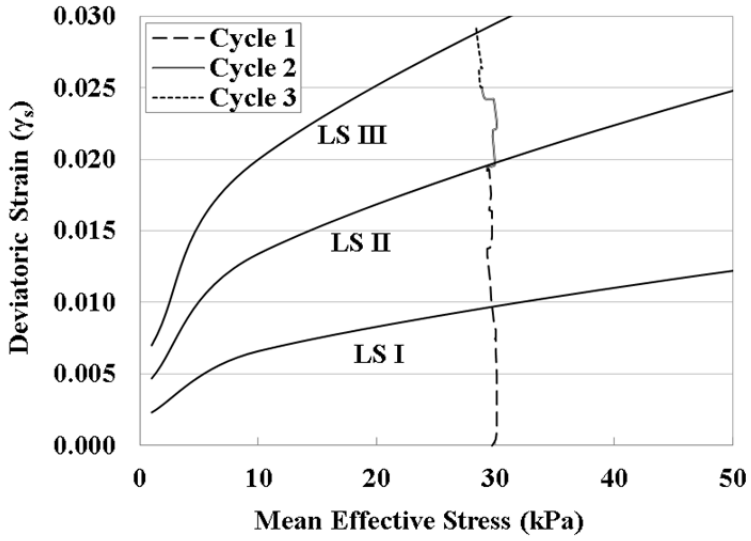

Figure 3.14 State of strains at toe in three cycles

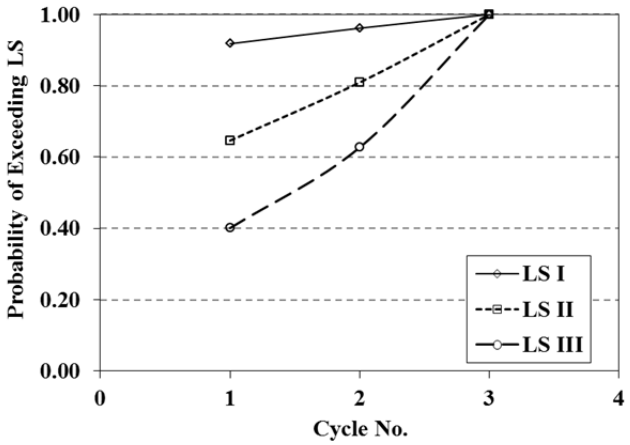

Figure 3.15 Probability of exceeding LS I, II and III vs cycles of rising and falling water

An estimation of the time to failure can be obtained from the inverse rate versus time graph as shown in Figure 3.16. A similar graph for estimating the time to failure due to creep in slopes was presented by Tavenas and Leroueil (1981). By extending the last portion of the curve and intersecting with the time axis at the very small values of inverse rate (Y axis), one can estimate the time to failure for this slope under current loading condition.

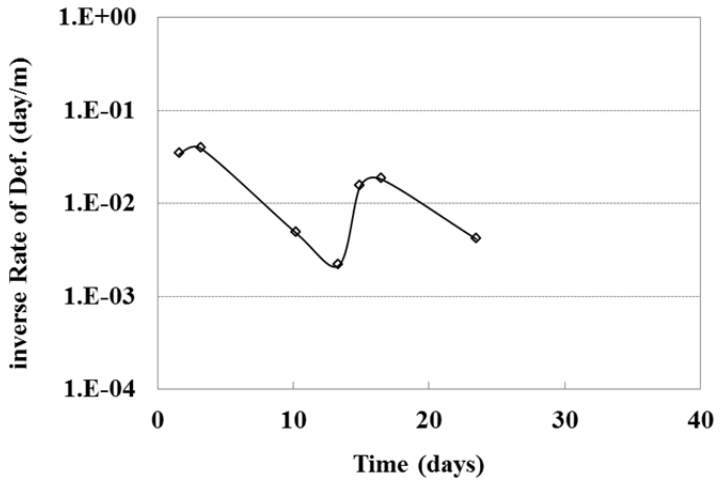

Figure 3.16 Estimation of time to failure from observed rate of deformation

3.8 Summary and Conclusions

The effect of geometry and loading conditions on the probability of exceeding prescribed performance limit states for flood protection earth embankments was performed in this paper. Based on the results of this study, the following conclusions are advanced:

The size of an embankment model has a direct impact on the limit state values. In a larger embankment model, the shear zone propagates deeper for failure to occur. Therefore, the shear strains at LS I, II and III and the corresponding deformations at the toe are higher as well. (Failure is defined in the model when shear strains increase instantaneously and displacements occur in the failed zone without any increase in time)

The time to exceed LS I, II and III increases as the size of an embankment model become larger. For example, failure occurs after 4.6 days in the model with a size factor of 0.1 compared to 12 days for a model with a size factor of 0.2. This is mainly because the saturation front reaches the critical level in less time in a small dam, considering that the hydraulic conductivities are the same.

In a dam with steeper side slopes the mobilized shear stresses are higher within the downstream slope and foundation. In the study model, the impact was between 30 to 40 percent higher shear stresses in a dam with side slopes of 1:2.5 compared to side slopes of 1:4. This results in higher magnitudes of shear strains horizontal deformation at the toe area. For example, after two weeks of water rising in the reservoir and sustained at the maximum

pool level, the magnitudes of horizontal deformations at toe are 0.16m, 0.08m, 0.055m and 0.048m for embankment models with side slopes of 1:2.5, 1:3, 1:3.5, and 1:4, respectively.

The results showed that it is important to consider the time history of loading in an embankment model, because failure can occur due to the accumulation of plastic shear strains under cycles of loading and unloading corresponding to the rising and falling of water in the reservoir. Such an accumulation of plastic strains leads to permanent deformations at the toe area and as a result, the probabilities of exceeding LS I, II and III increase with the cycles of rise and fall. For instance, for the studied model, probabilities of exceeding LS III are 40%, 63% and 100% in three cycles.

CHAPTER 4

4. EFFECT OF WOODY VEGETATION ON SEEPAGE-INDUCED DEFORMATION AND RELATED LIMIT STATE ANALYSIS OF LEVEES

4.1 Introduction

Levees often provide flood protection during flooding events and in many cases they are subjected to sustained high water elevations during severe storms. Natural plants and vegetation often grow on levees, and their roots can pose problems in the hydraulic seepage domain, which in turn may affect a levee's structural and hydraulic stability.

Since the occurrence of hurricanes Katrina and Rita, the condition assessment of levees has been the focus of many studies (Christian 2008, Sills et al. 2008, Bea and Cobos-Roa 2009). As a part of these investigations, attention has focused on the effects of localized deficiencies on the instability of levees, including deficiencies caused by woody vegetation. Several failures have been found to be facilitated by pre-existing defects in the levee foundation or embankment, with the impact of these defects exacerbated by the increase in water elevation due to flooding. Examples of localized deficiencies include tree roots and woody vegetation (whether dead or vital) that compromise stability by changing the hydraulic flow regime. Similarly, the impact of woody vegetation becomes important when considering the impact of pore water pressure and flow pattern on the stability of slopes (Gray et al., 1991). Whether the presence of roots has a positive or negative effect on the integrity of levees is itself a controversial issue in the literature. A study on the effect of tree

roots on levee stability was reported by Corcoran (2011). Significant testing and modeling was performed to assess the effect of roots on levees' soil structure using both seismic and conventional testing approaches as well as Lidar for mapping root shapes. In general, the study concluded that the presence of roots can contribute to either the stability or instability of a slope through mechanical and hydraulic mechanisms. Similar conclusion was presented by Greenway (1987). The beneficial hydrological effects of roots, mentioned in Greenway (1987), include: i) foliage interception of rainfall, causing absorptive and evaporative losses that reduce the amount of infiltration, and ii) moisture extraction from the soil that is lost to the atmosphere via transpiration, leading to lower positive pore pressure. These two effects, however, can be negligible during and immediately after a storm event when excessive amounts of rainfall and runoff storm water suddenly appear in the environment. On the other hand, instability due to woody vegetation can arise from the possible formation of piping channels along the decaying roots and the associated variation in hydraulic conductivity values. Although there are attempts in the literature to estimate the distribution of hydraulic conductivity in the field using statistical and optimization approaches (e.g. Das et al, 2012), few considered the effect of roots on such a distribution. A recent study by Corcoran et al (2011) stated that "statistical comparison of means did not produce conclusive evidence that tree roots influence the average hydraulic conductivity of a soil layer."

The definition of *deformation-based limit states* and the development of the interdependency of emerging failure modes are also lacking in the current literature. An improved framework to incorporate the levels of levee functionality is important for the

support of the Federal Emergency Management Agency (FEMA) National Flood Insurance Program. At present, if a levee is not accredited, even though it provides a level of protection, it is considered not to exist when FEMA digital flood insurance rate maps are developed. Such a binary approach may be simple to implement but has significant implications for many communities across the nation. The concept of limit states provides a graded scale that can enable a better assessment of the vulnerability of earth structures, and corresponding failure modes.

Work in this paper is focused on investigating the effects of changes in hydraulic conductivity due to the presence of woody vegetation in terms of exceeding performance limit states that describe the functionality of the levee. A review of the variation in hydraulic conductivity with the presence of roots is presented, and the impact of such variation on the probability of exceeding a given limit state over time is investigated. A levee in the Sacramento, California district is modeled using the finite element approach, and coupled seepage-deformation analyses are performed using hydraulic properties that represent the initial unsaturated and saturated regions of the embankment and foundation layers. A framework is provided for establishing performance limit states based on the critical state stress-strain levels for the embankment soil. Results are discussed in view of the limit states and associated strain and deformation levels, the probability of exceedance due to changes in the hydraulic characteristics of the profile, and the duration of high water levels.

4.2 Background

Greenway (1987) summarized the beneficial and adverse effects of vegetation on slope stability. Among the adverse impacts, two are related to the increase in seepage due to i) the increase in soil permeability, and ii) the creation of desiccation cracks due to the depletion of moisture in the soil. FEMA (2005) provided an overview of problems caused by woody vegetation in its "Technical Manual for Dam Owners" that described several factors that compromise safety, such as "decaying roots that create seepage paths and internal erosion", "uprooted trees that produce large voids and reduce freeboard" and "loosening compacted soil." A comprehensive literature review of publications pertinent to the presence of vegetation on levees was published in December 2010 by the United States Army Corps of Engineers Corcoran et al (2010). This report provided a review and summary of more than 200 documents on levees and woody vegetation and was followed by a report in 2011 that included extensive results from laboratory and field testing as well as modeling. The work by Corcoran et al (2011) investigated the effect of healthy woody vegetation on levee stability and concluded that the effect of roots on levees is a complex process that remains unquantifiable given the number of factors influencing the interaction. Ghestem et al. (2011) suggested that the presence of roots may lead to landslides by creating preferential flow paths around dead and decaying roots, and around decayed roots that are occupied by living roots, and that channels may form around such living roots.

In contrast, several studies that investigated the effects of roots on the stability of slopes reported a reinforcing effect of the vegetation. Nilaweera and Nutalaya (1999) studied seven tree species and estimated that these trees' roots contribute to increased stability by providing pull-out resistance and a tensile strength component to the system. Schwarz et al. (2010) employed the so-called *Wu model* and *fiber bundle model* (developed by Wu et al., 1979 and Pollen and Simon, 2005, respectively) to estimate the reinforcement effects of roots. Their overall conclusion, based on the stress-strain behavior of the roots, was that the reinforcement effect mobilized at a higher strain range than mobilizes due to suction or cementation effects. Other researchers also have reported on case studies that document the changes in hydraulic conductivity and the shear strength of soils with roots (Gabr et al. 1995, Zhou 1998, Bibalani et al. 2006, Abdi et al. 2010, and Buryloya et al. 2011). However, in the case of levees or embankment dams, the level of vulnerability associated with changes in hydraulic conductivity due to woody vegetation and associated seepage effects remains unclear. These effects are among the reasons for limiting vegetation growth on levees and earthen dams (USACE, 2009).

The issue of analyzing the effects of roots on hydraulic conductivity and associated seepage conditions lends itself to the use of a probabilistic approach. USACE technical letters, ETL 1110-2-547 (1997), ETL 1110-2-556 (1999), and ETL 1110-2-561(2006), provided summaries of several probabilistic approaches as well as applications to simple geotechnical problems. In these examples, probabilistic analysis was applied to a single failure mode (either seepage failure or slope instability) using the traditional concept of

factor of safety (FS). When attempting to correlate the probability of failure to a factor of safety, however, Griffiths and Fenton (2001) and Wang et al. (2011) found that, depending on where FS = 1 occurs, spatial variability can impact the estimated probability of failure (P_f). For example, if the location of FS = 1 is at the center or toward the upper tail of the probability distribution, a high variance of the FS leads to a low estimated probability of failure, which may not be a conservative estimate.

On the other hand, the application of the probabilistic approach is highly dependent on the availability of data that define the statistical distribution of the various analysis parameters. Both the collection and availability of such data in geotechnical engineering are often lacking. In response, Duncan (2000) suggests a simple method to estimate the probability of failure using the Taylor series and knowledge of the statistical parameters of a given property. Where limited data are available for the input parameters, a method termed the *three sigma rule* (Duncan 2000) is used to estimate the standard deviation of the random variables. The method is relatively simple to implement and, therefore, has the advantage of being easily applied by practitioners.

4.3 Effect of Roots on Hydraulic Conductivity

A series of field and laboratory hydraulic conductivity tests was conducted by Brizendine (1997) to characterize the impact of woody vegetation on hydraulic conductivity at four levee sites. The scope of the work included both laboratory and field testing. The site selection criteria for the study included the existence of woody vegetation and the availability

of piezometer data with historical records. The four levee sites studied are: i) Tallula, Issaquena County, Mississippi, ii) Sny Island, Pike County, Illinois, iii) Skagit Dike, Skagit County, Washington, and iv) Elkhorn Boat Launch, Sacramento County, California. The laboratory testing was conducted using flexible wall permeability tests on retrieved undisturbed samples, and the field data were obtained from a two-stage borehole hydraulic conductivity testing device (Brizendine, 1997). For each levee site, testing was conducted for a with roots section, located at the drip-line of a stand of trees on the landside of the levee, as well as for a without roots section located a significant distance away from the woody vegetation. Table 4.1 summarizes the results of the laboratory and field hydraulic conductivity tests.

Table 4.1 Laboratory and field hydraulic conductivity (units in m/s) [Brizendine, 1997]

	Tallula		Sny Island		Elkhorn		Skagit	
	W*	**W/O****	**W**	**W/O**	**W**	**W/O**	**W**	**W/O**
Laboratory Tests								
Test No.	n = 11	n = 3	n = 13	n = 10	n = 11	n = 14	n = 5	n = 8
Mean	1.96×10^{-9}	5.82×10^{-10}	2.23×10^{-8}	1.11×10^{-8}	6.88×10^{-7}	1.03×10^{-6}	3.02×10^{-6}	1.06×10^{-6}
SD	2.28×10^{-9}	2.50×10^{-10}	3.37×10^{-8}	1.72×10^{-8}	7.31×10^{-7}	5.87×10^{-7}	1.17×10^{-6}	5.16×10^{-7}
COV	116.33	42.96	151.12	154.95	106.25	56.99	38.74	48.68
Field Tests								
Test No.								
Mean	n = 5	n = 5	n = 6	n = 7	n = 5	n = 7	n = 5	n = 4
SD	5.28×10^{-8}	5.86×10^{-9}	2.78×10^{-7}	2.55×10^{-7}	6.12×10^{-6}	1.63×10^{-5}	2.51×10^{-6}	2.70×10^{-5}
COV	5.54×10^{-8}	3.18×10^{-9}	2.05×10^{-7}	1.36×10^{-7}	5.25×10^{-6}	3.87×10^{-5}	1.41×10^{-6}	2.14×10^{-5}
	104.9	54.2	74.00	53.35	85.33	237	56.2	79.4

*** With Roots** **SD: Standard Deviation**
****Without Roots** **COV: Coefficient of Variation**

Results from the laboratory testing indicate that the presence of woody vegetation in the soil either leads to a higher mean value of hydraulic conductivity, as seen in the Tallula, Sny Island and Skagit sites, or it causes the hydraulic conductivity to decrease, as seen in the Elkhorn site. From the field hydraulic conductivity results, the measured mean values and coefficients of variation for the *with roots* test locations are higher in Tallula and Sny Island than in the *without roots* locations. However, the opposite trend is observed at the Elkhorn and Skagit sites.

The results from the study thus do not yield a consistent trend from either the laboratory or field hydraulic conductivity tests, and unfortunately, no characterization of the status of vegetation/root types was performed to assist in the explanation of the results. The lack of a trend in the hydraulic conductivity also may be due to the complexity of taking the measurements, especially in capturing a representative test domain for both the field and laboratory set-ups. For example, during field testing, a small crack in the soil can have a pronounced effect on the results, and the k-value may vary from one location to another by an order of magnitude, even without considering the effects of the woody vegetation. A similar conclusion was presented by Corcoran et al (2011).

4.4 Study Model

The Elkhorn Levee is modeled and analyzed for deformational stability using the finite element program, Plaxis, and the limit equilibrium program, Slope/W. The hydraulic parameters and presence of roots in the soil are represented by the variation in the magnitude

of the hydraulic conductivity. The model accounts for *time to saturation* with the rise in water level through the use of soil water characteristic curves (SWCCs). The coupled seepage/deformation analysis yields information about the emerging shear zones and associated strain levels. The analysis results are presented within the critical state framework to define performance limit states for the levee.

The Elkhorn Levee is located within Reclamation District No. 1000 in Sacramento County, California. This area is protected from flooding by the easterly levee of the Sacramento River. Figure 4.1 presents the geometry, soil layers and finite element mesh of the Elkhorn Levee site. The soil profile consists of a four-layer system whereby the levee is constructed from silty sand (SM-ML) over a thin layer of sandy clay (CL) with low hydraulic conductivity. Under the CL layer is 2.1 m of SM-ML soil with properties similar to those of the top layer. Beneath this layer, the soil is mostly silty sand (Brizendine, 1997). Limit equilibrium slope stability analysis of the Elkhorn Levee was conducted using the Slope/W program (Slope/W, V5), and the results were used to validate the results from the numerical study.

4.4.1 Domain Discretization and Properties

The model is discretized using 15-node triangular plane strain elements. The finite element mesh consists of approximately 5,200 elements and 42,000 nodes. Figure 4.1 presents the geometry and discretized mesh. The embankment side slopes are 1V:2.5H on the upstream side of the levee, and 1V:2.3H and 1V:3.3H on the downstream side of the levee.

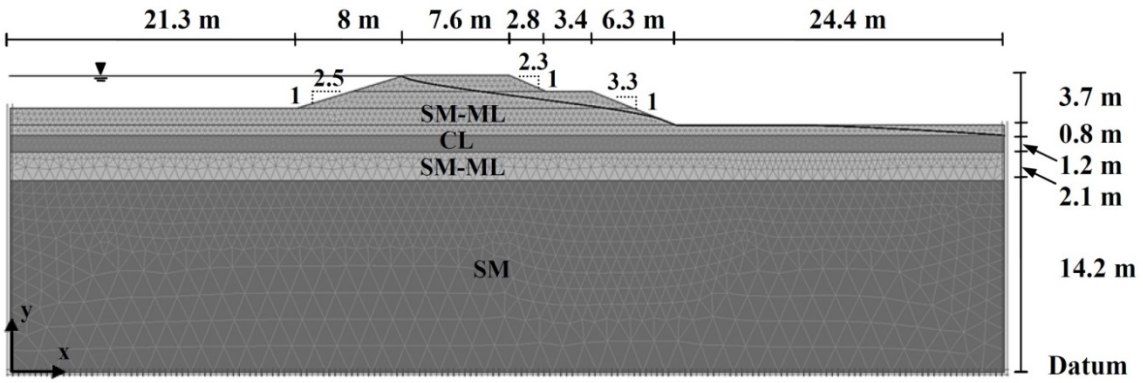

Figure 4.1 Elkhorn Levee: Geometry and discretized mesh

The properties of the SM-ML layer that constitutes the body of the levee, and the SM-ML layer beneath the CL layer, are similar. Table 4.2 shows the properties of the three soil types. Values for the soil unit weights were measured from retrieved undisturbed soil tubes. Field hydraulic conductivity and statistical parameters as presented in Table 4.1 were used in the analysis. The strength parameters were selected based on the correlation with the void ratios (after the U.S. Department of the Navy, 1986) and other reported values in the literature (Salgado et al. 2000, Tint et al. 2007). The measured liquid limits and specific gravity were used to estimate the compression index (Nagaraj and Murty, 1985), and the values for the modulus of elasticity were estimated from the correlation with the compression index (Plaxis, 2010).

Table 4.2 Soil properties

Soil Type	γ (kN/m^3)	k_m (m/s)	k_{SD} (m/s)	c (kPa)	Φ (°)	E_{50} (kPa)	E_{ode} (kPa)	E_{ur} (kPa)
SM-ML	18.0	7.6×10^{-7}	7.1×10^{-7}	3.8	32°	3.5×10^{3}	2.8×10^{3}	2.6×10^{4}
CL	18.4	1.9×10^{-7}	1.3×10^{-7}	3.8	30°	2.9×10^{3}	2.3×10^{3}	2.1×10^{4}
SM	17.9	1.7×10^{-6}	N/A	1	34°	-	-	5.0×10^{6}

Notation:

γ = Unit weight
E_{50} = Secant stiffness in drained triaxial test
E_{ode} = Tangent stiffness for oedometer loading
E_{ur} = Unloading / reloading stiffness
k_m = Mean k-value
k_{SD} = Standard deviation of k-value
c = Cohesion
Φ = Friction angle

In order to model a levee in a marginal failure condition, a reduction factor of 2.2 was applied to the soil strength parameters. This factor was obtained by using the soil strength reduction finite element method (SSRFEM), as described by Huang and Jia (2009). In the numerical analyses, the hardening soil (HS) model was used as the constitutive model for the SM-ML and CL layers, and the Mohr-Coulomb plasticity model was used for the bottom layer. The HS model simulates both soft and stiff soils (Schanz and Vermeer, 1998). In comparison to the Mohr-Coulomb model, the yield surface of the HS model is not fixed in the principal stress space and can expand due to plastic strain. The stiffness of the soil decreases under deviatoric stress, resulting in irrecoverable plastic strain. In a drained triaxial test, hardening soil model can be approximated with a hyperbola similar to the hyperbolic model by Kondner (1963) and Duncan and Chang (1970), but different in that it utilizes the theory of plasticity instead of the theory of elasticity to include dilation effects, and provides

for a yield cap (Plaxis, 2010). The two yield curves in triaxial condition are expressed by (Schanz et al., 1999):

$$f_{12} = \frac{q_a}{E_{50}} \frac{(\sigma_1 - \sigma_2)}{q_a - (\sigma_1 - \sigma_2)} - \frac{2(\sigma_1 - \sigma_2)}{E_{ur}} - \gamma^p \text{, and}$$

$$f_{13} = \frac{q_a}{E_{50}} \frac{(\sigma_1 - \sigma_3)}{q_a - (\sigma_1 - \sigma_3)} - \frac{2(\sigma_1 - \sigma_3)}{E_{ur}} - \gamma^p$$

where q_a is related to the ultimate deviatoric stress (q_f) with a parameter R_f described as:

$$q_f = \frac{6 \operatorname{Sin} \varphi_p}{3 - \operatorname{Sin} \varphi_p} (p + c \operatorname{Cot} \varphi_p) \qquad \text{and} \quad q_a = \frac{q_f}{R_f}$$

The plastic shear strain (γ^p), which is the hardening parameter, is defined with the following equation assuming that the plastic volumetric strain (ε_υ^p) is small:

$$\gamma^p = \varepsilon_1^p - \varepsilon_2^p - \varepsilon_3^p = 2\varepsilon_1^p - \varepsilon_\upsilon^p \approx 2\varepsilon_1^p$$

E_{50} is the stiffness modulus for primary loading given by:

$$E_{50} = E_{50}^{ref}\left(\frac{\sigma'_3 + c\,Cot\,\varphi_p}{\sigma^{ref} + c\,Cot\,\varphi_p}\right)^m$$

where E_{50}^{ref} is the reference stiffness modulus at a reference stress (σ^{ref}).

For unloading-reloading, another stress-dependent stiffness modulus is used:

$$E_{ur} = E_{ur}^{ref}\left(\frac{\sigma'_3 + c\,Cot\,\varphi_p}{\sigma^{ref} + c\,Cot\,\varphi_p}\right)^m$$

where E_{ur}^{ref} is the reference stiffness modulus at a reference stress (σ^{ref}).

Flow rule in the HS model is defined as:

$$\dot{\varepsilon}_{\upsilon}^{p} = \sin\psi_m\ \dot{\gamma}^p$$

where ψ_m is the mobilized dilatancy angle.

Because all or some parts of the top layer (i.e., the SM-ML layer) might be above the phreatic surface at the various stages of modeling (simulating a rising reservoir level), the unsaturated hydraulic properties are used for these sections. Figure 4.2 shows the soil water characteristic curves (SWCCs) for the various levels of saturated hydraulic conductivity (k_{sat}) used in the model. The k-value is a parameter that changes in the analyses to simulate the

effect of roots, and the appropriate SWCC is assigned to the top layer based on the saturated k-value. Table 4.3 presents the Van-Gunechten parameters pertinent to the SWCCs.

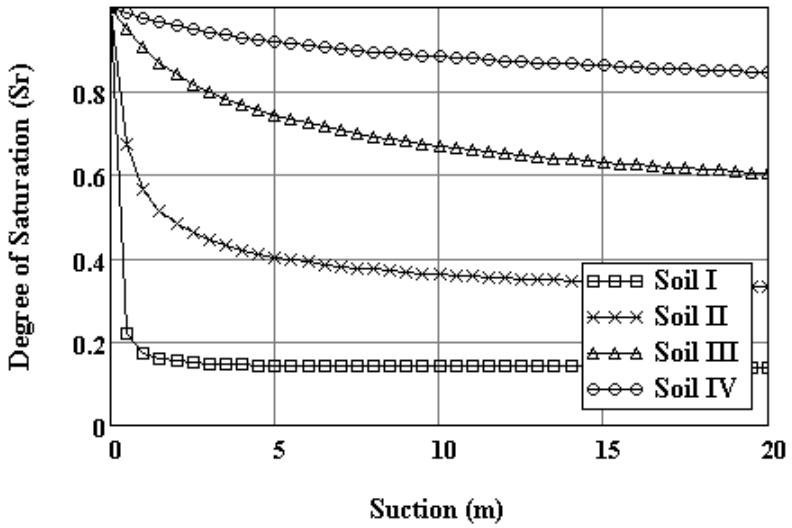

Figure 4.2 SWCCs for SM-ML layers with various k_{sat} values (Plaxis, 2010)

Table 4.3 Van-Gunechten parameters for various soils

Soil	k_{sat} (m/s)	n	α (1/m)	θ_{res}
Soil I	5×10^{-5}	2.28	3.78	0.139
Soil II	5×10^{-6}	1.48	1.80	0.256
Soil III	5×10^{-7}	1.23	0.30	0.207
Soil IV	5×10^{-8}	1.09	0.15	0.194

4.4.2 Loading and Boundary Conditions

The boundary conditions include the restriction of horizontal deformation on both sides of the soil profile as well as restriction of horizontal and vertical deformations at the lower boundary of the model. The flow boundary conditions include a no-flow boundary at the bottom of the model and a free-seepage boundary at the downstream side of the levee. On the left and right sides of the foundation layers, constant head boundaries are applied that are equal to the total hydraulic head.

A steady-state seepage condition, representing a 'sunny day' water elevation is first established by running the model, followed by a rise in water elevation with time to represent a flooding scenario. For the steady-state step, the upstream side of the levee is modeled as a constant pore pressure boundary, and for the transient steps it is modeled as a time-dependent pore pressure boundary.

4.4.3 Modeling Steps

Staged construction is first employed to build the model levee. During the construction of the levee in three layers, the water level is assumed to be at the elevation of 17.5 m (EL. 17.5, see Figure 4.1), which is the top of the CL layer. In the next step, it is assumed that the water reaches the heel of the levee (EL. 19.6 m) and that a steady-state condition occurs. To model a storm flooding, the water level is increased with an assumed rate of 0.06 m per hour until reaching a maximum elevation of 21.9 m. This relatively high rate of rise was observed recently at the Bourbeuse River Levee (NOAA, 2011). In the model

application, the water level is sustained for several days, and its effect on the flow and deformation responses is analyzed.

4.4.4 Roots and Change in k-value

Two models are analyzed herein. The first model assumes that the impact of roots leads to a change in k-value for the entire body of the levee. This case provides an upper bound of impact of the k-value on the estimated limit states of the levee. The various k-values used in the analyses are guided by those presented in Table 4.1. On the other hand, according to Gray et al. (1991), most of the plant roots are concentrated within the top meter from the surface, although the recent study by Corcoran (2011) indicated potentially deeper zones to a depth of few meters. A second model configuration is used in which the roots affect only the hydraulic properties of the levee within 0.75 m from the surface. As mentioned earlier, because no conclusive data exist regarding an increasing or decreasing impact of roots on hydraulic conductivity values, two cases of 0.1 k, and 10 k are applied to the top 0.75 m layer, where k is the hydraulic conductivity of the embankment layer (i.e., the SM-ML layer). The coefficient of variation of the k-value for this 'root' layer is assumed to be similar to that for the embankment layer.

4.5 Results

4.5.1 Limit Equilibrium and Numerical Analysis

A limit equilibrium model is analyzed using the Slope/W program along with the numerical simulation of the Elkhorn Levee, mainly to verify the results from the numerical

model. The limit equilibrium model in the Slope/W program is shown in Figure 4.3 (a), which presents the failure surface that corresponds to FS = 1. In parallel, Figure 4.3 (b) presents the results from the numerical analysis that indicates the location of the emerged failure surface. Similar to the Slope/W model results, as the flow regime in the numerical model reaches a steady-state condition, with the water elevation at the maximum level, a failure surface emerges at the downstream slope. These results serve to validate the computed behavior obtained from the numerical approach.

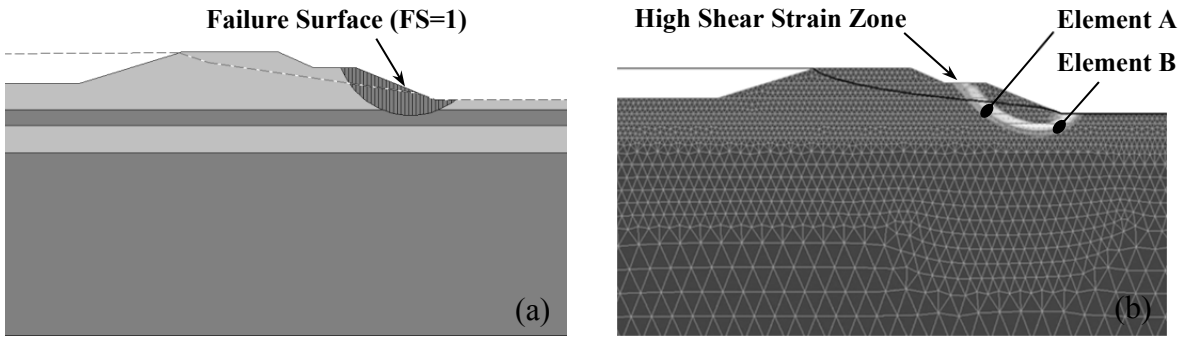

Figure 4.3 Failure zone in (a) Slope/W and (b) Plaxis models

4.5.2 Limit States

Khalilzad and Gabr (2011) presented a definition of performance limit states as follows:

LS I: minor deformations, no discernible shear zones, low gradients (i.e., $i < 0.4$) throughout the levee and foundation,

LS II: medium (repairable) deformations, dispersed plastic zones with moderate strain values, tolerable gradients less than critical (e.g., i = 0.4 ~ 0.8), and,

LS III: major deformations, breaches and critical gradients at key locations (i.e., i > 0.8, boiling and fine material washing at the location of the toe), high strain plastic zones and emerging shear bands.

The approach taken to define these limit states is developed further based on soil responses under deviatoric stress. Figure 4.4 shows the simulated stress-strain responses obtained from drained triaxial compression tests using the soil parameters presented in Table 4.2 for the SM-ML layer.

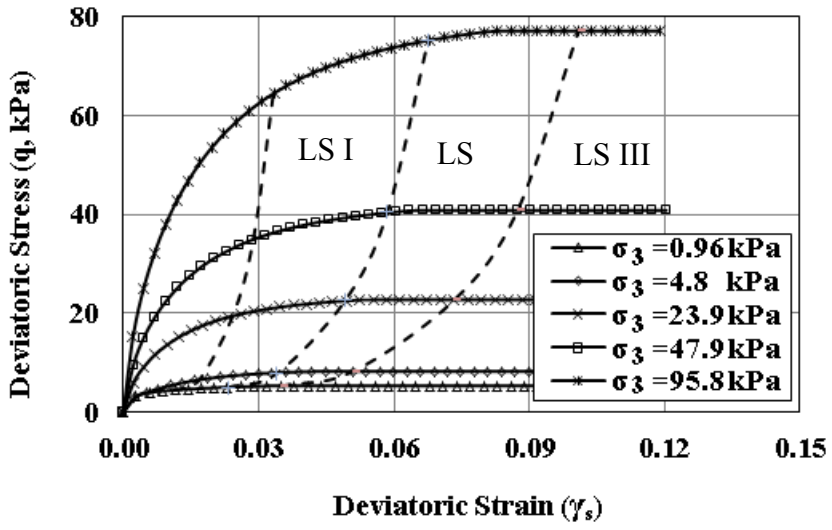

Figure 4.4 Triaxial test simulations of SM-ML soil

In this case, it is proposed that LS III is expressed as the onset of the critical state condition at each confining pressure with deviatoric strains corresponding to LS III and varying as a function of confining stress. For an illustration of this concept, LS I and LS II are defined at 33% and 67% of the critical deviatoric strain at LS III, respectively. At this time, this definition requires further verification in terms of associated performance metrics, such as the formation of shear bands and the occurrence of high gradients in relation to deformation and strain levels.

Figure 4.5 shows the deviatoric strain versus mean effective stress relationship for an element at the toe as well as for two elements in the shear zone (see Figure 4.3). The stress-strain path for these three locations, as shown in Figure 4.5, indicates a loading history that corresponds to the construction of the levee in layers, and then to the rise of the water level in the reservoir, and then remains at the maximum level for the simulation time of 30 days. Assuming that the toe area is the focus of the analysis, three deviatoric strains of 0.018, 0.032 and 0.047 are associated with LS I, LS II, and LS III, respectively. The stress path at the toe area is in the form of lateral extension and one of the advantages of tracking the toe area as an indicator of localized performance status is that this area can be inspected visually and surveyed in the field. Hansen and Roshanfekr (2012) also confirmed that the toe area in dams is a primary zone of engineering concern.

The horizontal deformation levels of the toe, at LS I, LSII, and LS III, are obtained from the corresponding deviatoric strains, as shown in Figure 4.6. In this case, three

horizontal deformations, 26 mm, 41 mm, and 58 mm are estimated as LS I, LS II and LS III, respectively, with 58 mm representing the onset of failure.

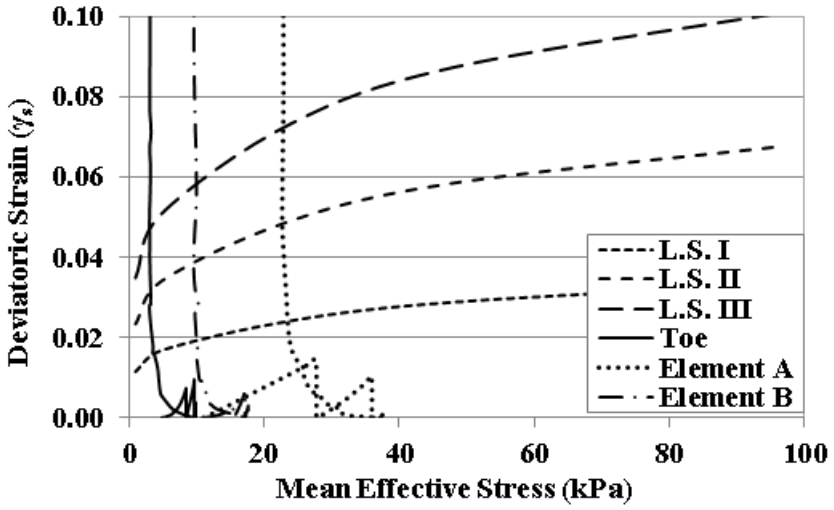

Figure 4.5 Limit states based on deviatoric strain

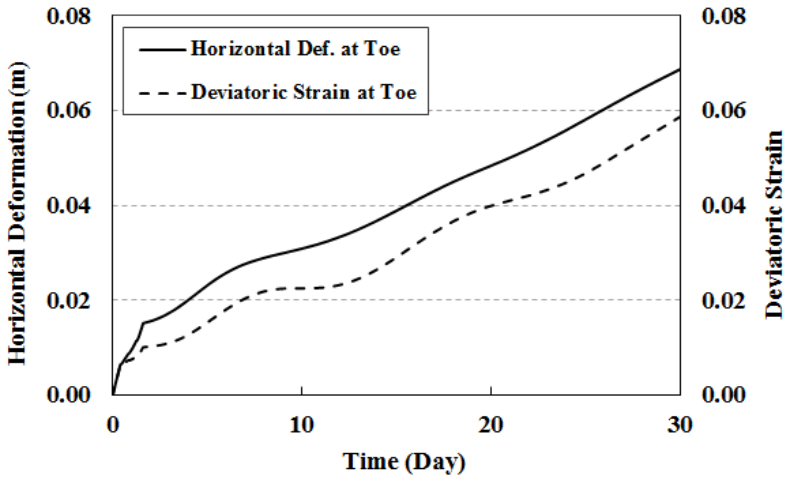

Figure 4.6 Horizontal deformation corresponding to deviatoric strain at toe

4.5.3 Exceedance Assessment

The probability of exceeding a given limit state is estimated, based on the deformation levels at the toe, as water rises in the reservoir and remains at the maximum level. Figure 4.7 shows the changes in horizontal deformation of the toe due to the variations in hydraulic conductivity of the SM-ML and CL layers (i.e. mean k-value plus/minus standard deviation of hydraulic conductivity). Over time, the horizontal deformation of the toe increases with a higher rate of increase for the higher values of hydraulic conductivity. This occurrence is due to the progression of the saturation front over time. As water remains at the maximum elevation in the reservoir, the phreatic line rises within the levee embankment and the saturation front advances until ultimately reaching the steady state

condition. This occurrence then leads to a reduction in soil suction and consequently induces a reduction in the effective stress, which in turn causes a decrease in the shear strength. In addition, the increase in pore water pressure is accompanied by seepage forces that contribute to an increase in strain magnitude.

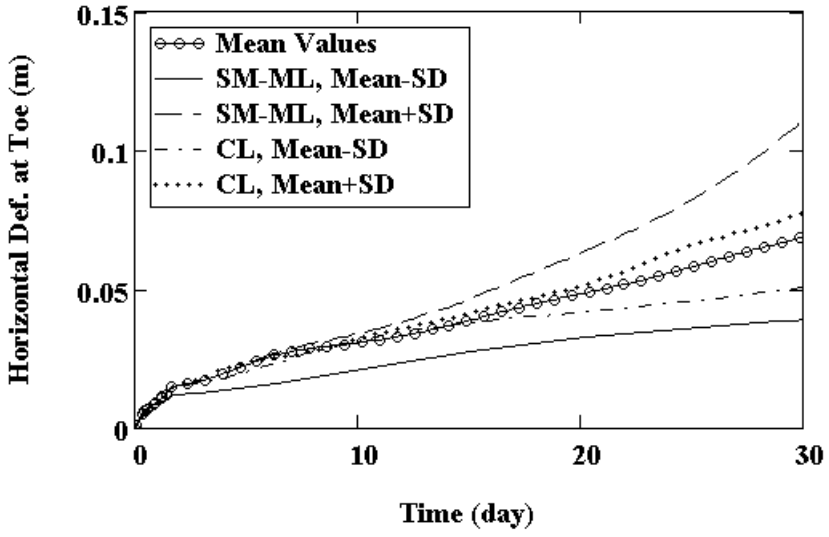

Figure 4.7 Horizontal deformation of toe for variations of k-value about its mean

Table 4.4 shows an example of a worksheet that has been developed to estimate the probability of exceeding a given limit state based on the results from the numerical model and using the Duncan (2000) approach. The model is analyzed twice for each random variable with the mean value plus/minus standard deviation of the variable. A normalized target parameter (i.e. horizontal deformation at toe normalized to the limit states) is used to

calculate the standard deviation of N function (N is equal to the limit state value divided by the horizontal deformation of toe). The mean value of N is also obtained from the finite element analysis of the model using mean values of all input parameters. The reliability index (β) and the probability of exceeding each limit state $P(E.L.)$ are calculated from the following equations:

$$\beta = \frac{E[X]}{SD_X}$$

$$P(E.L.) = \Psi(-\beta)$$

where $E[X]$ is the expected value of function X, SD_X is the standard deviation of function X, and $\Psi(-\beta)$ is the cumulative distribution function of the standard normal distribution evaluated at $-\beta$.

After 10 days, the probability of exceeding LS I, LS II, and LS III are 78%, 19%, and 0.02%, respectively, as shown in Figure 4.8. In all three cases, the probability of exceeding a given limit state increases with time in accordance with the advancement of the saturation front.

As the high water level is sustained, the probability of exceeding LS I reaches 97% after 20 days. For the same time period, the probability of exceeding the LS II and LS III is 73% and 37%, respectively. From a deterministic perspective, it should be noted that this

levee is already at the state of failure based on the limit equilibrium analysis. On the other hand, and despite the high probability of exceeding LS III, the hydraulic gradients at the toe, which correspond to the case with mean k-values, are 0.42, 0.52, and 0.57 after 10, 20 and 30 days, respectively. These findings demonstrate the inadequacy of condition assessments that are undertaken using a deterministic single performance matrix.

Table 4.4 Calculating the probability of exceeding limit states (after 10 days)

Hydraulic Conductivity					LS I (S_1 = 2.2 cm)		LS II (S_2 = 4.1 cm)		LS III (S_3 = 5.7 cm)	
Soil Type	**μ (m/s)**	**σ (m/s)**	**ι+/-σ (m/s)**	**S (cm)**	**$N=S_1/S$**	**ΔN**	**$N=S_2/S$**	**ΔN**	**$N=S_3/S$**	**ΔN**
SM-ML	7.6×10^{-7}	7.1×10^{-7}	5.3×10^{-8}	2.1	1.238	-0.473	1.952	-0.746	2.762	-1.056
			1.5×10^{-6}	3.4	0.765		1.206		1.706	
CL	1.9×10^{-7}	3.5×10^{3}	6.0×10^{-8}	3.1	0.839	-0.026	1.323	-0.041	1.871	-0.058
			3.2×10^{-7}	3.2	0.813		1.281		1.813	

	LS I	LS II	LS III
SD	0.237	0.374	0.529
Mean	0.839	1.323	1.871
COV	0.283	0.283	0.283
β	-0.773	0.870	2.121
R=Ψ(β)	0.220	0.808	0.983
P(E.L.)	0.780	0.192	0.017

Notations:

μ=Expected value of hydraulic conductivity
σ=Standard deviation of hydraulic conductivity
S=Horizontal deformation of the toe
N=Normalized deformation
COV=Coefficient of variation
β=Reliability index
R=Reliability

P(E.L.)=Probability of exceeding limit state

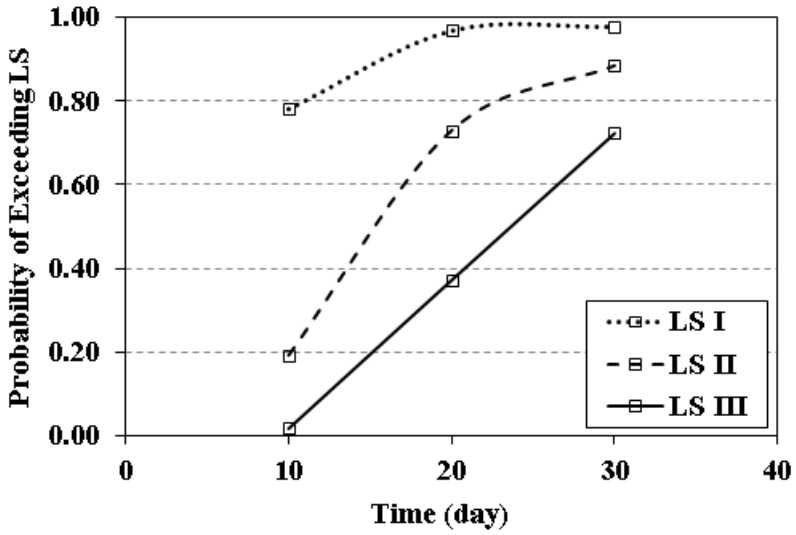

Figure 4.8 Probability of exceeding each limit state versus time

Figures 4.9 (a) and (b) present the effect of the variation in hydraulic conductivity on the deformation response. The data shown in Figure 4.9 (a) are a magnification of the first 48 hours of simulation. As the k-value of the top layer (SM-ML) increases, the horizontal deformation of the toe also increases, indicating the considerable effect of the k-value on the response of the levee. This effect becomes more pronounced at higher values of hydraulic conductivity.

After 24 hours, the horizontal deformation of the toe for a levee with hydraulic conductivity of 5×10^{-5} m/s is approximately three times more than that with hydraulic conductivity of 5×10^{-8} m/s. As shown in Figures 4.9 (a) and (b), when the hydraulic conductivity of the SM-ML layer is 5×10^{-5} m/s, the levee reaches LS III after about 4 days,

whereas it takes 12 days to reach LS III for the levee with hydraulic conductivity of 5×10^{-6} m/s. For the k-values of 5×10^{-7} m/s and 5×10^{-8} m/s, the time durations are 17 and 22 days, respectively.

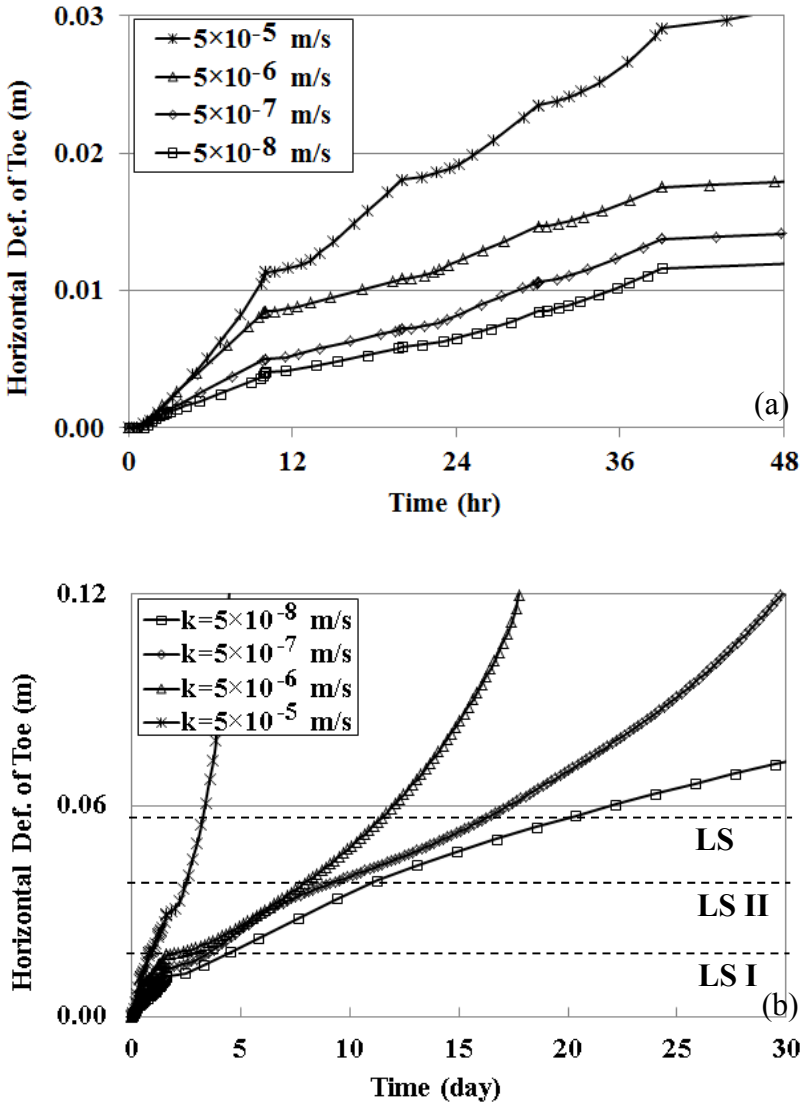

Figure 4.9 Effects of hydraulic conductivity: (a) 2 days, and (b) 30 days

4.5.4 Effects of Limited 'Root' Layer

Figure 4.10 shows the results of the variation in hydraulic conductivity for a 0.75 m top layer with roots. It seems that for both cases of 10 k and 0.1 k, the horizontal deformation of the toe is less than that for the 1.0 k case. This phenomenon is due to the differences in seepage pattern and distribution of pore pressure for these three cases. A 0.1 k layer at the top of the flow domain has a considerable impact on the deformation and flow responses with a rising water level, as water flow pathway is through a layer with relatively low hydraulic conductivity in order to reach the embankment layer underneath with the higher hydraulic conductivity of 1.0 k.

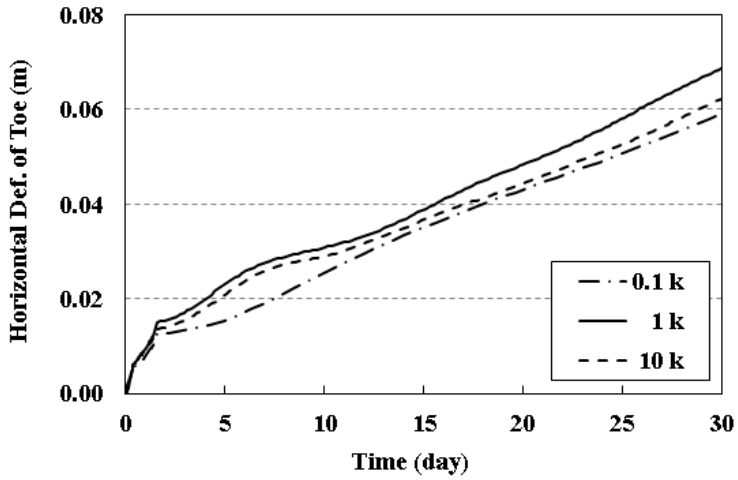

Figure 4.10 Effects of variation of hydraulic conductivity in top 0.75 m of soil

The total head drops substantially through this low k layer. After the saturation front reaches the 1.0 k layer, the hydraulic properties of the 1.0 k layer play a more important role, and the deformation levels become closer to the initial 1.0 k case (i.e., without the top 'root' layer). On the downstream side of the levee, the 'root' layer in this case hinders the advancement of the saturation front, resulting in less deformation over time. Thus, the presence of a 'root' layer with hydraulic conductivity of 0.1 k near the top leads in this case to less deformation than in the case with no roots. Figures 4.11 (a) and (b) show the responses of the phreatic surface for the case of 0.1 k versus 1.0 k.

For the second scenario, in which the 'root' layer has a hydraulic conductivity of 10 k, deformation levels are again lower compared to the case without 'roots'. This is because the downstream side of the levee with the 10 k layer behaves similarly to toe drainage, thereby leading to a lower phreatic surface at the zone closest to the toe (see Figure 4.11 (a) versus (c)).

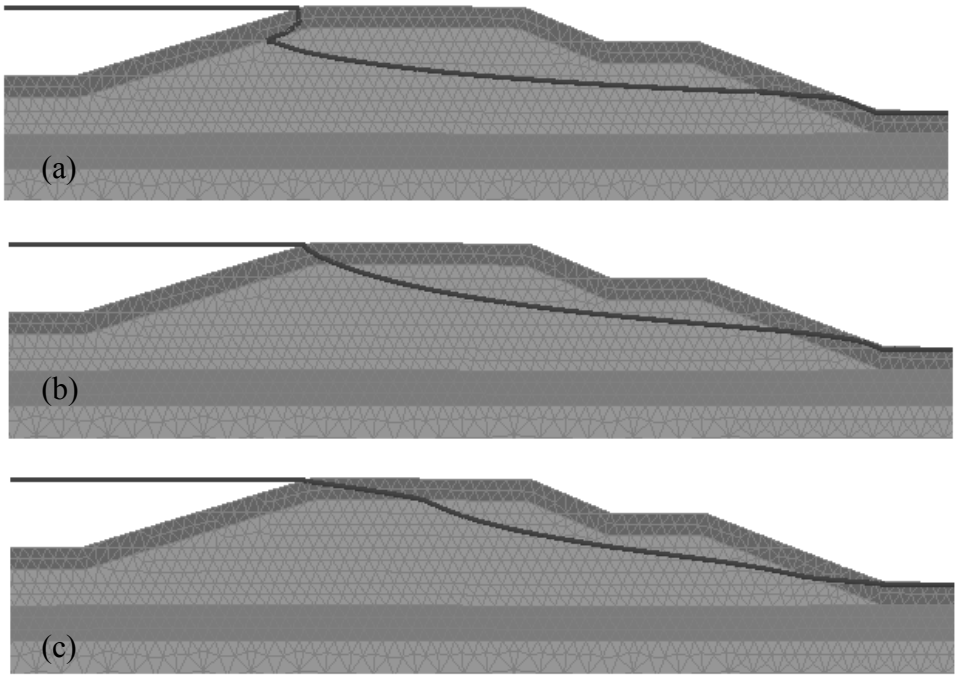

Figure 4.11 Saturation front for different cases after 30 days: i) 0.1 k, ii) 1.0 k, and iii) 10 k

Figure 4.12 presents the effects of varying the k-value within the 'root' layer, based on the probability of exceeding LS III. For all three cases, the probability of exceeding LS III increases with time. For the 0.1 k case, the probability of exceedance is the lowest of the three cases after each period of 10, 20 and 30 days, and such probability decreases by 1.3%, 15.9% and 11.6% after 10, 20 and 30 days, respectively.

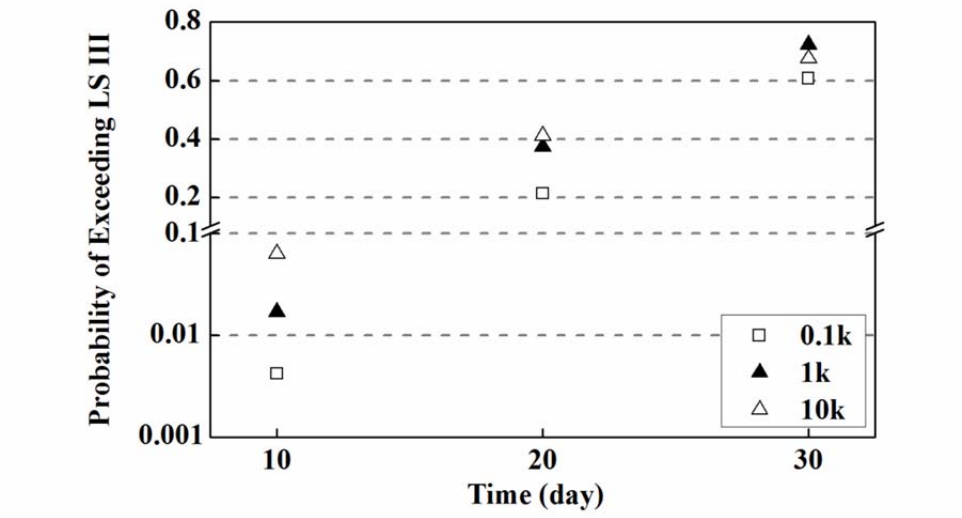

Figure 4.12 Effects of variation of k-value in top 0.75 m layer on the probability of exceeding LS III

In addition, the variation of the k-value in the 'root' layer with hydraulic conductivity of 10 k, leads to a higher probability of exceeding LS III after 10 and 20 days. However, after 30 days the exceedance probability is lower than with the 1.0 k-value. Such probability increases 4.7% and 3.9% after 10 and 20 days, respectively, but decreases by 4.6% after 30 days. The reason for this trend is mainly due to the large difference in deformation levels for the 10 k case compared to the 1.0 k case after 30 days. These results show that the subject of whether the presence of roots leads to high or low k-values and the related impacts needs to be analyzed in the context of a transient high water level, as the probability of exceedance is also dependent upon the duration of a sustained water level.

The estimated hydraulic gradient values at the toe for the three cases indicate that the highest is estimated for the 0.1 k case, as shown in Figure 4.13. While the gradient at the toe increases over time for all three cases, it is close to the critical value of 1.0 for the 0.1 k case as the saturation front develops within the embankment. For the 1.0 k and 10 k cases, the gradient levels are 0.6, and 0.22, respectively. In the case of the 0.1 k layer, this 'root' layer blankets the downstream side of the levee at the seepage face, thus causing a large hydraulic head differential that leads to a critical gradient condition. This phenomenon occurs despite the low probability of exceeding LS III from the deformation perspective. On the other hand, although the hydraulic gradient is lower for the 10 k case compared to the 1.0 k case, the probability of exceeding the deformation-based LS III is higher for the 10 k case at 10 and 20 days of sustained high water elevation. These results illustrate the necessity of obtaining the coupled flow and deformation responses of the embankment to gain a full understanding of expected performance under severe storm conditions.

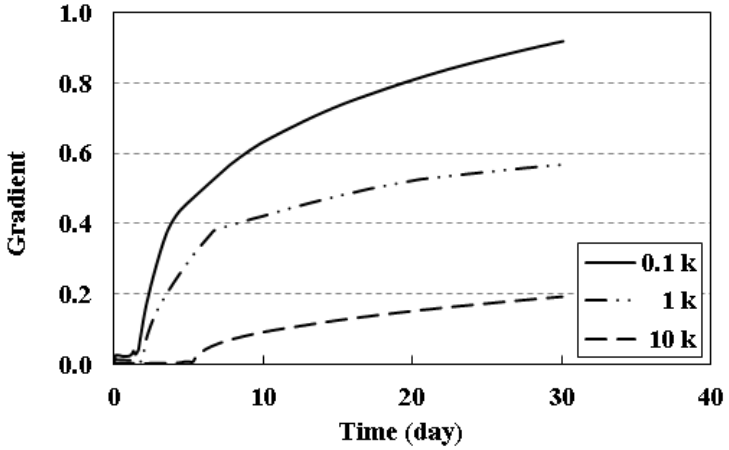

Figure 4.13 Gradient at the toe versus time for three cases

4.6 Summary and Conclusions

The results from laboratory and field hydraulic conductivity tests conducted by Brizendine (1997) at four levee sites, with and without roots, are summarized and presented. The values and distribution of the hydraulic conductivity parameters are used to estimate the probability of exceeding predefined limit states. A combination of numerical modeling, a definition of limit states based on the framework of critical state soil mechanics, and simple probability analyses are used to quantify three limit states of performance (LS I, LS II, and LS III) as well as the probability of exceedance under hydraulic loading. A case study of Elkhorn Levee is presented to demonstrate the applicability of the limit state concept. The effect of change in hydraulic conductivity due to the presence of woody vegetation on the

stability of the levee is investigated under the assumption that woody vegetation impacts either the whole embankment or only the 'root' layer that has a thickness of 0.75 m from the ground surface. The toe area is used as an indicator location for condition assessment with regard to the definition of *limit state*. Maximum deformations commonly occur in this location and can be visually inspected and surveyed. In addition, high gradients are observed in this area, and these critical gradients can be problematic, causing piping and internal erosion. Based on the results of this study, the following conclusions are advanced:

Field and laboratory hydraulic conductivity data from four levee test sites show no clear trend to support the notion that woody vegetation leads to either high or low values of hydraulic conductivity. However, the testing protocol that was used for the original study did not include characterization of the roots in terms of shape, distribution, or the extent of their decay. Knowledge of these parameters is necessary to interpret the possible effects of woody vegetation on the hydraulic conductivity data and to explain the observed trends. Even then, it seems that such an effect will have to be evaluated on a site specific basis.

Consideration of the transient nature of hydraulic loading provides a more comprehensive insight into the temporal responses of an embankment. Even though the levee case study is modeled in a marginal condition of stability, the probability of exceeding LS III after 10 days of sustained maximum water level is only 2%, based on limit equilibrium analysis. This finding signifies the relatively high probability of functionality of the levee at this point. The probability of exceeding LS III, however, increases over time to 37% and 72% after 20 and 30 days, respectively. These data signify a high probability of failure and

demonstrate the importance of defining the duration of hydraulic loading during and after the occurrence of severe storms.

The impact of woody vegetation on the changes in hydraulic conductivity of the flow domain plays a significant role in determining the time it takes to exceed LS III. If woody vegetation leads to a reduction in k-value from 5×10^{-5} m/s to 5×10^{-6} m/s, the time it takes to reach LS III increases from 4 days to 12 days. This amount of time can be critical in terms of performing preventive and rehabilitation efforts and mitigating failure hazards.

In modeling a 0.75 m top 'root' layer, the results show lower toe deformation for both cases of 0.1 k and 10 k than in the 1.0 k case (without a 'root' layer). The total head drops substantially across the 0.1 k layer, and the low k-value also hinders the advancement of the saturation front, resulting in less deformation over time. In the second scenario where the 'root' layer is modeled with hydraulic conductivity of 10 k, the deformation levels are also lower than for the case without a 'root' layer, mainly because the downstream side of the levee with the 10 k layer functions in a manner similar to toe drainage, leading to a low phreatic surface at the zone closest to the toe.

Despite the fact that the lowest value of probability to exceed LS III is found for the 0.1 k case, from the deformation aspect, critical levels of gradient are observed at the toe for this case after 30 days. Even though the probability of exceeding LS III is higher for the 10 k case than for the 0.1 k case, the computed gradients are lower. This finding again demonstrates the inadequacy of a condition assessment that is determined by a deterministic single performance matrix.

CHAPTER 5

5. ASSESSMENT OF REMEDIAL MEARURES TO MITIGATE HAZARD IN EMBANKMENT DAMS USING PERFORMANCE LIMIT STATES ANALYSIS

5.1 Introduction

The application of probabilistic analysis in the geotechnical engineering has gained acceptance during recent years as a supplemental approach providing insight into performance under a design event and potential associated risk (Wolff, 1994; Moellmanna et al., 2011). The limited use of probabilistic approaches in earth embankments has not only been due to the lack of databases available to perform the probabilistic analyses but also due to the unfamiliarity of the practicing professionals with the probabilistic techniques. The assessment of risk including the uncertainty in the hazardous event is needed for assessment of structure's vulnerability, and uncertainty in exposure. Facilitating the incorporation of such parameters, as decision variables in risk assessment, is therefore of paramount importance to allow for not only a meaningful condition assessment and cost effective specification and implementation of the remedial actions, but also an improved communication of the risk level to the public. To this end, the concept of deformation-based limit states (LS) for protective earth structures is introduced by Khalilzad and Gabr (2011) and provides a graded measure (versus the binary classification of safe/unsafe) of the safety margin under a specified storm loading. Such an approach provides a rational basis for

condition assessment of the structure as it is progressively loaded over time with multiple storms as well as the efficacy of remedial actions.

Using traditional deterministic analysis with the single values for strength, stiffness and hydraulic properties have led to several failures, even though, the design have been performed according to the engineering codes (Sherard, 1987; Chen et al., 1992; and Rogers et al., 2008). In such cases, remedial measures are required to downgrade the level of progressive failure and perhaps alter the failure mechanism to a less critical one over. A remedial design starts with evaluating the existing conditions to estimate the severity of the problem and assess potential factors leading to failure. In some important cases, it is accompanied with a monitoring program to assess the response before and after remedial measures (Ghorbani et al., 2012; and Mann, 2013).

This is especially true nowadays that with the advancement of computer technology, data management programs and intelligent instruments, real time assessment of the response of a dam or a levee can be performed under various loading condition such as during severe storm events. However, in a monitoring program, there is a need to establish some limit states and compare the measured quantities with those predefined values. Additionally, by incorporating these limit states into deformation-based probability analysis, probabilities of exceeding each limit state can be estimated as well.

The objective of this study is to investigate the effects of remedial measures on decreasing the probability of exceeding established performance limit states of earth embankments forming levees and dams. An embankment dam in the marginal stability

condition is analyzed using finite element approach and three remedial measures are implemented including constructing a downstream berm, adding a downstream drainage system, and an impermeable layer (cutoff wall) are modeled. The results of numerical modeling are incorporated into deformation-based probabilistic analysis and the impact of the remedial measures on the probabilities of exceeding limit states are presented and performance-based aspects of the remedial measures are discussed.

5.2 Background

Wahlstrom and Nichols (1969) presented the remedial measures undertaken during the construction of Dillon Dam in Colorado, where movements were observed during excavating the toe of a landslide having the potential of engulfing the intake structure by the adjacent landslide. To resolve the problem of increased deformations, a large volume of the landslide material was excavated and a gravel-fill dike was constructed on bedrock at the toe. In the study of the Gold Tailings dam in South Africa, Sully (1985) reported a minor failure which raised concerns about the future stability of the dam under high water condition and required controlling the phreatic surface to reduce the risk of seepage and stability issues. At first, installation of elevated drains within the body of the dam was recommended as a remedial measure, but later, more comprehensive seepage analysis of the dam provided results indicating that less costly remedial measures could be implemented instead. Mann and Snow (1993) presented a remedial design to stabilize the upstream slope of a 13.7 m high dam in Ohio where a crack was observed along the crest prior to filling the dam. Subsurface

explorations and testing revealed that either significant excess pore pressure along the failure surface or creep movements could be the reason for developing the crack. The main course of action in the remedial design of the dam included construction of a buttress on the upstream slope, repairing the crack by reconstructing the upper 3 to 4.5 m layer, and additional seepage control measures. Twenty years later, Mann et al. (2013) studied the 1993 remedial design using numerical analysis with the aid of performance monitoring data and showed that the creep movements continued to occur over time but at a decreasing rate. Mann et al (2013) concluded that the limit equilibrium analysis is not a robust measure of dam performance and it is only an indicator of safety of a dam relative to failure.

In another study, Nusir et al. (2002) reported seepage problems in an embankment dam in Jordan, where it was proposed to raise the crest of the dam to increase its storage capacity. This however, could worsen the existing seepage problems due to the presence of alluvial material under the foundation. The remedial actions suggested for controlling the seepage problems were constructing an upstream blanket, increasing the capacity of downstream relief wells and grouting in the likely seepage areas. Uddin (2005) studied the case of a hydroelectric power project dam where failure occurred following the emergence of major sinkholes in the embankment. They concluded that the failure happened due to several factors including shortened critical seepage path, inadequate filter protection, and design and quality control deficiencies. Remedial design was undertaken to return the dam to operational condition by excavating the embankment containing loose and free-draining material, placing granular backfill with controlled quality, and installing sand filters and drains. Richards and

Reddy (2005) used both numerical and analytical approaches to model a failure occurred in an embankment dam and concluded that the limit equilibrium method could lead to a more conservative design for a given shear strength.

On the other hand, probabilistic analysis has been widely developed and utilized in the geotechnical literature (Cornell, 1971; Alonso, 1976; Tang et al., 1976; Christian et al., 1994; Wolff, 1996; Wolff et al., 1996). A combination of random field simulation, seepage analysis, and slope stability analysis was employed by Gui et al. (2000) to study the effects of stochastic hydraulic conductivity on the slope stability of an embankment dam and concluded that the reliability index is very sensitive to the uncertainty of saturated hydraulic conductivity.

Srivastava et al. (2010) also investigated the effect of permeability parameter on the seepage and slope stability analysis using the finite difference approach. They assumed a lognormal distribution for the permeability as a random variable and reported that a lower value of correlation distance and coefficient of variation in the permeability parameter provides higher factor of safety values. Ahmed (2009) studied the problem of free surface flow through earth dams using a probabilistic method with the assumption of a lognormal distribution for the permeability and drew an important conclusion that numerical models over predict the amount of seepage flow through a homogenous dam formation and the measured flow in the field should be less than numerically calculated value. He also found that the water exit point on the downstream slope obtained from deterministic analysis is higher than its real location.

5.3 Study Model

An embankment dam is modeled using the finite element program Plaxis (Plaxis, 2010).The modeled dam geometry is obtained from the US Army Corps of Engineers technical manuals (USACE, 2006) and it represents an earth dam section with geological profile representative of the lower Mississippi valley where a three layer soil system including a shale layer at the bottom is overlain by a layer of alluvial soil with a relatively high hydraulic conductivity. Above the alluvial layer, a low permeability soil forms the top foundation layer and the body of the embankment dam. The side slopes are 4H:1V on both upstream and downstream sides of the embankment dam. The landside ground surface slopes at 50:1 and the river side slopes at 30:1. In this paper, a model with a size factor of 0.5 (i.e. scaling down the original geometry by 50%) has been used as the base case with the soil properties adjusted such that the dam is in a marginal stability condition. To obtain the soil properties corresponding to this condition, the dam is modeled in Slope/W (a limit equilibrium program) and the material strength is reduced until a factor of safety of 1.05 is reached. This factor of safety value is selected to represent the near-failure condition while preventing the numerical convergence issues. The geometry and meshing of the model are shown in Figure 5.1. The finite element mesh consists of approximately 47,000 nodes and 5800 elements. The 15-node triangular plane strain elements (Plaxis, 2010) are utilized to capture a better resolution of stress and deformation magnitudes.

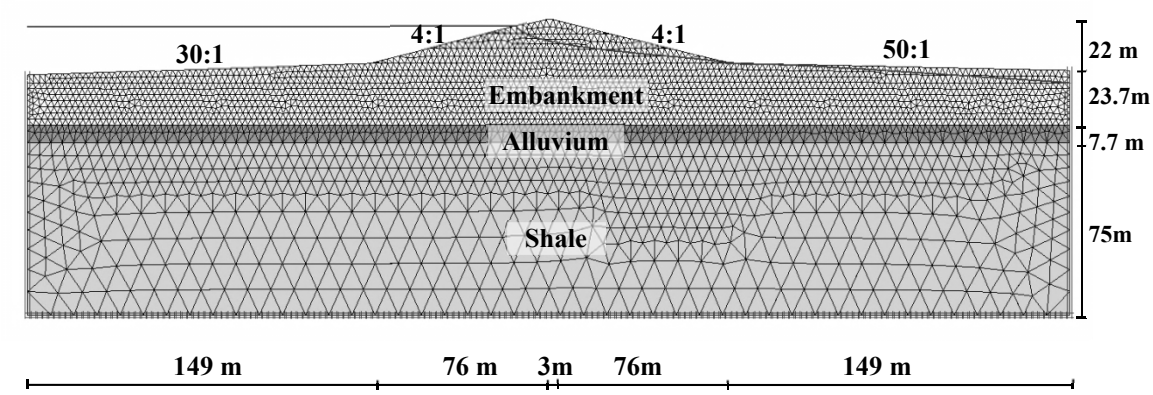

Figure 5.1: Model geometry and discretization

The soil properties of the embankment and foundation layers are presented in Table 5.1. As mentioned earlier, the soil strength parameters originally reported in USACE (2006) have been reduced by a factor of 1.55 in order to reach a safety factor of 1.05 in the model. This is consistent with the soil strength reduction method (SSRFEM) which is an approach to find the factor of safety using the finite element analysis (Huang and Jia, 2009). It is assumed that the soils are homogeneous within each layer, thus, no spatial variability is taken into account in the analysis.

Table 5.1. Soil properties

Soil Parameters	Embankment	Alluvium	Shale
γ (kN/m^3)	19.7	16.5	20.1
C (kPa)	0	0	0
Φ, Mean (°)	17.5	11.6	13.4
Φ, SD (°)	1.65	2.54	3.59
E_{50} (kPa)	6670	5000	33.3E3
E_{ode} (kPa)	5330	4000	26.7E3
E_{ur} (kPa)	20.0x10^3	15.0 x10^3	100.0 x10^3
k (m/day)	0.43	0.43	0.86 x10^{-9}
θ_{res}*	0.074	N/A	N/A
α (1/m)*	1.6	N/A	N/A
n*	1.37	N/A	N/A

*** Van-Gunechten parameters**

The constitutive response of the model domain is defined by the Hardening Soil (HS) model, as incorporated in Plaxis (Schanz et al., 1999). Unsaturated hydraulic properties are used for the embankment layer as all or some parts of the layer are above the phreatic surface at the different stages of modeling simulating rising reservoir level. The other two layers are saturated during the simulation time. The appropriate soil water characteristic curve (SWCC) is assigned to the top layer based on the saturated k value. The Van-Gunechten parameters pertinent to the SWCCs are also presented in Table 5.1.

5.3.1 Loading and Boundary Conditions

Horizontal deformations are restricted on both sides of the foundation soil profile and both horizontal and vertical deformations are restricted at the lower boundary of the model. The flow boundary conditions include no-flow boundary at the bottom of the model and free-

seepage boundary at the downstream face of the embankment. On the right side of the foundation layers, a constant head boundary equal to the total hydraulic head is applied. A steady state seepage condition, representing a "sunny day" water elevation is first established through a model run, followed by a rise in water elevation with time to represent a flooding scenario. For the steady state step, the upstream side of the embankment and the left side boundary are modeled as constant head boundaries, while for the transient steps they are modeled as time-dependent head boundaries.

5.3.2 Modeling Steps

The dam is modeled using the staged construction. Geostatic stress state is generated in the foundation layers and the embankment is placed in three layers with water level assumed to be at elevation 101m (EL. 101m, see Figure 5.1) which is 8 m below the toe of dam. Next, the water level is raised in several steps, allowing the steady state condition to occur, until it reaches around the mid-height of the dam (EL. 119.2 m). To model a storm situation, the water level is raised with an assumed rate of 0.08 m per hour until reaching to a maximum elevation of 125.3 m. This relatively high rate of rise was observed, for example, recently at Bourbeuse river levee (NOAA, 2011). The water level remains at this level for several days, and its effect on the flow and deformation responses of the embankment is investigated.

5.4 Probabilistic Approach and Limit States (LS)

Khalilzad and Gabr (2013, 2011b) presented deformation-based limit states for embankment dams and incorporated these into simple probabilistic analysis using the approach by Duncan (2000). The performance limit states are defined in terms of horizontal deformation at the toe as a key location indicating basal stability of the embankment. At this location, the stress path follows the form of an axial extension loading. The horizontal deformations are then correlated to levels of shear strain on the potential failure surface. A qualitative definition of the performance limit states (LS) was expressed by the authors as: LSI: minor deformations, no discernible shear zones, low gradients (i.e. i<1) throughout the embankment dam and foundation ; ii) LSII: medium (repairable) deformations, limited piping problems (i.e. i>1 within a shallow depth at the location of toe), dispersed plastic zones with moderate strain values, tolerable gradients less than critical; iii) LSIII: major deformations, breaches and critical gradients at key locations (i.e. boiling and fine material washing at the location of toe), high strain plastic zones and emerging shear bands (LS III). Although, it is challenging to quantify a set of limit states, representative of both flow and deformation response of an earth embankment, the authors in this paper endeavor to use coupled flow and deformation finite element model for the understanding these limit states, and their variation of various embankment parameters.

The probability of exceeding a given limit state is estimated, based on the deformation levels at the toe, as water rises in the reservoir and remains at the maximum

level. This occurrence is due to the progression of the saturation front over time. As water remains at the maximum elevation in the reservoir, the phreatic line rises within the levee embankment and the saturation front advances until ultimately reaching the steady state condition. This occurrence then leads to a reduction in soil suction and consequently induces a reduction in the effective stress, which in turn causes a decrease in the shear strength. In addition, the increase in pore water pressure is accompanied by seepage forces that contribute to an increase in strain magnitude.

Table 5.2 shows an example of a worksheet that has been developed to estimate the probability of exceeding a given limit state based on the results from the numerical model and using the Duncan (2000) approach. The model is analyzed twice for each random variable with the mean value plus/minus standard deviation of the variable. A normalized target parameter (i.e. horizontal deformation at toe normalized to the limit states) is used to calculate the standard deviation of N function (N is equal to the limit state value divided by the horizontal deformation of toe). The mean value of N is also obtained from the finite element analysis of the model using mean values of all input parameters. The reliability index (β) and the probability of exceeding each limit state $P(E.L.)$ are calculated from the following equations:

$$\beta = \frac{E[X]}{SD_X}$$

$$P(E.L.) = \Psi(-\beta)$$

where $E[X]$ is the expected value of function X, SD_X is the standard deviation of function X, and $\Psi(-\beta)$ is the cumulative distribution function of the standard normal distribution evaluated at $-\beta$.

5.5 Remedial Measures

Among many remedial measures that can be utilized to mitigate the hazard in an embankment dam, three are studied in the current paper: i) adding a berm to the toe of embankment; ii) installing a drainage system at the toe area, iii) decreasing hydraulic conductivity at a certain section (adding an impermeable curtain as a cutoff wall). These remedial measures are selected as examples for three different aspects of remedial effort (i.e. adding overburden stress to stabilize the failure surface, lowering phreatic surface to reduce the pore pressures, and decreasing hydraulic conductivity of soil to limit the amount of flow and increase the length over which the water head is dissipating). Effects of each action is investigated through deformation-based probabilistic analysis by comparing the probabilities of exceeding LS I, II, and III before and after implementing the remedial measures.

5.5.1 Downstream berm

A berm is constructed on the downstream slope over the toe area and the impacts on variation of exceedance probabilities are investigated. For comparison, two models with

different berm heights are analyzed. For simplicity, it is assumed that the soil properties of the berm layer conform to those of embankment layer. The berm has a side slope of 1V:4H, a height of 6 m in one model and 3 in another one, and the width at the top of berm is 12 m.

5.5.2 Drainage system at toe

The effect of adding a drainage system is investigated by modeling a 10-meter long drainage layer at the toe of an embankment dam. In order to entirely focus on the hydraulic impacts of the drainage layer, it is assumed that the soil strength properties of the layer conform to those of embankment material and only hydraulic conductivity of the drainage layer is increased to 1.7 m/day and 8.6 m/day.

5.5.3 Impermeable curtain

Decreasing hydraulic conductivity of embankment soil at a certain section of dam can also be used as a remedial effort. Three models are analyzed in which an impermeable curtain starting from the crest extends to three different depths (27 m, 45 m, and 60 m deep from the crest). In order to avoid convergence problems and also retaining the numerical mesh, these three depths were selected to correspond to the modeling layers. For simplicity, it is assumed that the soil strength parameters of the impermeable layer are similar to embankment layer and only the hydraulic conductivity decreased to 4.3×10^{-3} m/day which is about the hydraulic conductivity of bentonite mixes (Castelbaum and Shackelford, 2009).

5.6 Results and Discussions

Table 5.2 presents a sample spreadsheet developed to calculate the exceedance probabilities.

Table 5.2. Calculating the probability of exceeding limit states (after 10 days)

	Friction Angle				LS I (S_1 = 0.23 m)		LS II (S_2 = 0.46 m)		LS III (S_3 = 0.76 m)	
Soil Type	**μ (°)**	**σ (°)**	**μ+/-σ (°)**	**S (m)**	**N=S_1/S**	**ΔN**	**N=S_2/S**	**ΔN**	**N=S_3/S**	**ΔN**
Embankment	17.5	1.65	19.15	0.07	3.286	-2.434	6.571	-4.868	10.857	-8.042
			15.85	0.27	0.852		1.704		2.815	
Alluvium	11.6	2.54	14.14	0.135	1.704	-0.426	3.407	-0.852	5.630	-1.407
			9.06	0.18	1.278		2.556		4.222	
Shale	13.4	3.59	16.99	0.14	1.643	-0.249	3.286	-0.498	5.429	-0.823
			9.81	0.165	1.394		2.788		4.606	

	LS I	LS II	LS III
SD	1.242	2.483	4.103
Mean	2.091	4.182	6.909
COV	0.594	0.594	0.594
β	1.067	2.328	3.242
R=Ψ(β)	0.857	0.990	0.999
P(E.L.)	0.143	0.010	0.001

Notations:

μ=Expected value of friction angle
σ=Standard deviation of friction angle
S=Horizontal deformation of toe
N=Normalized deformation
COV=Coefficient of variation
β=Reliability index
R=Reliability

P(E.L.)=Probability of exceeding a limit state

5.6.1 Effect of Downstream berm

Figures 5.2a and 5.2b show the effect of constructing a berm at the toe on the horizontal deformation and gradient at the toe, respectively. The results show that in both

cases (constructing a 3m high or a 6m high berm), the horizontal deformations at the toe area dramatically decrease over time compared to the dam on which no remedial measures was performed. For example, horizontal deformations of 0.12 m, 0.19 m, and 0.32 m respectively after 10, 20 and 30 days of water remaining at high level, would decrease to 0.055 m, 0.07 m, and 0.077m after constructing a 6 m high berm at the toe. The expected horizontal deformation levels would be 0.065m, 0.075 m, and 0.095 m after 10, 20 and 30 days respectively, in case that a berm with 3 meters height is constructed at the toe. Such reduction in deformation levels can be explained as follows. As water remains at a high elevation in the pool, the phreatic surface within the dam begin to rise leading to higher pore pressures within the body of the dam and the toe area as well. Consequently, the effective stresses reduce and so does the shear strength of soils. This, in turn, leads to an increase in shear strain and deformation magnitudes. When a berm is constructed at the toe, the mean effective stresses at any depth below the toe increase. Therefore, the shear strain levels at which soil become plastic become higher and the existing loading condition develops less plastic points and less plastic shear strains. As a result, the deformations are also lower when there is a berm at the toe area. In a higher berm, the mean effective stress applied to the soil underneath in greater and so is the shear strain levels at which plasticity begins. Thus, less plastic strain and less deformation are developed at the toe for a 6 m high berm compared to a 3 m high berm.

Figure 5.2b shows that gradient decreases if a berm is added to the toe area and gradient values are less for a higher berm. However, the reduction in gradient values is not

pronounced. Comparing the “without Berm” case with “3 m high berm” and “6 m high berm” cases, the reduction is gradient values are approximately 3% and 6%, respectively.

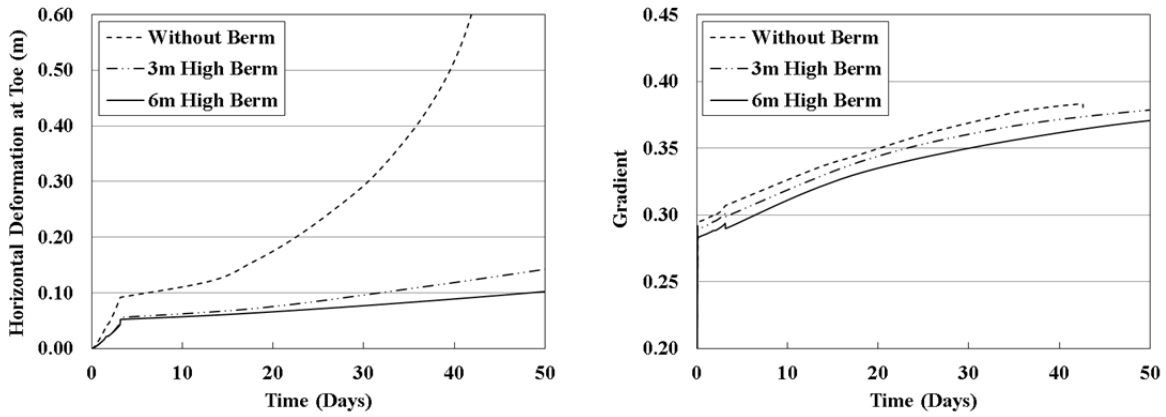

Figure 5.2: Effect of a berm at toe on a) Horizontal deformation (left), and b) Gradient (right) at toe

Figure 5.3a, 5.3b, and 5.3c present the variation of probabilities of exceeding LS I, II and III due to constructing berms with two different heights at the toe of the embankment dam. Since the impact is drastic, the probabilities are shown on a logarithmic scale in order to be able to differentiate between the curves. Even though the probabilities are very small in some cases, they have been reported herein because the values can be used in the risk analysis in combination with a high consequence and still produce a meaningful value (since risk is defined as: risk = probability of exceedance × consequences). For all three limit states, the exceedance probabilities decrease with construction of a berm at the toe and a

higher height of berm leads to lower value of exceedance probabilities. For example, probabilities of exceeding LS I after 30 days reduce by 1 and 2 orders of magnitude by adding berms with 3 m and 6 m height to the toe, respectively. The reason is due to the lower magnitudes of shear strain and deformation developed at the toe area with constructing a berm which was explained above.

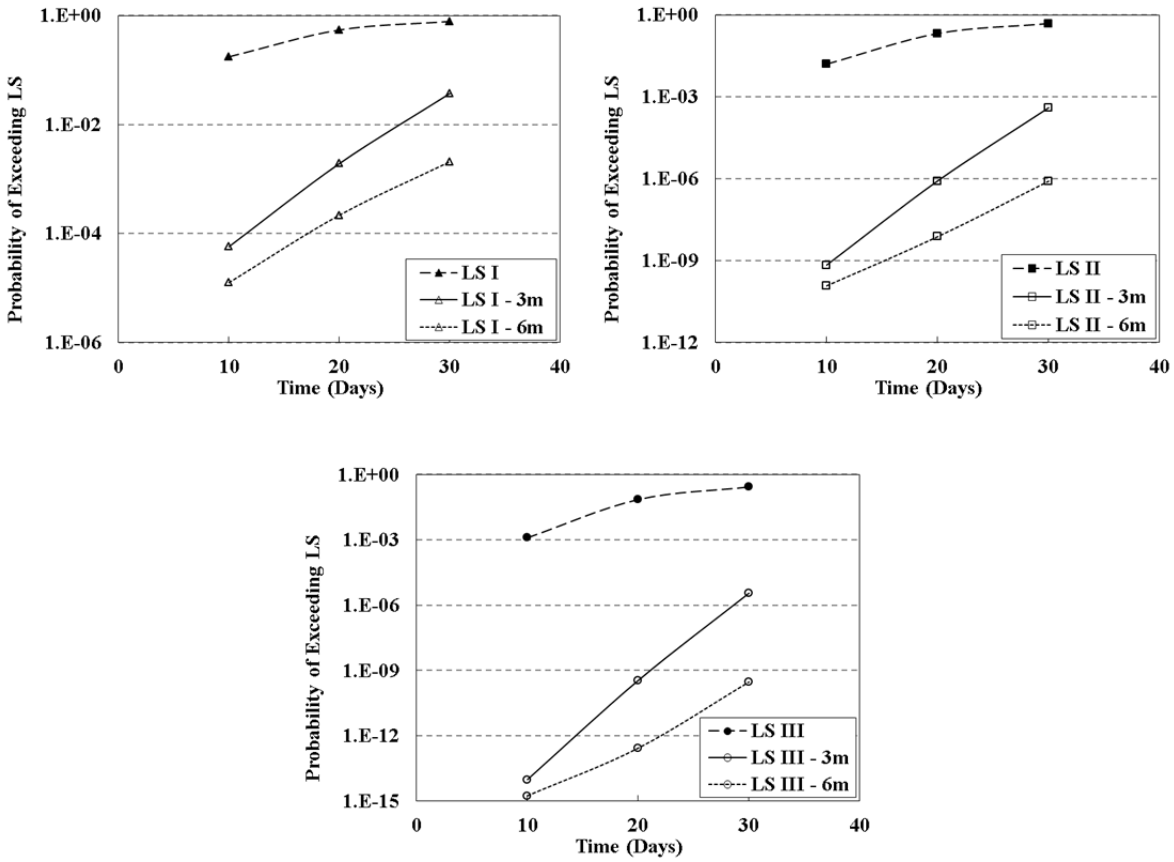

Figure 5.3: Effect of berm at toe on probabilities of exceeding LS I (top left), LS II (top right), and LS III (bottom)

5.6.2 Effect of impermeable curtain

Figures 5.4a and 5.4b show the horizontal deformation of the toe and gradient at the toe before and after constructing an impermeable curtain stating at the crest of dam and extending to three different depths (27 m, 45 m and 60 m). The results show that the deeper the impermeable curtain, the less the magnitudes of horizontal deformation and gradient at the toe. For example, after 20 days, the horizontal deformation at the toe reduces by 25%, 40% and 47% for cutoff walls respectively 27 m, 45 m, and 60 m deep. Similarly, the gradient reduces by 25%, 41%, and 50% after 20 days. This occurs because seepage path increases as the cutoff wall penetrates deeper. As a result, the total head dissipates more over a longer distance and pore pressure reduces. This coincides with a lower phreatic surface for deeper cutoff wall. Consequently, this is reflected to lower shear strains and less deformation at the toe.

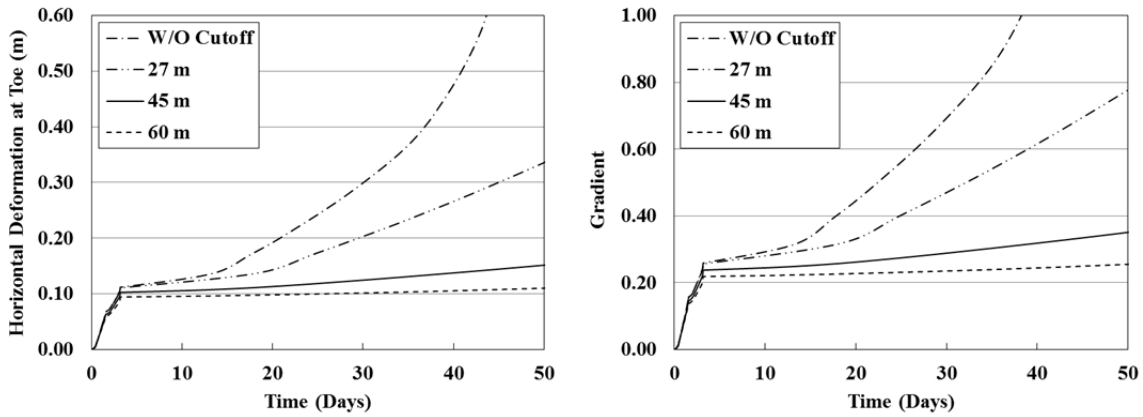

Figure 5.4: Effect of a berm at toe on a) Horizontal deformation (left) , and b) Gradient (right) at toe

The variation of probabilities of exceeding LS I, II and III due to constructing an impermeable curtain below the crest of the embankment dam is shown in Figure 5.5a, 5.5b, and 5.5c. The results show a considerable reduction in exceedance probabilities as the impermeable curtain penetrates deeper. For example, after 20 days, the probabilities of exceeding LS I for the embankment shown in Figure 5.1, is 55%. This value decreases to 35%, 14% and 8% for cutoff walls with 27 m, 45 m, and 60 m depths, respectively. The reason for the reduction is due to increased length of seepage path and lower phreatic surface for a deeper cutoff wall (as explained above).

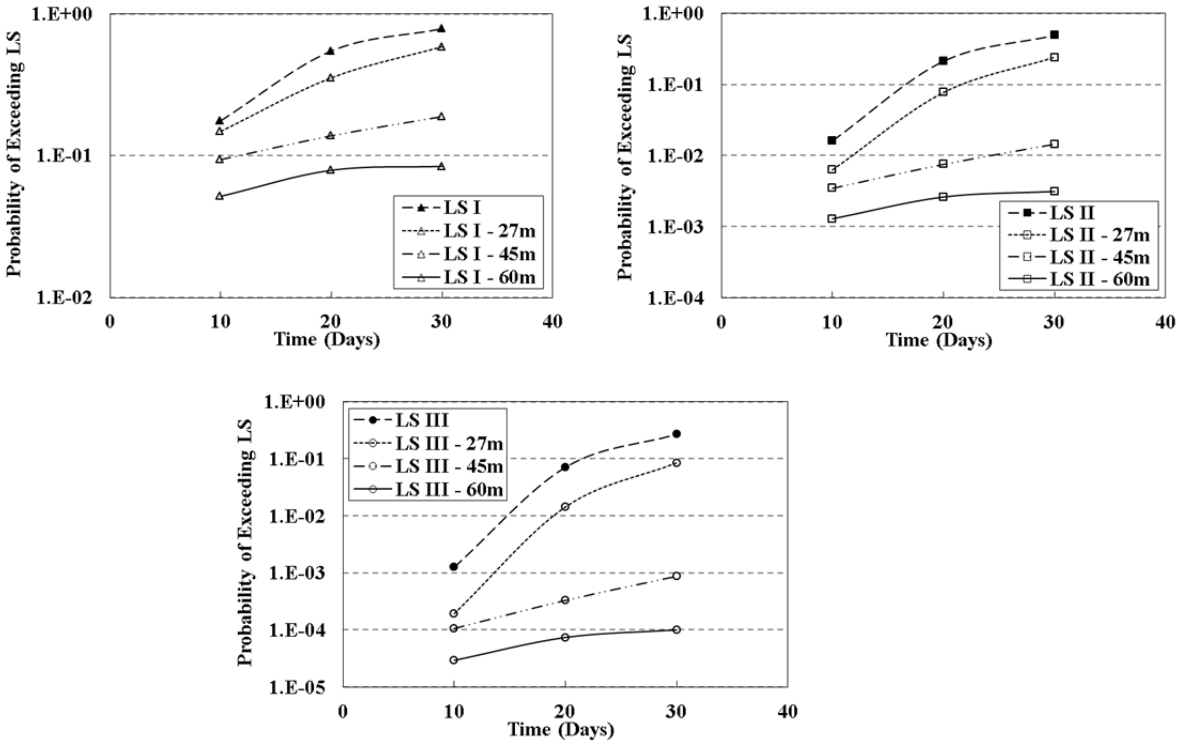

Figure 5.5: Effect of impermeable curtain on probabilities of exceeding LS I (top left), LS II (top right), and LS III (bottom)

5.6.3 Effect of drainage system at toe

Figures 5.6a and 5.6b present the horizontal deformation of the toe and gradient at the toe with and without having a drainage system at the toe. The results show that a toe drainage can considerably decrease the magnitudes of horizontal deformation, if the hydraulic conductivity is high enough to drain the water from area toe area. For example, after 30 days, the toe horizontal deformations are 0.14 m and 0.27 m for drainage system with hydraulic

conductivity of 8.6 m/day and 1.7 m/day, respectively. Without a toe drain, this value would be 0.3 m. The reduction is because of the drainage system lowering the phreatic surface and correspondingly the shear strains and deformations developed in the toe area are less due to reduced pressure head and less seepage flow forces. Gradients also decrease at the toe for the same reason. After 30days the toe gradients are 0.28 and 0.35 in toe drains with hydraulic conductivities of 8.6 m/ day abd 1.7 m/day, respectively. The quantity would be 0.37 without a toe drain.

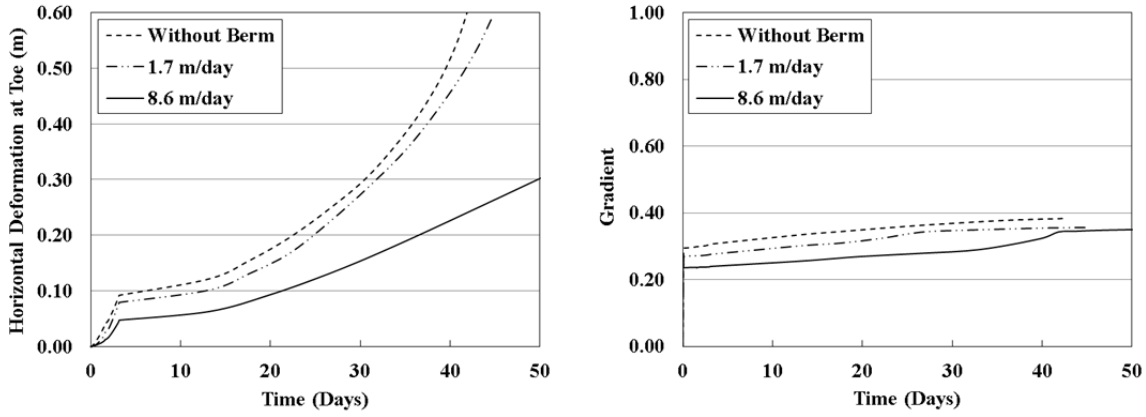

Figure 5.6: Effect of a drainage system at toe on a) Horizontal deformation (left), and b) Gradient (right) at toe

The variation of probabilities of exceeding LS I, II and III due to constructing a drainage system at the toe of the embankment dam is shown in Figure 5.7. The results show that the exceedance probabilities decrease with adding a toe drain to an embankment dam and the impact is higher if the hydraulic conductivity of the drainage system is higher. For

instance, after 20 days, probabilities of exceeding LS II decrease from 21% for no toe drain case to 14% and 6% for toe drains with hydraulic conductivities of 1.7 m/day and 8.6 m/day, respectively. The decrease in exceedance probabilities is due to lower phreatic surface at the toe area because of drainage system which results in lower shear strains and less deformation at the toe.

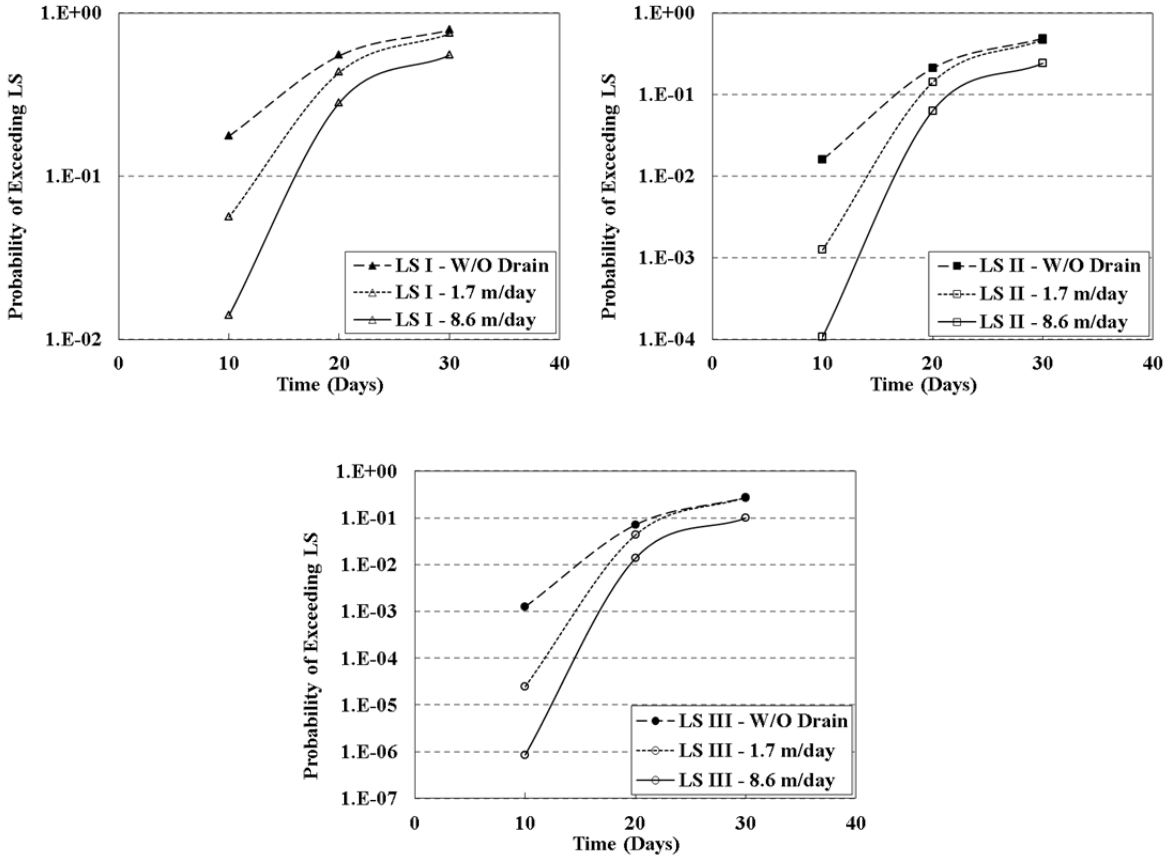

Figure 5.7: Effect of toe drainage on probabilities of exceeding LS I (top left), LS II (top right), and LS III (bottom)

5.6.4 Comparison of three remedial measures

Figure 5.8 shows a comparison of the three remedial measures presented herein. One case from each remedial measure is selected for this comparison which includes 6 m berm, 60m cut-off wall, and drainage layer with hydraulic conductivity of 8.6 m/day are the . The results show that constructing a berm at the toe leads to lower exceedance probabilities and thus seems to be the best approach, among the abovementioned remedial measure, to reduce the risk. This is because constructing a berm not only changes the flow regime by increasing the distance between the water entry point on the upstream side and the exit point on the downstream slope of the berm, but also it increases confining stresses at the toe area leading to smaller plastic strains and consequently smaller deformations at the toe.

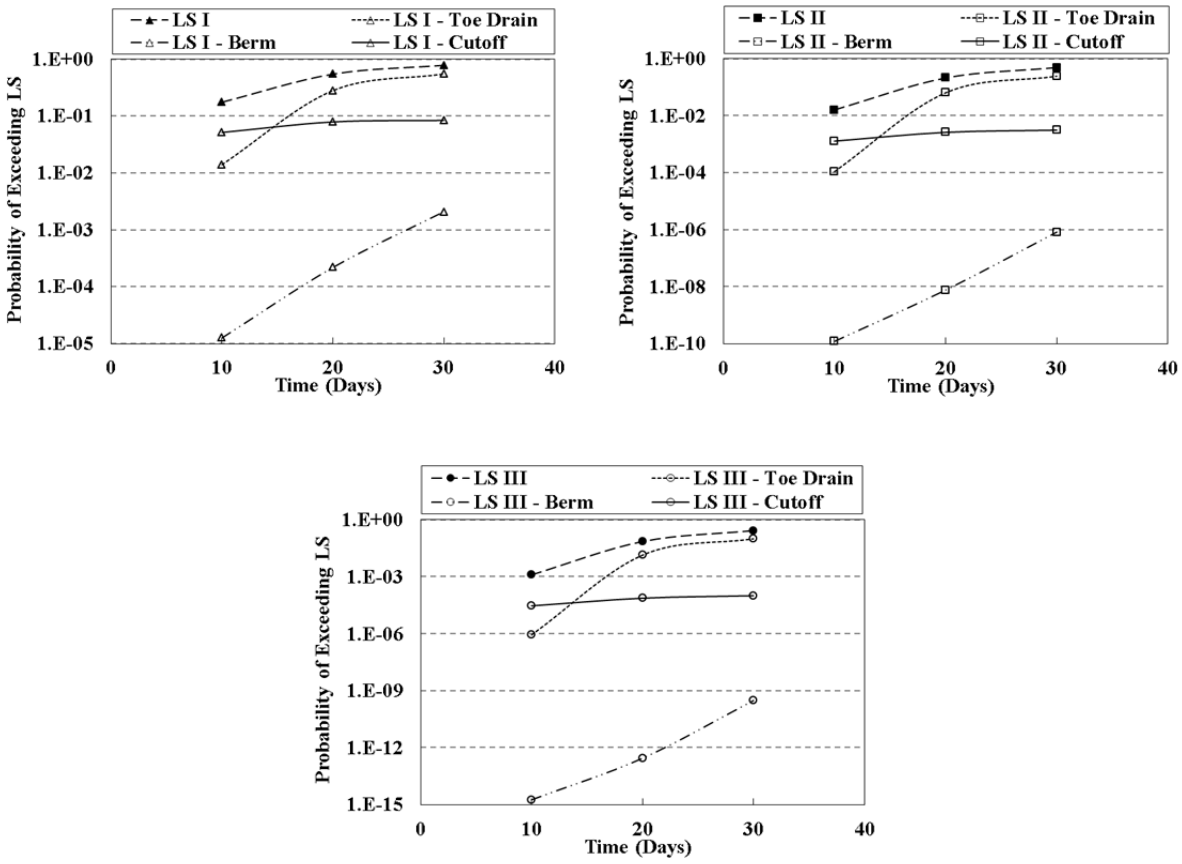

Figure 5.8: Probabilities of exceeding LS I, II, and III for three remedial measures

5.7 Summary and Conclusions

Three remedial measures are investigated which are related to various aspects of a remedy that might be thought for a problematic embankment dam (i.e. applying overburden stress, adding impermeable layer to limit seepage, and improving drainage to lower phreatic

surface.) The conclusions that can be drawn from the results of this study are summarized as follows:

Constructing a downstream berm as a remedial measure has a significant impact on the defamation levels at the toe. For example, due to the impact of a adding a 6 m high berm, after 30 days of water rising in the reservoir and remaining at high pool level, the horizontal deformations at toe is 0.077 m which would be 0.23 m if no berm was constructed. The quantity would be 0.095 m, for a 3 m high berm. Thus, even the smaller berm has a drastic impact on the deformation values. This can be attributed to the reason that mean confining pressures at any section under the toe increase and thus, less plastic shear strains develop in the toe area due to adding the berm.

A downstream berm as a remedial measure has a small impact on the toe gradient values and lead to a reduction of 3% and 6% in gradient value for berms with 3 m and 6 m height, respectively.

Exceedance probabilities decrease dramatically after constructing downstream berm. For instance, after 30 days, the probabilities of exceeding LS I reduce by 1 and 2 orders of magnitude due to constructing 3 m and 6 m high berms, respectively. This is also because of less shear strain developing in the toe area due to increased mean effective stresses.

Adding an impermeable curtain below the dam crest considerably reduces both deformation and gradient levels (e.g. after 20 days, the horizontal deformation at the toe reduces by 25%, 40% and 47% for cutoff walls respectively 27 m, 45 m, and 60 m deep. Similarly, the gradient reduces by 25%, 41%, and 50% after 20 days.) This occurs due to an

increased seepage path leading higher drop of pressure head and lower phreatic surface level. This in turn results in less strain and deformation magnitudes.

The exceedance probabilities decrease considerably due to adding an impermeable curtain below the dam crest. The impact can be as high as reducing probability of exceeding LS I from 55% to 8% after 20 days for a depth of penetration of 60 m. This is also due to the increase in seepage flow path and reduction of pressure heads, which leads to less strains and deformations at the toe.

The exceedance probabilities decrease with adding a toe drain to an embankment dam and the impact is higher where the hydraulic conductivity of the drainage system is higher. For instance, after 20 days, probabilities of exceeding LS II decrease from 21% for no toe drain case to 14% and 6% for toe drains with hydraulic conductivities of 1.7 m/day and 8.6 m/day, respectively. The decrease in exceedance probabilities is due to lower phreatic surface at the toe area because of drainage system which results in lower shear strains and less deformation at the toe.

CHAPTER 6

6. SUMMARY AND CONCLUSION

The first paper in Chapter 2 presents the results of coupled seepage/deformation analysis with the aim of estimating the probabilities of exceeding a pre-defined deformation limit state, with a focus on water storage and flood protection earth structures. Finite element analyses of an embankment dam where failure was estimated to occur with high water level in the reservoir were performed. Limit states were defined on the basis of deformation level and area of high seepage gradients. The approach presented in this paper utilized limit states that were defined based on potential emerging failure zones instead of using probability of exceeding a predefined value of factor of safety. Based on the assumptions made in this study and the analyses results, the following conclusions are presented:

i. By considering uncertainties in design soil properties, analyses indicated the earth embankment has a 100% probability of exceeding *Limit State I* and *II* and a 73% probability of exceeding *Limit State III* when the water level is at the maximum elevation (980 ft).

ii. This is in agreement with the deterministic analyses in which a factor of safety of less than unity is estimated for the embankment slope at water elevation of 980 ft (USACE, 2006).

iii. Analyses results suggested that at *Limit State I*, corresponding to 2.5 inches of lateral deformation at the crown, zones of high hydraulic gradients began to emerge. At *Limit State II*, corresponding to 5 inches of lateral deformation at the crown, the high gradient zones (above critical gradient) expands to a depth of 10 ft below the toe. In case of *Limit State III*, corresponding to 10 inches of lateral deformation at the crown, a substantial area on the high gradient zones below the toe extends to a depth of 20 ft.

iv. In these analyses, *Limit State I* can be considered the serviceability limit state while *Limit States II* and *III* can be considered intermediate and ultimate limit states, respectively. The flow rates through the dam for *Limit States I* was 200 gal/day per ft, but increased to 320 gal/day per ft for *Limit States II* and to 360 gal/day per ft for *Limit States III*.

Finally, selecting the definition of limit states for earth embankments is a challenging task because it requires a large database with quantifiable information on condition and corresponding performance levels. Coupled with modeling effort, mining databases such as the National Levee Database provided by the USACE may provide sufficient information for a better establishment of limit states in various modes. The advantage of this approach is not only in terms of avoiding confusion with factors of safety and their various definitions, but also in terms of a better communication of risk for county, city, state and federal officials.

The second paper in Chapter 3 presents the results of coupled seepage/deformation analysis with the aim of estimating the probabilities of exceeding a pre-defined deformation

limit state, with a focus on water storage and flood protection earth structures. Finite element analyses of an embankment dam where failure was estimated to occur with high water level in the reservoir were performed. Limit states were defined on the basis of deformation level and area of high seepage gradients. The approach presented in this paper utilized limit states that were defined based on potential emerging failure zones instead of using probability of exceeding a predefined value of factor of safety. Based on the assumptions made in this study and the analyses results, the following conclusions are presented:

i. By considering uncertainties in design soil properties, analyses indicated the earth embankment has a 100% probability of exceeding *Limit State I* and *II* and a 73% probability of exceeding *Limit State III* when the water level is at the maximum elevation (980 ft).

ii. This is in agreement with the deterministic analyses in which a factor of safety of less than unity is estimated for the embankment slope at water elevation of 980 ft (USACE, 2006).

iii. Analyses results suggested that at *Limit State I*, corresponding to 2.5 inches of lateral deformation at the crown, zones of high hydraulic gradients began to emerge. At *Limit State II*, corresponding to 5 inches of lateral deformation at the crown, the high gradient zones (above critical gradient) expands to a depth of 10 ft below the toe. In case of *Limit State III*, corresponding to 10 inches of lateral deformation at the crown, a substantial area on the high gradient zones below the toe extends to a depth of 20 ft.

iv. In these analyses, *Limit State I* can be considered the serviceability limit state while *Limit States II* and *III* can be considered intermediate and ultimate limit states, respectively. The flow rates through the dam for *Limit States I* was 200 gal/day per ft, but increased to 320 gal/day per ft for *Limit States II* and to 360 gal/day per ft for *Limit States III*.

Finally, selecting the definition of limit states for earth embankments is a challenging task because it requires a large database with quantifiable information on condition and corresponding performance levels. Coupled with modeling effort, mining databases such as the National Levee Database provided by the USACE may provide sufficient information for a better establishment of limit states in various modes. The advantage of this approach is not only in terms of avoiding confusion with factors of safety and their various definitions, but also in terms of a better communication of risk for county, city, state and federal officials.

The results from laboratory and field hydraulic conductivity tests conducted by Brizendine (1997) at four levee sites, with and without roots, are summarized and presented in the third paper in Chapter 4. The values and distribution of the hydraulic conductivity parameters are used to estimate the probability of exceeding predefined limit states. A combination of numerical modeling, a definition of limit states based on the framework of critical state soil mechanics, and simple probability analyses are used to quantify three limit states of performance (LS I, LS II, and LS III) as well as the probability of exceedance under hydraulic loading. A case study of Elkhorn Levee is presented to demonstrate the

applicability of the limit state concept. The effect of change in hydraulic conductivity due to the presence of woody vegetation on the stability of the levee is investigated under the assumption that woody vegetation impacts either the whole embankment or only the 'root' layer that has a thickness of 0.75 m from the ground surface. The toe area is used as an indicator location for condition assessment with regard to the definition of *limit state*. Maximum deformations commonly occur in this location and can be visually inspected and surveyed. In addition, high gradients are observed in this area, and these critical gradients can be problematic, causing piping and internal erosion. Based on the results of this study, the following conclusions are advanced:

Field and laboratory hydraulic conductivity data from four levee test sites show no clear trend to support the notion that woody vegetation leads to either high or low values of hydraulic conductivity. However, the testing protocol that was used for the original study did not include characterization of the roots in terms of shape, distribution, or the extent of their decay. Knowledge of these parameters is necessary to interpret the possible effects of woody vegetation on the hydraulic conductivity data and to explain the observed trends. Even then, it seems that such an effect will have to be evaluated on a site specific basis.

Consideration of the transient nature of hydraulic loading provides a more comprehensive insight into the temporal responses of an embankment. Even though the levee case study is modeled in a marginal condition of stability, the probability of exceeding LS III after 10 days of sustained maximum water level is only 2%, based on limit equilibrium analysis. This finding signifies the relatively high probability of functionality of the levee at

this point. The probability of exceeding LS III, however, increases over time to 37% and 72% after 20 and 30 days, respectively. These data signify a high probability of failure and demonstrate the importance of defining the duration of hydraulic loading during and after the occurrence of severe storms.

The impact of woody vegetation on the changes in hydraulic conductivity of the flow domain plays a significant role in determining the time it takes to exceed LS III. If woody vegetation leads to a reduction in k-value from 5×10^{-5} m/s to 5×10^{-6} m/s, the time it takes to reach LS III increases from 4 days to 12 days. This amount of time can be critical in terms of performing preventive and rehabilitation efforts and mitigating failure hazards.

In modeling a 0.75 m top 'root' layer, the results show lower toe deformation for both cases of 0.1 k and 10 k than in the 1.0 k case (without a 'root' layer). The total head drops substantially across the 0.1 k layer, and the low k-value also hinders the advancement of the saturation front, resulting in less deformation over time. In the second scenario where the 'root' layer is modeled with hydraulic conductivity of 10 k, the deformation levels are also lower than for the case without a 'root' layer, mainly because the downstream side of the levee with the 10 k layer functions in a manner similar to toe drainage, leading to a low phreatic surface at the zone closest to the toe.

Despite the fact that the lowest value of probability to exceed LS III is found for the 0.1 k case, from the deformation aspect, critical levels of gradient are observed at the toe for this case after 30 days. Even though the probability of exceeding LS III is higher for the 10 k case than for the 0.1 k case, the computed gradients are lower. This finding again

demonstrates the inadequacy of a condition assessment that is determined by a deterministic single performance matrix.

In the last paper presented in Chapter 5, three remedial measures are investigated which are related to various aspects of a remedy that might be thought for a problematic embankment dam (i.e. applying overburden stress, adding impermeable layer to limit seepage, and improving drainage to lower phreatic surface.) The conclusions that can be drawn from the results of this study are summarized as follows:

Constructing a downstream berm as a remedial measure has a significant impact on the defamation levels at the toe. For example, due to the impact of a adding a 6 m high berm, after 30 days of water rising in the reservoir and remaining at high pool level, the horizontal deformations at toe is 0.077 m which would be 0.23 m if no berm was constructed. The quantity would be 0.095 m, for a 3 m high berm. Thus, even the smaller berm has a drastic impact on the deformation values. This can be attributed to the reason that mean confining pressures at any section under the toe increase and thus, less plastic shear strains develop in the toe area due to adding the berm.

A downstream berm as a remedial measure has a small impact on the toe gradient values and lead to a reduction of 3% and 6% in gradient value for berms with 3 m and 6 m height, respectively.

Exceedance probabilities decrease dramatically after constructing downstream berm. For instance, after 30 days, the probabilities of exceeding LS I reduce by 1 and 2 orders of

magnitude due to constructing 3 m and 6 m high berms, respectively. This is also because of less shear strain developing in the toe area due to increased mean effective stresses.

Adding an impermeable curtain below the dam crest considerably reduces both deformation and gradient levels (e.g. after 20 days, the horizontal deformation at the toe reduces by 25%, 40% and 47% for cutoff walls respectively 27 m, 45 m, and 60 m deep. Similarly, the gradient reduces by 25%, 41%, and 50% after 20 days.) This occurs due to an increased seepage path leading higher drop of pressure head and lower phreatic surface level. This in turn results in less strain and deformation magnitudes.

The exceedance probabilities decrease considerably due to adding an impermeable curtain below the dam crest. The impact can be as high as reducing probability of exceeding LS I from 55% to 8% after 20 days for a depth of penetration of 60 m. This is also due to the increase in seepage flow path and reduction of pressure heads, which leads to less strains and deformations at the toe.

The exceedance probabilities decrease with adding a toe drain to an embankment dam and the impact is higher where the hydraulic conductivity of the drainage system is higher. For instance, after 20 days, probabilities of exceeding LS II decrease from 21% for no toe drain case to 14% and 6% for toe drains with hydraulic conductivities of 1.7 m/day and 8.6 m/day, respectively. The decrease in exceedance probabilities is due to lower phreatic surface at the toe area because of drainage system which results in lower shear strains and less deformation at the toe.

REFERENCES

Abdi, E., Majnounian, B., Genet, M., and Rahimi, H. (2010). "Quantifying the effects of root reinforcement of Persian Ironwood (Parrotia persica) on slope stability; a case study: Hillslope of Hyrcanian forests, northern Iran." *Ecological Engineering*; 36:1409-1416.

Ahmed, A. A. (2009). "Stochastic analysis of free surface flow through earth dams." Computers and Geotechnics 36: 1186-1190.

Alonso, E.E. (1976). "Risk analysis of slopes and its application to slopes in Canadian sensitive clays." Geotechnique, 26 (3), 453–472.

Bauer, J. and Pula, W. (2000). "Reliability with respect to settlement limit-states of shallow foundations on linearly-deformable subsoil", Computers and Geotechnics, 26 (2000) 281-308.

Bea, R., and Cobos-Roa, D. (2009). Discussion of "stability of I-walls in New Orleans during hurricane Katrina" by J. M. Duncan, T. L. Brandon, S. G. Wright, and N. Vroman. J. Geotechnical and Geoenvironmental Engrg, 135(12): 1995-1999.

Berilgen, M. M. (2007). “Investigation of stability of slopes under drawdown conditions.” Computers and geotechnics, 34 (2), 81-91.

Bibalani, G. H., Golshani, A. A., Najafian, K. A. (2006). “The traction effect of lateral roots of Gavan (Astragalus raddei) on soil reinforcement in Northwest Iran (rangelands of the Shanjan area of Shabestar).” Canadian Journal of Soil Science; 86:493-49.

Brizendine, A. L. (1997). “Risk Based Analysis of Levees.” Doctoral Dissertation submitted to The College of Engineering and Mineral Resources, West Virginia University.

Buryloa, M., Hudekb, C., Reya, F. (2011). “Soil reinforcement by the roots of six dominant species on eroded mountainous marly slopes (Southern Alps, France).” Catena; 84:70-78.

Callari, C., and Abati, A. (2009). "Finite element methods for unsaturated porous solids and their application to dam engineering problems", J. Computers and Structures, 87(7-8): 485-501.

Castelbaum, D. and Shackelford, C. (2009). ”Hydraulic Conductivity of Bentonite Slurry Mixed Sands.” J. Geotech. Geoenviron. Eng., 135(12), 1941–1956.

Charles, J. A., and Bromhead, E. N. (2008). "Contributions to Géotechnique 1948–2008: Slope stability and embankment dams" Géotechnique, 58 (5), 385 –389.

Christian, J. T. (2008), "SPECIAL ISSUE: Performance of Geo-Systems during Hurricane Katrina." J. Geotechnical and Geoenvironmental Engrg; 134 (5), 555-779.

Corcoran, M. K., Gray, D. H., Biedenharn, D. S., Little, C. D., Leech, J. R., Pinkard, F., Bailey, F., and Lee, L. T. (2010). "Literature Review –Vegetation on Levees." U.S. Army Corps of Engineers, ERDC SR-10-2.

Corcoran, M. K., Peters, J. F., Dunbar, J. B., Llopis, J. L., Tracy, F. T., Wibowo, J. L., Simms, J. E., Kees, C. E., McKay, S. K, Fischenich, J. C., Farthing, M. W., Glynn, M. E., Robbins, B. A., Strange, R. C., Schultz, M. T., Clarke, J. U., Berry, T. E., Little, C. D., and Lee, L. T. (2011). "Initial Research into the Effects of Woody Vegetation on Levees." ERDC, Technical Report to USACE HQ, Washington DC, Vol. I-IV.

Cornell, C.A. (1971). "First-order uncertainty analysis of soils deformation and stability", Proceedings of First International Conference on Application of Probability and Statistics in Soil and Structural Engineering (ICAPI), Hong Kong, 129–144.

Das, S., Samui, P., and Sabat, A. (2012). “Prediction of Field Hydraulic Conductivity of Clay Liners Using an Artificial Neural Network and Support Vector Machine.” Int. J. Geomech., 12(5), 606–611.

Duncan, J. M. (2000). “Factors of Safety and Reliability in Geotechnical Engineering.”, J. Geotechnical and Geoenvironmental Engrg; 126 (4): 307-316.

Duncan, J.M., and Chang, C.Y. (1970). “Nonlinear analysis of stress and strain in soil.” ASCE J. of the Soil Mech. and Found. Div., 96, 1629–1653.

FEMA. (2005). “Technical manual for dam owners, impacts of plants on earthen dams.” Washington, D.C., U.S. Dept. of Homeland Security, Federal Emergency Management Agency.

Fu, J., and Jin, S. (2009), "A study on unsteady seepage flow through dam", J. Hydrodynamics, 21(4): 499-504.

Gabr, M., Akram M., and Taylor, H. M. (1995). “Effect of Simulated Roots on the Permeability of Silty Soils.” American Society for Testing and Materials, Geotechnical Testing Journal, 118 (1), 112-116.

Ghorbani, M., Sharifzadeh, M., Yasrobi, S., and Daiyan, M. (2012). "Geotechnical, structural and geodetic measurements for conventional tunneling hazards in urban areas-The case of Niayesh road tunnel project". Tunneling and Underground Space Technology 31:1-8.

Gray, D.H., MacDonald, A., Thomann, T., Blatz, I., and Shields, F.D. (1991). "The effects of vegetation on the structural integrity of sandy levees." Technical Report No. REMR-EI-5, Vicksburg, MS: U.S. Army Waterways Experiment Station.

Greenway, D. R. (1987). "Vegetation and Slope Stability." Slope Stability. John Wiley and Sons, New York.

Griffiths, D. V., and Fenton, G. A. (2001). "Bearing capacity of spatially random soil: the undrained clay Prandtl problem revisited." Geotechnique, 51(4), 351-359.

Gui, S., Zhang, R., Turner, J., and Xue, X (2000). "Probabilistic Slope Stability Analysis with Stochastic Soil Hydraulic Conductivity". Journal of Geotechnical and Geoenvironmental Engineering 126(1): 1-9.

Hansen, D. and Roshanfekr, A. (2012). "Assessment of Potential for Seepage-Induced Unraveling Failure of Flow-Through Rockfill Dams." Int. J. Geomech., 12(5), 560–573.

Hart, D. J., Bradbury, K. R. and Feinstein, D. T. (2006), The Vertical Hydraulic Conductivity of an Aquitard at Two Spatial Scales. Ground Water, 44: 201–211. doi: 10.1111/j.1745-6584.2005.00125.x .

Huang M. S., Jia C. Q. (2009). "Strength reduction FEM in stability analysis of soil slopes subjected to transient unsaturated seepage." Computers and Geotechnics, 36(2), 93-101.

Huang M. S., Jia C. Q. (2009). "Strength reduction FEM in stability analysis of soil slopes subjected to transient unsaturated seepage", Computers and Geotechnics, 36(2), 93-101.

Khalilzad, M. and Gabr, M. A. (2011). "Deformation-Based Limit States for Earth Embankments." ASCE Conf. Proc. 397, 372 (2011), DOI:10.1061/41165(397)372, p. 3639-48.

Kim, Dae-ManMurielle Ghestem, Roy C. Sidle and Alexia Stokes. (2011). "The Influence of Plant Root Systems on Subsurface Flow: Implications for Slope Stability." BioScience, 61(11): 869-879.

Kohgo, Y., Takahashi, A., Asano, l. and Suzuki, T. (2006). "FEM consolidation analysis of centrifuge test for rockfill dam model during first reservoir filling", Proceedings of the

Fourth International Conference on Unsaturated Soils, 2006, Carefree Arizona, p. 2312 – 2323.

Kondner, R.L. (1963). “A hyperbolic stress strain formulation for sands.” Pan. Am. ICOSFE Brazil; 1, 289–324.

Lu, N., and Godt, J. (2008). "Infinite slope stability under steady unsaturated seepage conditions", Water Resources Research, 44(11), 1-13.

Mann, M. J., and Snow, R. E. (1993). “Analysis of slope failure and remedial design of an earth dam.” Stability and Performance of Slopes and Embankments –II, ASCE Geotechnical Special Publication No. 31.

Mann, M. J., Snow, R. E., and Klettke, A. J. (2013). “Remedial Design of An Earth Dam – 20 Years later”. GeoCongress 2013, San Diego, California, United States, March 3-6.

Meyerhof, G. G. (1982). “Limit States Design in Geotechnical Engineering”, J. Structural Safety, 1(1): 67-71.

Morrice, J. A., Valett, H. M., Dahm, C. N. and Campana, M. E. (1997). “Alluvial Characteristics, Groundwater-Surface Water Exchanged and Hydrological Retention in

Headwater Streams." Hydrological Processes, 11: 253–267. doi: 10.1002/(SICI)1099-1085(19970315)11:3<253::AID-HYP439>3.0.CO;2-J.

Moellmanna, A., Vermeera, P. A. and Hubera, M. (2011). "A probabilistic finite element analysis of embankment stability under transient seepage conditions", Georisk: Assessment and Management of Risk for Engineered Systems and Geohazards, Volume 5, Issue 2, p. 110-119.

Nagaraj, TS, and Srinivasa Murthy, BR (1985), "Prediction of the Preconsolidation Pressure and Recompression Index of Soils." Geotechnical Testing Journal, 8(4), pp. 199-202.

National Oceanic and Atmospheric Administration (NOAA, 2011), National Weather service, http://water.weather.gov/ahps2/hydrograph.php?wfo=lsx&gage=unnm7

Nilaweera, N.S., Nutalaya, P., 1999. Role of tree roots in slope stabilisation. Bulletin of Engineering Geology and the Environment 57, 337–342.

Nusier, O. K., Alawneh, A., and Malkawi, A. I. (2002). "Remedial measured to control seepage problems in the Kafrein dam, Jordan". Bulletin of Engineering Geology and the Environment 61 (2): 145-152.

Özera, A. T., and Bromwell, L. G. (2012). "Stability assessment of an earth dam on silt/clay tailings foundation: A case study." Engineering Geology, Vol. 151, 29 November 2012, 89-99.

Phoon, K.K and Kulhawy, P.H., (2008). "Serviceability limit state reliability-based design", In: Phoon, K.K. ed. Reliability-based Design in Geotechnical Engineering - Computations and Applications. London, UK: Taylor & Francis, 344--384.

Plaxis (Version 2010), User's Manual, Plaxis Company.

Pollen, N., Simon, A., (2005). "Estimating the mechanical effects of riparian vegetation on stream bank stability using a fiber bundle model." Water Resour. Res. 41, W07025.

Reclamation District 1000 (RD1000) website, (2012) http://www.rd1000.org

Richards, K. S., and Reddy, K. R. (2005), "Slope Failure of Embankment Dam under Extreme Flooding Conditions: Comparison of Limit Equilibrium and Continuum Models." Geo-Frontiers Congress 2005, Austin, Texas, United States, January 24-26; http://dx.doi.org/10.1061/40787(166)30.

Rogers, J. D., Boutwell, G. P., Schmitz, D. W., Karadeniz, D., Watkins, C. M., Athanasopoulos-Zekkos, A. G., and Cobos-Roa, D. (2008). "Geologic Conditions Underlying the 2005 17th Street Canal Levee Failure in New Orleans". Journal of Geotechnical and Geoenvironmental Engineering 134(5): 583-601.

Salgado, R. (2000). "Shear strength and stiffness of silty sand." J. Geotech. Eng., ASCE, Vol. 126, No. 5, 451-462.

Schanz, T., P.A Vermeer, P.G. Bonnier (1999). "The Hardening Soil Model: Formulation and Verification", Beyond 2000 in Computational Geotechnics-10 Years of PLAXIS © 1999 Balkema, Rotterdam, ISBN 90 580940 X.

Schanz, T., Vermeer, P.A. (1998). "Special issue on pre-failure deformation behaviour of geomaterials." Géotechnique; 48, 383–387.

Schanz, T., Vermeer, P.A., and Bonnier, P.G. (1999). "The Hardening Soil Model: Formulation and Verification", Beyond 2000 in Computational Geotechnics-10 Years of PLAXIS © 1999 Balkema, Rotterdam, ISBN 90 580940 X.

Schwarz, M., Preti, F., Giadrossich, F., Lehmann, P., and Or, D. (2010). "Quantifying the role of vegetation in slope stability: A case study in tuscany (italy)." Ecological Engineering, 36(3), 285-291. doi:10.1016/j.ecoleng.2009.06.014.

Seed, R.B, Mitchell, J.K., and Seed, H.B. (1990). "Kettlemen Hills waste landfill slope failure, II: stability analysis." Journal of Geotechnical Engineering, ASCE, 116 (4): 669–690.

Sherard, J. L. (1987). "Lessons from the Teton Dam Failure". Engineering Geology 24: 239-256.

Sills, G. L., Vroman, N. D., Wahl, R. E., and Schwanz, N. T. (2008). "Overview of New Orleans levee failures: Lessons learned and their impact on national levee design and assessment" J. Geotechnical and Geoenvironmental Engrg, 134(5): 556-565.

SLOPE/W (Version 5), User's Manual, GEO-SLOPE International, Ltd.

Stark, T. D., and Duncan, J. M (1991) "Mechanisms Of Strength Loss In Stiff Clays," Journal of Geotechnical Engineering, ASCE, Vol. 117, No. 1, pp. 139-154.

Sully, J. P. (1985). "Geotechnical aspects of remedial design for a gold tailings dam". International Journal for Numerical and Analytical Methods in Geomechanics 9 (6): 589-598.

Sun, H., Li, S., Xiong, W., Yang, Z., Cui, B., and Tao-Yang. (2008). "Influence of slope on root system anchorage of pinus yunnanensis." Ecological Engineering, 32(1), 60-67. doi:10.1016/j.ecoleng.2007.09.002.

Tang, W.H., Yucemen, M.S., Ang, A.H.S. (1976). "Probability-based short term design of soil slopes", Can. Geotechnical J., 13, 201–215.

Tavenas and Leroueil (1981). "Creep and failure of slopes in clays." Can. Geotech. J., 18, 106-120.

Tint, K., Kim, Y., Seo, I. and Kim, D. (2007). "Shear behavior of overconsolidated Nakdong river sandy silt." Korean Society of Civil Engineers, 11(5), pp. 233-241.

Udin, N. (2005). "Lessons Learned: Failure of a Hydroelectric Power Project Dam". Journal of Performance of Constructed Facilities; 19 (1): 69-77.

U.S. Army Corps of Engineers, (1990). "Engineering and Design, settlement analysis", Engineering Manual No. 1110-1-1904, Dept. of the Army, Washington D.C., 30 September 1990.

U.S. Army Corps of Engineers, (1997). “Introduction to probability and probability methods for use in geotechnical engineering.” Engr. Tech. Letter No. 1110-2-547, Dept. of the Army, Washington D.C., 30 September 1997.

U.S. Army Corps of Engineers, (1999). “Risk-based analysis in geotechnical engineering for support of planning studies.” Engr. Tech. Letter No. 1110-2-556, Dept. of the Army, Washington D.C., 28 May 1999.

U.S. Army Corps of Engineers, (2006). “Reliability analysis and risk assessment for seepage and slope stability failure modes for embankment dams.” Engr. Tech. Letter No. 1110-2-561, Dept. of the Army, Washington D.C., 31 January 2006.

U.S. Army Corps of Engineers, (2009). “Engineering and Design: Guidelines for Landscape Planting and Vegetation Management at Levees, Floodwalls, Embankment Dams, and Appurtenant Structures.” ETL 1110-2-571.

US Navy (1986). “Soil Mechanics, Foundations, and Earth Structure.” NAVFAC Design Manual DM-7.2, Washington, D.C.

Viratjandr, C. and Michalowski, R. L. (2006). "Limit analysis of submerged slopes subjected to water drawdown". Canadian geotechnical journal, 43 (8), 802-814.

Wahlstrom, E. E., and Nichols, T. C. (1969). “The morphology and chronology of a landslide near Dillon dam, Dillon, Colorado”. Engineering Geology 3 (2): 149-174.

Wang, Y., Cao, Z., and Au, S. K. (2011). “Practical reliability analysis of slope stability by advanced Monte Carlo simulations in spreadsheet.” Canadian Geotechnical Journal, 48(1), 162-172.

Wellington C. D. and Vlachaki, C. (2004). “Serviceability limit state criteria for the seismic assessment of R/C building”, 13th World Conference on Earthquake Engineering, Vancouver, B.C., Canada.

Wolff, T.F. (1994). "Evaluating the reliability of existing levees" Rep., Res. Proj.: Reliability of existing levees, prepared for U.S. Army Engineer Waterways Experiment Station Geotechnical Laboratory, Vicksburg, Miss.

Wolff, T.F. (1996). “Probabilistic slope stability in theory and practice”, proceeding of uncertainty, Geotechnical Special Publication, No. 58 1. ASCE, Madision, WI, 419–433.

Wolff, T.F., Demsky, E.C., Schauer, J. and Perry, E. (1996). “Reliability Assessment of Dike and Levee Embankments”, Proceeding of uncertainty, Geotechnical Special Publication, No. 58 1. ASCE, Madison, pp. 636–650.

Wu, T.H., McKinnell, W.P., and Swanston, D.N. (1979). “Strength of tree roots and landslides on Prince of Wales Island, Alaska. Can.” Geoth. J., 16, 19–33.

Yu; S., R. Salgado, S. W. Sloan, and J. M. Kim (1998) “Limit Analysis Versus Limit Equilibrium for Slope Stability, “Journal of Geotechnical and Geoenvironmental Engineering, ASCE, 124 (1). pp. 1-11.

Zhang, L. M. & Ng, A. M. Y. (2005). “Probabilistic limiting tolerable displacements for serviceability limit state design of foundations”, Geotechnique, 55, No. 2, 151–161.